

ME519/ME525: MAE Group Project

Demonstrating the use of the Soft Systems Methodology to drive a Blended Wing Body Feasibility Study

Group O:
Steven Munn, Lewis McBride, Toni Barr, Nian Liu, Craig Melrose and Aidan Wood

MAE Project Adviser: Dr Mohammed Afsar

Version Date: 29/03/2021

Word Count: 34,426

Website: <https://bwbliners.netlify.app/>

Abstract

The emerging goal of carbon neutrality by 2050 across the globe encouraged a revisit of revolutionary technologies such as the Blended Wing Body (BWB) aircraft. The aim of this project was to investigate the feasibility of a BWB aircraft for long haul flights by analysing the technical and economic performances of such concept through an iterative design process using the Soft Systems Methodology (SSM). The wicked design problem was broken into its requisite sub-systems, where a global study to a complex aircraft design problem was iterated. The project was split in to 6 inter-dependent departments (Aero-dynamics, Structures, Propulsion, Materials, Economics and Legal) using the SSM, with their interactions and inter-reliances mapped before a design concept was iterated via a manual, multidisciplinary design optimisation approach. Through the progression of each department and within the whole team, the final designed BWB concept was able to hold 562 passengers in a 2-class configuration; up to 31.8% higher volume of cargo compared to B747-8F when operate as a freighter. Up to 9% acquisition cost reduction from the A380 was achieved for the BWB; at full passenger load, the BWB achieved up to 12.5% Direct Operating Cost (DOC) reduction per nm-pax and 18% less CO_2 emission compared to the Airbus A380. The BWB was found to represent a feasible design concept that, with further advances in engine technology, could represent the next step forward in commercial aviation. The SSM adopted for this study was concluded to provide a strong basis by which the design could be broken down to work through the problem within the team.

Acknowledgements

Deepest gratitude must be expressed to Dr Mohammed Afsar, who was the advisor for this project. His support and encouragement have been vital to the depth of the scope, and regular communication ensured focus and motivation, allowing the project to be completed to the highest standard.

Additionally, special regards must be paid to Rohella Muhel for his support in semester 1 as a CFD consultant, where his extensive subject expertise confirmed the correct and optimum procedure was being implemented.

Finally, thanks must be given to Dr David Butler for providing the project management workshops and information, through which supplied a solid basis for the team mechanics throughout the project.

Contents

Nomenclature	7
1 Introduction	16
1.1 Global Aim and Department Objectives	16
2 Project Management	19
2.1 Project Overview	19
2.2 Project Scope	20
2.2.1 Project Phasing	21
2.2.2 Base Requirements	22
2.3 Working Structure	23
2.3.1 Roles & Responsibilities	23
2.3.2 Working Procedures	27
2.4 Systems Engineering	31
2.4.1 Soft Systems Methodology (SSM)	31
2.4.2 Application of 4 Activities Model	35
2.4.3 Design Roadmap	40
2.4.4 Multi-Disciplinary Optimisation (MDO) Approach	42
2.4.5 Design Stage Reviews	42
2.4.6 Requirements Definition	43
2.4.7 Fault Analysis - Non-Compliance to Requirements	44
3 Literature Overview	45
4 Design Boundaries	46
4.1 Constraints Diagram	46
4.2 Regulations	47
5 The Design Process	49
5.1 Aerodynamics and Structures	49
5.2 In the context of the Global Design	49
5.2.1 Inter-dependencies	49
5.2.2 Inputs and Outputs	50
5.2.3 Key Performance Indicators	50
5.2.4 Manual Optimisation	51
5.3 Literature Review	51
5.4 Methodology	52
5.4.1 ONERA M6 Flow Verification	52
5.4.2 CFD Verification Problem Modelling	52

5.4.3	Verification Results	53
5.5	BWB Modelling	55
5.5.1	FEA Modelling	55
5.5.2	CFD Modelling	55
5.5.3	Resource Cap and weeArchie HPC	59
5.5.4	Mesh Convergence	59
5.6	Iterative Results	60
5.6.1	Iteration 1 - Initial Design	60
5.6.2	Iteration 2 - Basic Shape Adjustments	63
5.6.3	Iteration 3 - Aerofoil Alterations	68
5.6.4	Iteration 4 - Wing Twist	72
5.6.5	Iteration 5 - Taper Ratio, Sweep and Winglet Addition	75
5.6.6	Results Overview and Discussion	77
5.6.7	Ribs and Spar Internal Structure	79
5.6.8	Wing Structure Topology Optimisation	83
5.6.9	Fuselage Structure	85
5.7	Stability and control	88
5.7.1	Static Stability	88
5.7.2	Static Margin	89
5.7.3	Control Surfaces and Dynamic stability	90
5.8	Interior Layout	91
5.8.1	Cabin Layout Methodology	92
5.8.2	Consolidated Layout Design	94
5.8.3	Evacuation Considerations	96
5.8.4	Cargo-Passenger Configuration	100
6	Propulsion	106
6.1	In the context of the Global Design	106
6.1.1	Inter-dependencies	106
6.1.2	Inputs and Outputs	106
6.1.3	Key Performance Indicators	108
6.2	Literature Review	109
6.2.1	Weight Estimation	109
6.2.2	Engine Placement and Configuration	109
6.2.3	Alternative Engines and Fuel Sources	111
6.2.4	Experimental Propulsive Technologies	112
6.3	Weight Estimation and Propulsion Parameters	114
6.4	Engine Selection Process	117

7 Materials	119
7.1 In the context of the Global Design	119
7.1.1 Inter-dependencies	119
7.1.2 Inputs and Outputs	119
7.1.3 Key Performance Indicators	119
7.2 Literature Review	120
7.3 Methodology	122
7.4 Results	123
7.4.1 Wing Spars	123
7.4.2 Fuselage Frame	125
7.4.3 Fuselage Shell	126
7.4.4 Wing Skin	128
8 Economics and Environmental Impacts	131
8.1 In the Context of the Global Design	132
8.1.1 Inter-dependencies	132
8.1.2 Inputs and Outputs	132
8.1.3 Key Performance Indicators	133
8.2 Development Cost	133
8.2.1 Methodology	133
8.2.2 Results	136
8.3 Direct Operating Cost	140
8.3.1 Methodology	140
8.3.2 Results	144
8.4 Results Interpretation	148
8.4.1 Development Cost	148
8.4.2 Direct Operating Cost	148
9 Discussion	150
9.1 Soft Systems Methodology	150
9.2 The BWB Concept	150
9.2.1 Technical Feasibility	150
9.2.2 Practical Feasibility	152
9.2.3 Economic Feasibility	152
9.2.4 Environmental Feasibility	152
10 Conclusion	154
11 Future Work and Perspectives	156
11.1 Aerodynamics	156
11.2 Structure and Stability	156
11.3 Interior Layout	156

11.4 Propulsion	157
11.5 Materials	157
11.6 Economics	158
12 Appendices	166
12.1 Appendix A : Semester 1 Gantt Chart	166
12.2 Appendix B : Semester 2 Gantt Chart	167
12.3 Appendix C : ONERA M6 Mesh Characteristics	168
12.4 Appendix D: Regulations of Predominant Importance of Regarding Transport of Cargo in Passenger Compartment	169
12.5 Appendix E : Malaysia Airlines Interior Layout Drawing	171
12.6 Appendix F : A380 Cargo Loading Calculations	172
12.7 Appendix G : BWB Cargo Loading Calculations	176
12.8 Appendix H : MATLAB Script for Weight Estimation	179
12.9 Appendix I: Development Cost Breakdown	193
12.10 Appendix J(a) : DOC per nm-pax Comparison for 4-Engine	194
12.11 Appendix J(b) : DOC per nm-pax Comparison for 3 and 4-Engine	195
12.12 Appendix K: Evacuation simulation	196
12.13 Appendix L: Required material operating temperature	210

Nomenclature

$\frac{T}{W}$	Thrust-to-weight ratio	
$\frac{W}{S}$	Wing loading	N/m^2
γ	Ratio of specific heat of air	
λ_{aft}	Aft taper ratio	
ρ	Air density	kg/m^3
<i>AMC</i>	Acceptable Means of Compliance	
<i>AOA</i>	Angle of attack	<i>degree</i>
<i>APU</i>	Auxiliary power unit	
<i>BPR</i>	Engine bypass ratio	
<i>BWB</i>	Blended wing body	
<i>c.g</i>	Centre of Gravity	
C_D	Drag Coefficient	
C_L	Lift coefficient	
C_{AC}	Aircraft acquisition cost	\$
$C_{d_{max}}$	Maximum drag coefficient	
$C_{d_{min}}$	Minimum drag coefficient	
$C_{L_{max}}$	Maximum lift coefficient	
<i>CAD</i>	Computer aided design	
<i>CFD</i>	Computational fluid dynamics	
<i>CFRP</i>	Carbon fibre reinforced polymer	
<i>CPI</i>	Consumer Price Index	
<i>CS – 25</i>	Certification Specifications for Large Aircraft	
<i>DOC</i>	Direct Operating Cost	
<i>EASA</i>	European Aviation Safety Agency	
<i>ENP</i>	Engine price	\$

f_{comp}	Composite fraction in the airframe	
FEA	Finite element analysis	
h	Maximum cargo height	m
HAS	Human Activity Systems	
IOC	Indirect Operating Cost	
l	Loading area length	m
L/D	Lift to Drag Ratio	
l_{lat}	Total loading area length (including access)	m
M	Mach number	
m_{AA}	Weight of aircraft air-conditioning and anti-icing	kg
m_{aft}	Weight of the aft of the aircraft	kg
m_{APU}	Weight of aircraft APU	kg
m_{cabin}	Weight of aircraft cabin	kg
M_{cruise}	Cruise Mach number	
m_{elec}	Weight of aircraft electicals and electronics	kg
$m_{eng-dry}$	Engine dry weight	kg
m_{fuel}	Weight of fuel	kg
m_{furn}	Weight of aircraft furnishings	kg
m_{gear}	Weight of aircraft landing gear	kg
m_{HP}	Weight of aircraft hydraulics and pneumatics	kg
m_{opi}	Weight of aircraft operating items	kg
$m_{payload}$	Weight of payload	kg
m_{prop}	Weight of propulsion systems	kg
m_{sc}	Weight of aircraft surface controls	kg
Ma_c	Cruising Mach number	
MAC	Mean Aerodynamic Chord	m

MAE	Mechanical & Aerospace Engineering	
MDO	Multi-Disciplinary Optimisation	
MSP	Aircraft list price	\$
$MTOW$	Maximum take-off weight	kg
$MUSCL$	Monotonic Upstream-centred Scheme for Conservation Laws	
MWE	Aircraft empty weight	kg
N	Number of units produced over 5 years	
n_c	Number of compressor stages	
N_{la}	Number of loading areas	
$N_{passengers}$	Number of passengers	
N_{pp}	Number of engines	
NP	Neutral Point	
OPR	Overall pressure ratio	
P_{BORROW}	Loan amount	\$
pax	Number of passenger	
Q_{FLGT}	Flight time per year	hr
R	Air gas constant	kJ/kgK
R_{labour}	Labour rate	$\$/hr$
S	Wing area	m^2
S_{aft}	Aircraft aft area	m^2
S_{cabin}	Aircraft cabin area	m^2
S_{ref}	Wetted area	m^2
S_{sc}	Surface controls area	m^2
S_{wing}	Wing area	m^2
SAF	Sustainable Aviation Fuel	
SFC	Specific fuel consumption	kg/kNs

SSM	Soft Systems Methodology	
T	Engine thrust	N
t	Flight time	s
T_a	Air temperature	K
T_c	Cruise thrust	kN
$t_{available}$	Aircraft available time per year	hr
t_{block}	Flight block time	hr
T_{sl}	Sealevel Engine thrust	N
TAT	Turnaround Time	hr
TAW	Tube-and-wing	
TOW	Take-off weight	kg
V	Maximum cargo volume	m^3
V_H	Maximum level airspeed	$KTAS$
V_{cruise}	Cruise speed	m/s
$V_{lift-off}$	Lift-off speed	m/s
V_{sect}	Total section cargo volume	m^3
V_{stall}	Stall speed	m/s
w	Section width	m
$W_{airframe}$	Airframe weight	lbf
W_{ENG}	Engine weight	kg

Table of Figures

1	Project Overview.	19
2	London to Shanghai flight path [7].	22
3	Group hierarchical structure.	24
4	The 7 Step Model diagram [10].	32
5	Ease-Benefit matrix [10].	34
6	Overview of the simplified, more fluid SSM process [8].	34
7	Project Rich Picture.	36
8	Project Activity Model.	37
9	Project ease-benefit matrix.	38
10	Design Roadmap.	41
11	Constraints diagram produced based on the counterpart aircraft A380.	46
12	ONERA M6 Pressure Plot Results.	54
13	BWB Mesh: Fluid Domain.	56
14	BWB Body Mesh.	56
15	BWB Wingtip Mesh Refinement.	57
16	BWB Trailing Vortex Refinement.	57
17	BWB Mesh $y+$	58
18	Render of initial design 3D CAD model.	61
19	CFD pressure contours for base design at $Ma = 0.84$ and $AOA = 3^\circ$	61
20	FEA stress analysis of initial design wing.	62
21	Base Design.	63
22	Wing shapes investigated.	64
23	Boundary conditions for FEA analysis.	65
24	Ansys FEA Von Mises stress for base wing design showing with maximum stress between middle and tip wing sections.	65
25	Ansys FEA Von Mises stress for angular sweep wing design with maximum stress at root to main wing transition.	66
26	Mk.2 CFD pressure coefficient.	67
27	Aerofoil Comparison: yellow - SC(2)-0714; dark blue - Eppler 403; green - Eppler 417 and light blue - Whitcomb.	68
28	Eppler 417 aerofoil design.	69
29	Ansys FEA Von Mises stress for smooth sweep Eppler wing design with maximum stress occurring as in Figure 25 to a lesser magnitude.	69
30	Plot of Lift/Drag vs AOA for the Eppler wing geometry at $Ma = 0.84$	70
31	Pressure contours on Eppler wing geometry at $Ma = 0.84$ and $AOA = 2^\circ$	71
32	Mk.3 Pressure Contours.	71
33	Diagram depicting wash in and washout on twisted wings [30].	73
34	3D CAD Model of twisted wing.	73
35	Mk.4 Pressure Contours.	74

36	Mk.5 Pressure Contours.	77
37	L/D vs Mach No. for all design iterations.	78
38	Render of initial rib and spar structure without skin.	79
39	FEA depicting the gross deformation occurring within the root.	81
40	Improved structure with 0.16m thick ribs and extra reinforcing ribs around root-main wing transition.	81
41	Logarithmic stress contour with skin stress below 100MPa.	82
42	Internal structure stress contour with maximum stress at spar and last rib.	82
43	Render of current iteration of internal structure featuring mass saving cut outs.	83
44	Output of Solid works Topology optimisation tool used as design reference.	84
45	FEA stress contours results for the iteration 11 design.	84
46	Sketch illustrating the increase of differential pressure as altitude is increased.	85
47	Structural concepts for BWB designs [27].	86
48	3D CAD Model of initial fuselage structure section design.	87
49	3D CAD model of fuselage section iteration 6 showing design improvements.	87
50	FEA stress Analysis of iteration 12.	88
51	Locations of point masses on aircraft in longitudinal direction.	89
52	Example control surface layouts from different projects on similarly sized BWB concepts.	91
53	Cabin floor placement.	92
54	Initial layout design.	93
55	Cabin layout - passenger.	94
56	Cabin layout - cargo.	95
57	A380 validation simulation. Red dots indicate individuals. Blue areas represent seating and orange areas represent emergency exits.	98
58	BWB single-class simulation. Worst-case: all aft exits unavailable. t = 50 seconds. Red dots indicate individuals. Blue areas represent seating and orange areas represent emergency exits.	99
59	Colour coded A380 layout for seating formations considered.	102
60	Colour coded BWB layout for seating formations considered [48].	104
61	Propulsion Iteration Cycle.	108
62	Airbus ZEROe concept range [58].	112
63	Ashby's method of materials selection. Adapted from [75].	121
64	Materials selection chart for wing spars [71].	124
65	Materials selection chart for fuselage shell [71].	128
66	Materials selection chart for wing skin [71].	129
67	East-Lake production cost flow diagram, derived from equations [18].	134
68	Minimum list price per unit for different produced units in 5-year period.	137
69	Development cost distribution.	137
70	Production costs and revenue for break-even analysis.	139

71	Effects of production units in 5-year period on the number of sold aircraft for break-even.	139
72	Direct operating cost flow diagram, derived from equations [18].	141
73	Direct operating cost flow diagram using AEA method, derived from equations [83]	141
74	A380 DOC contribution for long haul flights at normal fuel price.	145
75	DOC contribution comparison for long haul flights at different fuel prices using the AEA model for BWB final design iteration.	145
76	DOC contribution comparison for short haul flights at different fuel prices using the AEA model for BWB final design iteration.	145
77	DOC per nm-pax for different design iterations compared to A380 and B747. .	147
78	DOC per nm-pax for the BWB 3-engine configuration for the final design iteration for long haul flights compared to the BWB 4-engine configuration, A380 and B747.	147
79	ONERA M6 Meshing Characteristics	168
80	DOC per nm-pax for BWB 4-engine configurations through different design iterations at various fuel price scenarios for long haul and short haul flights compared to A380 and B747.	194
81	DOC per nm-pax for the BWB 3-engine configuration for the final design iteration at various fuel price scenarios for long haul and short haul flights compared to the BWB 4-engine configuration, A380 and B747.	195

Table of Tables

1	Team member roles.	23
2	Technical roles descriptions.	25
3	Myers-Briggs results.	26
4	Management roles descriptions.	27
5	Summary of the key differences between soft and hard approaches [9].	31
6	KPIs and dependencies.	43
7	KPIs and feasibility criteria.	44
8	Initial input parameters for constraint diagram construction [19].	46
9	ONERA M6 Experimental Flow Parameters [28].	52
10	ONERA M6 Meshing Parameters.	53
11	Simulation Re Numbers.	58
12	Base Design Mesh Convergence Study.	59
13	Grid Independence study for internal structure using tetrahedral elements. .	60
14	Base Design L/D for Varying Mach No.	62
15	Lifting surface area and subsequent wing loading of each design.	64
16	Stress and deflection results of wing shapes under loading.	66
17	Base Design L/D for Varying Mach No.	67
18	FEA analysis results for smooth sweep Eppler wing.	70
19	Mk. 3 L/D for Varying Mach No.	72
20	Stress results for FEA analysis of initial design with different spar shapes. .	73
21	Mk4 L/D for Varying Mach No.	75
22	Stress results for FEA analysis of different wing modifications.	76
23	Mk. 5 L/D for Varying Mach No.	76
24	Grid Independence study for internal structure using tetrahedral elements. .	80
25	Stress results for FEA analysis of initial design with different spar shapes. .	80
26	Stress and deflection results for FEA analysis of iteration 6.	82
27	Stress and deflection results for FEA analysis of iterations 7-10.	83
28	Stress results comparison of manual optimisation vs using topology function.	84
29	Mass, stress and deflection results for FEA analysis of iterations 11 - 13. .	85
30	Stress results comparison between different iterations.	88
31	Point masses and their locations.	89
32	Typical seating dimensions and chosen dimensions, adapted from [34].	92
33	Typical lavatory count, adapted from [34].	93
34	Cargo container dimensions.	94
35	Passenger capacity comparison between A380 and BWB.	95
36	Cargo volume comparison between B747-8F and BWB.	96
37	Available cargo loading lengths for each section.	102
38	A380 loading area volumes.	103
39	BWB loading area volumes.	105

40	Propulsion parameters.	107
41	Weight component breakdown.	115
42	A380 performance values for comparison [54].	116
43	Thrust requirements for engine configurations.	117
44	Selected engine performance characteristics.	118
45	Explanation of each output from the translation stage. Adapted from [75]. .	122
46	Translation for wing spars.	123
47	Assessment of supporting documentation for possible materials families. .	125
48	Translation for fuselage frame.	126
49	Translation for fuselage skin.	127
50	Translation for wing skin.	129
51	Development Labour Cost. [18]	134
52	Other Development Costs. [18]	135
53	Total Development Cost. [18]	135
54	Used parameters for A380 development cost analysis.	136
55	Minimum list price for break-even assuming 67 units produced in a 5-year period.	137
56	Breakdown development costs for each analysed aircraft using the Eastlake model.	138
57	Number of units required to be sold for break-even for different listing prices. .	138
58	DOC - Eastlake model, adapted from [18].	142
59	Available hours per year and corresponding Turnaround Time [83].	142
60	DOC - AEA, adapted from [83] and [85].	143
61	Range and block time for long and short haul flights.	144
62	Fuel prices. [83]	144
63	A380 DOC per nm-pax for short and long haul flights at normal fuel price using the Eastlake and AEA models, and compared to the AEA results from literature [83].	144
64	DOC per nm-pax (\$) for long haul flight.	146
65	DOC per nm-pax (\$) for short haul flight.	146
66	CO_2 emissions for long haul flight.	147
67	CO_2 emissions for short haul flight.	148
68	Breakdown development costs for each analysed aircraft using the Eastlake model.	193

1 Introduction

Commercial aviation is a huge industry throughout the world and in 2019, airlines throughout the world had a combined revenue of around \$872 Billion [1] US Dollars over millions of flights per year. From its inception in 1968 the ‘tube and wing’, widely seen throughout the world today, has been extensively optimised for use as the preferred commercial aircraft design. Progression in commercial aviation has somewhat slowed over the past few decades. With the emerging goal of carbon neutrality by 2050 across the globe, aviation sectors have shifted towards cleaner technology solutions [1], which encouraged introduction of revolutionary technologies such as Blended Wing Body (BWB) aircraft.

Not to be confused with flying wing aircraft, where there is no distinct fuselage or wing structures, a BWB aircraft is one in which the wing and body structures are blended together without a clear dividing line [2]. Contrary to popular belief, the BWB concept is not a new notion. The first theoretical idea developed regarding a BWB design was in the early 1920s by Nicolas Woyevodovsky, which developed to take the form of the Westland Dreadnought built by the British Aeroplane Company Limited in 1924 [3]. However, it stalled and crashed on its initial flight, causing severe injuries to the pilot, thus the idea was cancelled with no further aircraft manufactured. Besides a brief reappearance in the 1940s with experimental aircraft from Miles (M.26 and M.30) and McDonnell (XP-67), with which were multiple disadvantages including engine problems, the concept lay largely forgotten until it came to the interest of NASA and Boeing in the 1990s. X-48B models developed by NASA and Boeing were tested in wind tunnels as early as 2006 at the Langley Research Centre with further testing continuing from 2007-8 at the Dryden Flight Research Centre [4]. Building upon the knowledge gained, a 6 percent scale model with a 13 foot wingspan was tested in the Langley Research centre in 2016 to compare with data retrieved at the Ames Research Centre, with the designated next step to be tests with a manned demonstrator [5]. Since publication of these intentions, Airbus have released a BWB concept of their own, dubbed the MAVERIC, which excelled from a simple sketch to tested demonstrator in just three years [6]. Airbus predict the MAVERIC would allow a 20% fuel saving in comparison to conventional aircraft utilising similar engines, and hope to revolutionise the industry with their model.

1.1 Global Aim and Department Objectives

The aim of the project was to investigate the feasibility of a BWB aircraft for long haul flights from London to Shanghai by analysing the technical performances as well as economics of such concept through an iterative design process. Soft Systems Methodology (SSM) was employed throughout the design framework to better understand the inter-dependencies between various design parameters and choices, considering the multi-disciplinary nature of this project.

From the comparison of performance to current similar aircraft, and identification of advantages and disadvantages of the design, a further objective was to achieve successful performance development, making the configuration more competitive with current aircraft, through iterative design processes.

In terms of the aims of the Aerodynamics department, the main aim was to iterate a BWB aerodynamic model in order to assess its performance against current conventional aircraft. Through CFD analysis of the BWB airframe, performance this performance could be measured. This would be completed in conjunction with other departments to ensure any design decision made in the Aerodynamics department would not negatively impact the performance of the others, and where they may do so, assess the trade-off with the other department to deliver a compromise and feasible solution.

The structural analysis undertaken was aimed to assess whether the design and aerodynamic performance were structurally feasible. Initially, the aircraft was modelled as a solid body, assessing different wing designs for structural characteristics in tandem with their aerodynamic performance, before taking the most optimum design forward to be modelled as a rib and spar structure, optimised to create an efficient design. Thereafter, creating an internal structure concept for the fuselage to allow for more accurate weight estimations and basic stability analysis. The cabin seating layout was constructed for both 1-class and 2-class configurations for determining the maximum passenger capacity to inform the Direct Operating Cost (DOC). The available cargo volume for the cargo-passenger configuration was calculated based on the seating layout; the maximum cargo capacity when configured as a freighter was estimated.

Propulsion requirements were outlined through comparison to A380 performance and through an iterative cycle based on basic thrust equations. A weight estimation method was also constructed in order to provide a more accurate estimate to be used in design calculations. Subsequently, engine selection for the required calculated parameters was undertaken and the benefits of various engines placements were explored. Brief consideration to the use of alternative fuel sources was additionally given.

In addition to structural design and analysis of the BWB, a preliminary materials selection study using Ashby's method was undertaken for a limited number of key structural elements. These included the wing spars, wing skin, fuselage frame, and inner fuselage skin. Performing materials selection aimed to ensure the structural design was feasible in terms of existing aerospace materials.

Based on the aircraft characteristics of each design iteration, the development cost and minimum number of sold aircraft units for break-even were determined using the Eastlake

model, the DOC per nautical mile per passenger for both long and short haul flights at low, normal, and high fuel prices was investigated using the AEA model. Both the development cost and DOC results were compared to the counterpart aircraft A380 in order to determine the economic viability of the final BWB design.

2 Project Management

2.1 Project Overview

As a starting point for the management of the project it was imperative to define the baseline motivations and goals, in order to assure all of the relevant parties had consistent knowledge. Figure 1 details the key characteristics of the project outline agreed upon by the team.

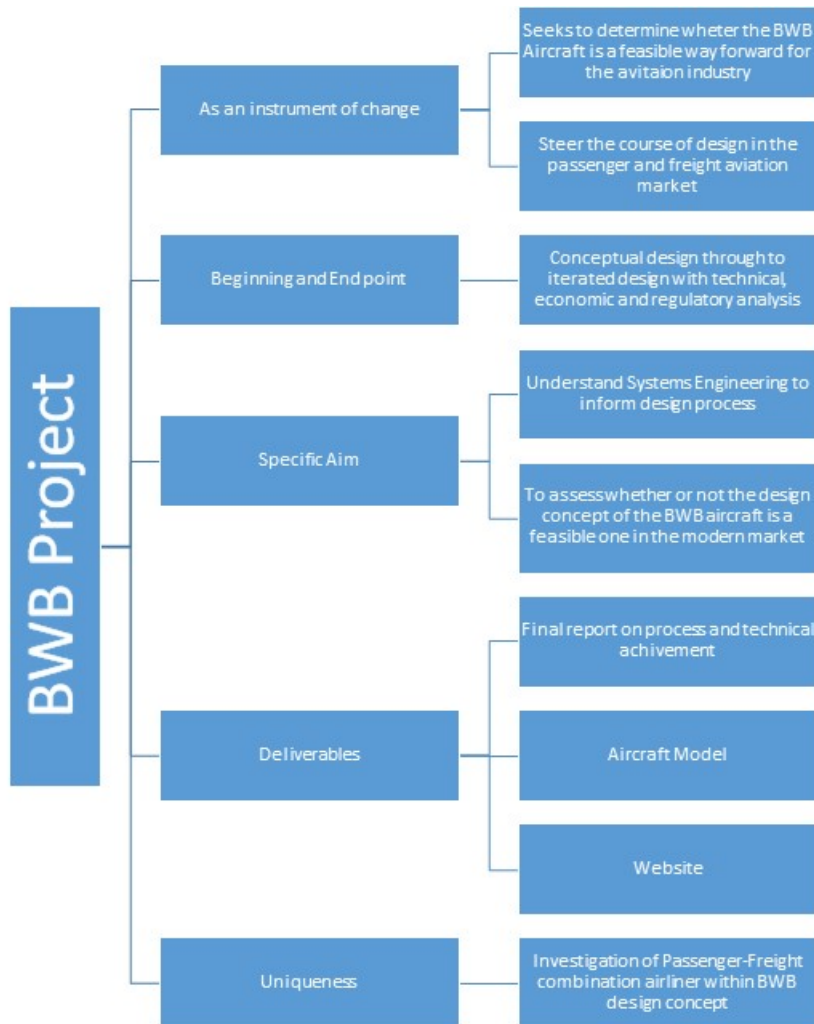


Figure 1: Project Overview.

2.2 Project Scope

By the complex nature of the project itself, along with the time and resource constraints set by the project brief, it was also important to define the scope of the project. This would allow for the setting of achievable goals.

The aim of the project was to be achieved by conducting an aerodynamic study, structural analysis, propulsion performance analysis and economic study, while ensuring all aspects of the operation of the aircraft met industrial legislation.

Aspects deemed within the scope of the project, and which will be exhibited, include:

- Basic preliminary aircraft design
- Aerodynamic CFD (Computational Fluid Dynamics)
- Structural integrity FEA (Finite Element Analysis) study
- Propulsion selection investigation
- Industrial legislation investigation
- Design comparison with conventional aircraft
- Manually optimised aircraft design
- Basic internal layout and analysis
- Material consideration
- Economic study

Aspects deemed out of the scope of the project include:

- Detailed aircraft design
- Aircraft systems investigation
- Manufacturing procedures
- Consideration of configuration for alternative routes
- Detailed internal layout
- Material selection at components level

2.2.1 Project Phasing

The need for a systematic approach was further agreed upon by the team members, therefore a project phasing plan was determined with deadlines for interim deliverables and project milestones (see Gantt charts in Appendix A & B). The following phasing was established:

1. Initiation and Specification Phase

- Introductory meeting
- Project definition
- Literature review

2. Initial Design Phase

- Constraints diagram
- Determination of design loop
- Conceptual design and analysis

3. Preliminary Design Phase

- Further analysis
- Potential design changes
- Design review

4. Iterative Design Phase

- Manual optimisation of preliminary design
- Continual analysis
- Design review

5. Delivery Phase

- Finalisation of deliverables
- Presentation of deliverables

In applying this rigid structure, the team agreed that progress could be adequately monitored with clear, agreed upon deadlines and achievable targets.

2.2.2 Base Requirements

For the examination of the feasibility of the design for long haul flights, such as London to Shanghai, it had to be ensured that the aircraft would be able to cover such a distance and be of similar, if not increased, calibre of the aircraft already traversing the route.

The London to Shanghai flight path itself, exhibited in Figure 2, requires a range of 4966nm (9197km) [7], upon which the Airbus A380 is among the most prevalent aircraft and, as such, was used as a real world comparative. For qualification of the design to be classed as a BWB, there was an elementary stipulation of smooth blending between the fuselage and wing structures. In addition, a constraints diagram was constructed which informed the furthering of the design concepts and which will be detailed in Section 4.

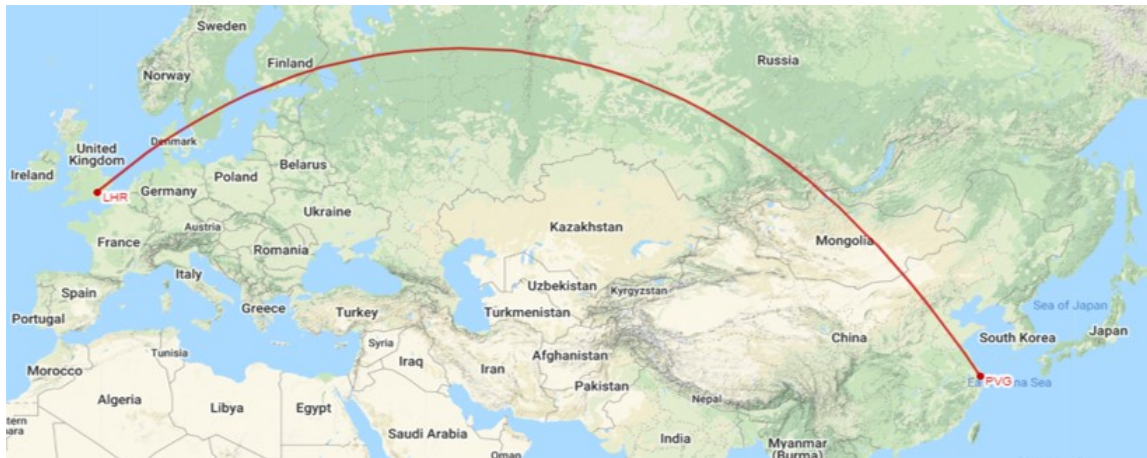


Figure 2: London to Shanghai flight path [7].

Regarding the project deliverables, these were categorized into three main outputs:

- Interim review
- Final review
- Website generation

The interim review consisted of the production of a 2500 word report detailing the work achieved to date and an overview of the management of the project, and a 15 minute presentation regarding the progress with a subsequent question and answer session. As can be seen in Appendix A, the majority of the design conception and intense simulations were to be completed prior to the interim report, with the second semester primarily reserved for iterative cycle progressions for design improvement and surrounding concerns.

The final review consisted of the production of a final report giving reflections upon the project management and overview of the technical achievements of the project, and 25 minute presentation regarding the project with a subsequent question and answer session.

Parallel to the work undertaken for the final review, a website was required to be generated, with independent hosting, showcasing the context of the project and the project achievements.

2.3 Working Structure

2.3.1 Roles & Responsibilities

Distribution of Roles

After collaboration to devise the project outline and general timeline, roles were designated within the team, based on person interests, aptitudes and psychometric testing. While each member would have a technical role working on the, predominantly, engineering based aspects of the project, it was also deemed necessary for members to take on a management based role to adequately cover the various aspects of conducting the project. Detailed below are the members respective roles (shown in Table 1) and the hierarchical structure (shown in Figure 3) by which the team would operate. Engineering roles were matched to group members based on previous experience; for example, Steven was matched with the CFD department for the project as he had previously completed a project studying winglet geometries in the cruise phase of flight.

Group Member	Technical Role	Management Role
Steven Munn	Aerodynamics	Group Leader
Lewis McBride	Structures & Stability	Technical Manager
Toni Barr	Legal Assessment & Propulsion	Regulatory Manager
Nian Liu	Economics	Web Designer
Craig Melrose	Propulsion & Stability	Client Relations
Aidan Wood	Materials & Practicality	Administrator & Web Designer

Table 1: Team member roles.

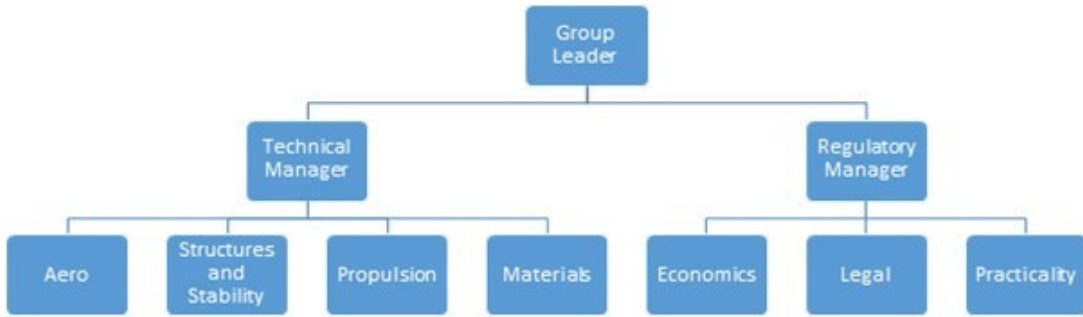


Figure 3: Group hierarchical structure.

Technical Roles

With team accord, it was agreed that the roles would naturally be somewhat fluid due to the inter-dependency of the aspects within each department, and it was established that the team are able offer assistance in any role to support the progression of the project. The primary responsibilities of each role is detailed in Table 2.

Role	Responsibility
Aerodynamics	Analysing the aerodynamic performance of any proposed design, looking for key values in terms of L/D.
Structures	Overcoming issues pertaining to the structural integrity of the aircraft and structural optimisation.
Stability	Ensuring static stability is within an adequate range to make a successful design.
Propulsion	Outlining propulsion requirements from baseline calculations, using these in the determination of the aircraft mass, engine selection and engine placement.
Materials	Responsible for optimum material selection for the structural elements of the aircraft.
Economics	Assess the economic viability of any such design in order to ascertain the benefits and drawbacks in financial terms, while drawing comparisons with current, conventional aircraft.
Legal Assessment	Ensure any legal requirements dictated by notified bodies of the aviation industry are met in the design, for its proposed application.

Table 2: Technical roles descriptions.

Management Roles

The management roles were less flexible due to their inherent nature, however effective teamwork and consistent communication from all team members was required in order for optimum performance in all roles. The primary responsibilities of each role are detailed in Table 4. In assignment of management roles, a Myers-Briggs Personality Test was undertaken by each group member in order to ascertain who would be suited to leadership roles. The results of the testing is displayed in Table 3. Steven and Lewis were matched with the Commander personality type denoting natural-born leaders who are decisive with a drive towards accomplishment, and thus were assigned Group Leader and Technical Project Manager respectively. Toni and Aidan were matched with the Architect personality type which is decisive, rational and enjoy working with facts and figures to expand their knowledge, and thus were assigned Regulatory Manager and Administrator. Further to this, due to

Aidan's extensive coding knowledge and experience, he was further given the role of Chief Web Designer. Nian was matched with the Defender personality type who are efficient hard-workers with careful attention to detail and analytical abilities, and thus was assigned the role of Web Designer to support Aidan in the large undertaking to ensure aesthetically pleasing and comprehensive website. Craig was matched with the Protagonist personality type who are passionate, charismatic and enjoy helping others, so was a natural fit for the role of Client Relations.

Team Member	Myers-Briggs Type
Steven Munn	ENTJ - Commander
Lewis McBride	ENTJ - Commander
Toni Barr	INTJ - Architect
Nian Liu	ISFJ - Defender
Craig Melrose	ENFJ - Protagonist
Aidan Wood	INTJ - Architect

Table 3: Myers-Briggs results.

Role	Responsibility
Group Leader	Responsible for general running of the group, ensuring deadlines were met and progress was being made, as well as creating meeting agendas and producing meeting notes.
Project Manager (Technical)	Responsible for ensuring progress in the technical department of the technical roles (Structures, Stability, Propulsion & Aerodynamics).
Project Manager (Regulatory)	Responsible for ensuring progress within the regulatory area of the technical roles (Legal, Economics & Practicality).
Administrator	Responsible for compiling work records and organisation of any completed work, organising meeting times within the group and ensuring effective group communication.
Client Relations	Responsible for interaction with the client (advisor) and output of the deliverables, with the help of the team members.
Web Designer	Responsible for the construction of the website to showcase the work of the team.

Table 4: Management roles descriptions.

2.3.2 Working Procedures

Managing Interactions

While a hierarchical structure had been devised, it was agreed within the team, that in terms of design and technical contribution, all members would be equal; therefore, it was determined at the outset that the team would establish regular round-table meetings in order to track individual and group progress, and have formal discussions about project aims and work presented to the supervisor. Furthermore, an emphasis was placed on the provision that there would be opportunity for informal conversation so as to enjoy working on a project with new colleagues and to learn from the diverse range of characters.

Communication with those involved in the project took the forms of:

- Twice weekly team meetings via Zoom involving all team members to discuss updates and areas to be raised with MAE (Mechanical & Aerospace Engineering) project supervisor at the next meeting.

- Twice weekly supervisor meetings via Zoom for Semester 1, decreasing to weekly supervisor meetings in Semester 2, involving all team members (where possible) and MAE supervisor to discuss the progress of the project, enquire about any areas of uncertainty and outline future steps.
- Slack project channel providing a constant communication link between all team members to clarify issues, share information and work collaboratively.
- Once a semester project management clinics via Zoom to ensure management was being optimised and provides an opportunity for help to facilitate improvement.

Conflict Resolution

Throughout the project, there were a couple of main conflicts that were encountered between departments within the team. The first main conflict encountered was within the Propulsion department. It was originally planned to conduct a fully manual optimisation and analysis of the propulsion system, including modelling the chosen engines themselves and integrating these on to the fuselage in Solidworks, then conducting various CFD investigations into the different configurations chosen for test. This would allow us to exactly pinpoint the correct propulsion system for the design through in-depth analysis. However, it was soon identified by the Propulsion department to be a very challenging and lengthy feat to complete as part of the project. It was agreed that the initially proposed plan for propulsion could be considered as a project in itself with the various different areas that would have to be accounted for, such as modelling of the engine internals, engine cycles, engine redundancy studies and the complex analysis of airflow through the engines. This in turn would negatively impact the other areas of the project and was hence deemed outwith the scope of the project.

The conflict was raised in a respective manner to the team through one of the many weekly meetings that was undertaken towards the end of the first semester and the issue was received well by all, whereby the group leader then suggested to democratically decide on the course of action regarding the propulsion research. The Propulsion department produced a revised plan in which there would no requirement to implement any CFD analysis of the engines integrated on to the fuselage, allowing the Propulsion department to focus on delivering a basic propulsion system for future optimisation, while helping out other areas of the project. This plan was well accepted and the team decided democratically to proceed along this route for the benefit of the project. Overall, the conflict was met with very little opposition and only a few early concerns between other members of the team. These concerns were resolved by presenting a clear and concise outline of how the change would aid the project as a whole and any opposing views were put to one side as the team continued on united.

Another major conflict encountered was the decision on whether to manually or autonomously optimise the design. The proposal of autonomous optimisation was presented to the team by two team members, who revealed interest in exploring the opportunity. The trade-off was that although it would require a significantly higher amount of initial work, optimisation would be quicker achieved, potentially outweighing the initial effort/complexity of implementation. The suggestion of autonomous optimisation was presented to the team by said members and was immediately met with some conflict on how beneficial the process would be to the project. Both arguments were posed to the team, again in a respectful manner. The consensus then was taken by the team that autonomously iterating the design was not necessary for a project of this level, despite the inevitable benefits in the long run. The design requirements could be excellently met through the manual iteration of the design as a group, therefore this was the chosen method. This naturally disheartened and disappointed said members, however communication and teamwork skills were utilised to overcome these conflicts and disappointments to deliver a high quality project over the course of the year.

Progress Reporting

Progress within different departments of the project were communicated to the entire team and advisor through the meeting structure outlined previously. Preceding the meetings with the advisor, the team would hold an independent meeting whereby each would create a PowerPoint presentation, where applicable, detailing their work which would be presented to the team. Such an activity allowed for the team to be fully knowledgeable on the progress to date, make enquiries regarding clarification or information which interlinked into their own department, and discuss what the future steps of the project would entail. Despite members having means of communication on general projects aspects and some members being required to work closely together on their work when highly dependent, these meetings allowed everyone to consolidate their overall knowledge of the project and provided ample opportunity for information sharing. These meetings additionally proved useful in creating an agenda for the following meeting with the advisor regarding topics of conversation and questions the team wished to ask.

Furthermore, when any member was dependent on information or assistance from other team member(s) before a team meeting, this was resolved through the use of the Slack channel or organisation of impromptu Zoom meetings between those necessary to involve. Any progress made or points of interest to be raised to the attention of the collective were included in the independent team meetings.

Taking on a similar form, team progress was presented to the advisor, not only utilising the previously mentioned PowerPoints, but through the exhibition of generated models and of any relevant documents created which would aid in the absorption of the new information. Aforesaid mediums were presented according to the agenda ensuring adequate time for re-

ports on all aspects of the project, questions from the team to the advisor and any queries from the supervisor to be addressed. During the meetings the advisor also included time to enquire to how the team were feeling with respect to the enjoyment of the project in addition to learning, how the group dynamic was working and for some informal discussion to build a mutual bond. Having made note of any recommendations and answers provided by the supervisor, quick recap team only meetings followed which allowed for summation of the next steps of the project and delegations of tasks and internal deadlines.

Interim Review

The feedback from the interim review proved highly beneficial for the future progress of the project, especially towards the final review, as it allowed understanding of how the project presentation, management and team interaction were perceived by an unrelated outside body. The brevity of the feedback initially caused some confusion as to what improvements could be applied, however further expansion was given after a request for supplementary clarification. From the feedback, the main areas of improvement identified were:

- Clear exhibition of the logical stages of the project and detailed iterative loops which accounts for areas interactions, supplemented with comments
- Further details regarding implementation of project management techniques and/or methods
- Increased transparency regarding the team interactions and dynamics to present how individual progress informed the complete progress of the team
- Clarification on the manner of optimisation used and what would deem the design feasible in the opinion of the team

After reflection of the feedback on both a team level and in conjunction with the advisor, it was concluded that care would be taken to address the aforementioned points in the final review. In order to account for this, it was kept in constant consideration that the future assessors would not be acquainted with the work undertaken, therefore all processes and interactions within the team should be detailed in a clear concise manner. A consensus was taken as to how to marry effectively the organisational aspect of the project with the technical achievements so that a complete understanding could be gained, whereby the internal structure of the team and stages of the project would be outlined previous to the display of technical work. Such a format would facilitate comprehension regarding the interaction of the team in the completion of the various stages of the project, with attention that all points for improvement were included.

2.4 Systems Engineering

2.4.1 Soft Systems Methodology (SSM)

Systems thinking was first introduced in the 1950s with the intention of providing a universal language and framework which would be able to express and solve any problems encountered in a diverse range of disciplines, encouraging the unity of science [8]. Problems encountered can generally be regarded as either a hard system or a soft system, where appropriate hard or soft approaches would be required to tackle them. At its essence, in hard systems engineering the problem world is systemic, whereas in soft systems engineering the process of enquiry is systemic. The predominant areas of contrasting perception are in the problem definition, nature of the organisation, model and the outcome.

Developed explanation of the differences in the previous areas are discussed in the Systems thinking article on the project website, however they can be encapsulated by the following statement: a hard approach is a regimented and detail-oriented process whereby a solution to an easily defined problem is achieved, where a soft approach is a fluid and adaptable process promoting consideration of human nature and the transience of perceived optimal solutions. The key differences are summarised in Table 5.

	Hard Approach	Soft Approach
Problem Definition	Straight-forward and singular	Multi-faceted and problematic
Organisation Nature	Constant, robotic	Must be negotiated and human nature accounted for
Model	Accurate representation of the real world	A way of generating debate and insight about the real world
Outcome	Product or recommendation	Progress achieved through learning

Table 5: Summary of the key differences between soft and hard approaches [9].

The 7 Step Model

The 7 Step model is as demonstrated in Figure 4 and can be seen to differentiate the steps regarding if they are to be considered in the real world or in the systems thinking world (i.e. how reality affects the problem and how human actions can influence how reality affects the

problem). The most important components of the 7 Step model are the Rich Picture, the conceptual model, formulating root definition(s) and the formal systems model [10]. An initial noticeable difference in comparison to other models is the use of round shapes and curved arrows used in hand drawn diagrams. Typically, the style conveys the fact that this is a working model which is relevant in the current climate and undermines the certainty of rigid shapes and straight arrows to give a more human and organic feel [8]. Additionally, the use of 7 steps is the optimal number dictated by Miller's work on human perception, whereby he determined that the human brain can cope with around 7 items or concepts at once [8].

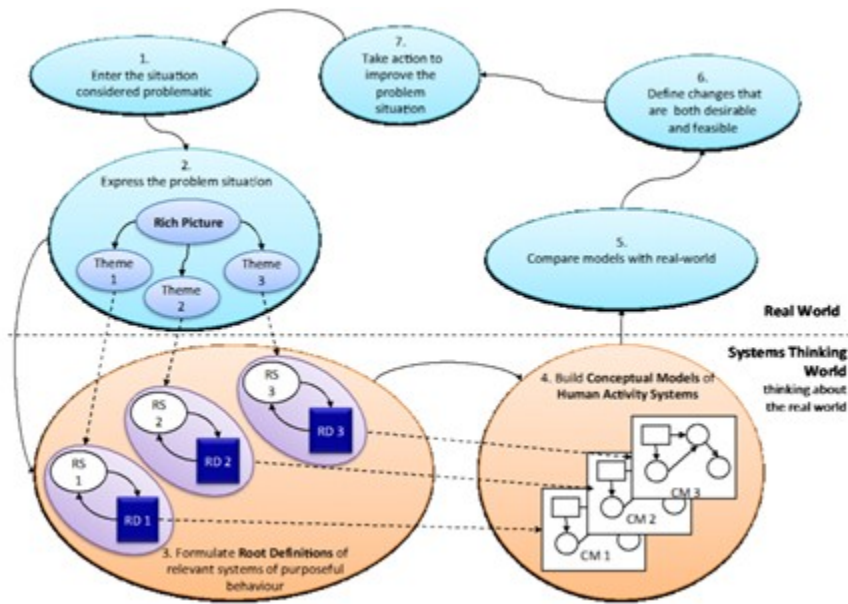


Figure 4: The 7 Step Model diagram [10].

Step 1: Appreciate the situation. Define the scope of the problem from all contexts and perspectives before undertaking research surrounding the problem such as key stakeholders, current performance, latest innovation and any issues.

Step 2: Express the situation. It is recommended by Checkland that this be achieved through the creation of a Rich Picture which encompasses various perceptions surrounding the problem. The Rich Picture is a pictorial representation of the problem with its surrounding factors which allows for better representation due to the increased density of information provided. It should allow for differences of interpretation, agreement on found interpretations and to identify the themes for the systems.

Step 3: Formulate root definitions. The root definition should capture the transformation performed by the system, as it is from this that all logical steps to achieve this transformation are derived.

Step 4: Build conceptual model of the human activity system. Produce a logical view of the activities necessary to achieve a system purpose. The conceptual model should focus on 7 ± 2 activities of roughly the same scale where each activity description begins with an imperative or command verb. An arrow should be used to display logical dependence and numbers can also be incorporated for traceability. Being developed for Human Activity Systems (HAS), monitoring and controlling must be introduced so that the variability in the performance from humans can be assessed. The conceptual model should be a system which can adapt and survive in a changing environment, hence, according to Checkland, “any [human activity] system model is thus a combination of an operational subsystem and a monitoring and control system” [10]. The monitoring and control approach was expressed as the 3 E’s:

- Effective: is the systems doing the right thing
- Efficacy: is the system producing the desired result
- Efficient: is the system using the minimum resources

From the 3 E’s, two levels of monitoring and control were deemed necessary where the first would regard the efficiency and efficacy of the operational activities, and the second would regard the effectiveness of the monitored and controlled operational activities.

Step 5: Compare the model with the real world. The comparison of the output of the model to the real world allows for discussion as to where the improvements could be made. Such improvements should be noted and then assessed in the next step.

Step 6: Define desirable and feasible changes. Generally, not all improvements can be made to a system due to restrictions in resources (people, time, funding etc.). Therefore, any improvement(s) should be vetted to see which are desirable in principle and feasible to implement [8]. This process could be completed from a discussion or through the establishment of a ease-benefit matrix, as shown in Figure 5. The size of the circle indicates the quantity of resources required. Upon the decision of improvement(s) to be implemented, a logical order and timescale should be decided.

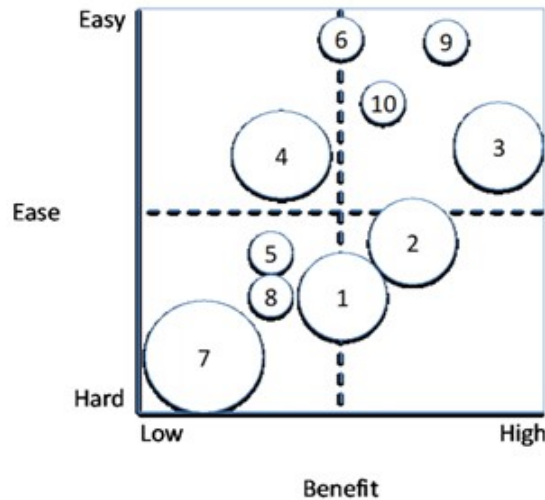


Figure 5: Ease-Benefit matrix [10].

Step 7: Take action to improve the problem. Implement the improvement(s) decided upon. This will provide new data for further improvement or issues, and so the process repeats.

The 4 Activities Model

With the concept progressing with experience, Checkland subsequently established the 4 Activities model, outlined in Figure 6), which is better suited to the flexible application of the method. The 4 Activities model essentially encapsulates all seven steps previously described in a broader and more relaxed format, which better facilitates the ever-changing nature of the problems being tackled.



Figure 6: Overview of the simplified, more fluid SSM process [8].

The 4 Activities are defined [8]:

1. Finding out about a problem situation including any cultural or political context (Step 1).
2. Formulating some relevant purposeful activity model(s) (Steps 2-4).
3. Debating the situation, using the model(s), seeking
 - (a) Changes which would improve the situation and are regarded as both desirable and feasible (Steps 5 & 6), and
 - (b) The accommodations between conflicting interests which will enable action-to-improve to be taken.
4. Taking action in the situation to bring about improvement (Step 7).

2.4.2 Application of 4 Activities Model

1. Finding out about a problem situation, including any cultural or political context.

The initial project description specified considering the feasibility of a BWB aircraft as an alternative to the conventional aircraft model for short and long haul commercial flights. After team discussion with the project supervisor regarding the project scope and specifications that would deem an aircraft feasible, the project aim and objectives were decided upon, as stated previously. Consequently, investigation into BWB aircrafts, and current large passenger aircraft performance was undertaken, in addition to the general topics of legislation and economic models.

2. Formulation of relevant purposeful activities models.

In order for a comprehensive overview, from which the root definitions and associated activities would be derived, a rich picture was created as seen in Figure 7.

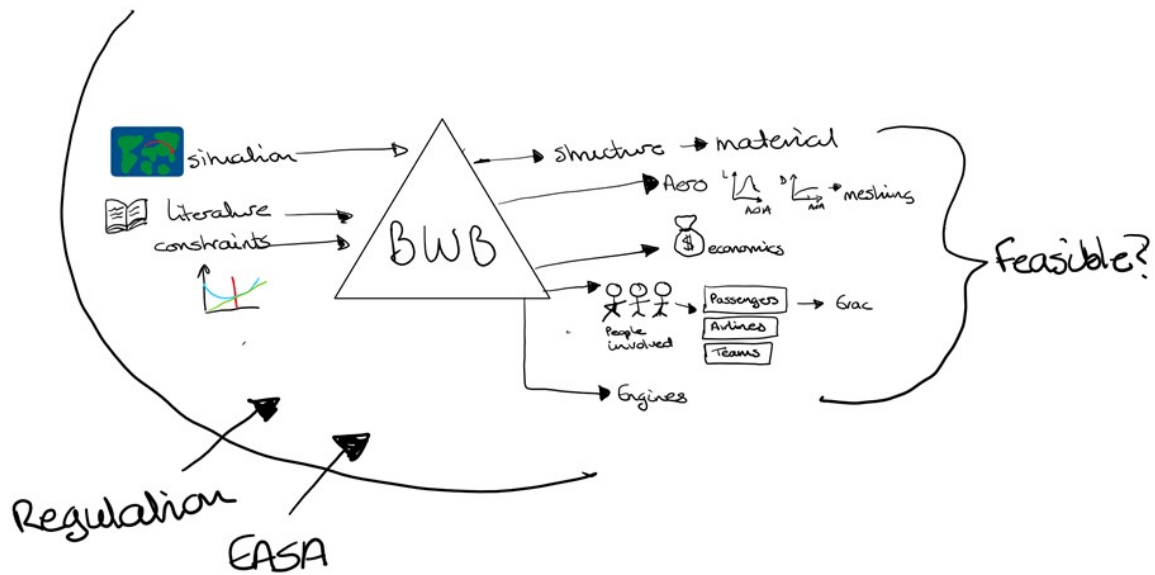


Figure 7: Project Rich Picture.

Resulting from the rich picture, the following root definition was decided upon:

Produce a feasible BWB concept which is comparable to current aircraft, with an element of exceedance in performance.

Following Miller's 7 ± 2 rule and Checkland's logical procedure for building activities models [8], the main project aspects were decided and the activities model constructed based on their dependencies, as seen in Figure 8.

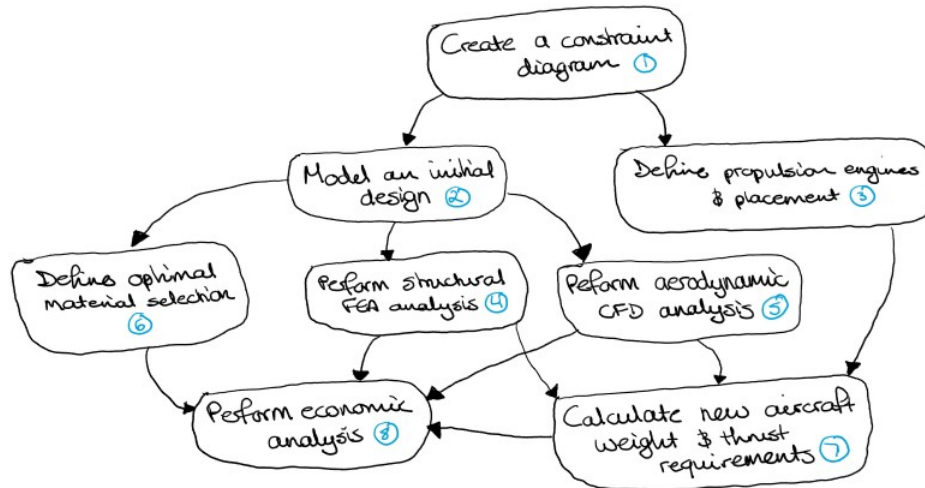


Figure 8: Project Activity Model.

Due to the complex multi-disciplinary nature and limited time of the project, the scope and limitations of the iterative activities were decided:

Model of designs: Limited to 5 iterations where the depth of the modelling was of the basic aerodynamic shape and sections of support structure. Detailed aspects such as landing gear, flaps etc were not included. The production, and any subsequent changes of the model, would be manually altered.

Aerodynamic CFD analysis: Limited to 5 iterations where the depth of the simulations was restricted to calculate values of lift and drag coefficients, used to calculate L/D, at a cruise design point.

Structural FEA analysis: Limited to 5 iterations where the depth of the simulations was restricted to calculate values of von Mises and principal stresses, and deflection. The simulations were limited to the effects weight and lift, with no fuel or emergency considerations.

Economic analysis: The scope of the analysis would be to provide a working overview of the conditions for break-even and operational costs, limited to the design iterations performed, utilising existing economic models used in the industry.

3. Debating the situation, using the models, seeking changes which are desirable and feasible.

The results of the initial design, after the first completion of the activities model, were ensured to meet the requirements of the constraints diagram and compared to the performance and specifications of an A380 aircraft. From the comparison, outlined below are the possible improvements considered:

1. Wing design optimisation - accounting for aerodynamic and structural issues
2. Novel engine design
3. New engine configuration
4. New material application
5. Alternative engine/fuel source
6. ANSYS or software optimisation of aerodynamic and structural performance
7. Addition of winglets
8. Ashby's Method for determining the optimum materials
9. Structural optimisation

To aid in the determination of the most desirable and feasible improvements, the possibilities above were entered into a ease-benefit matrix (see Figure 9)

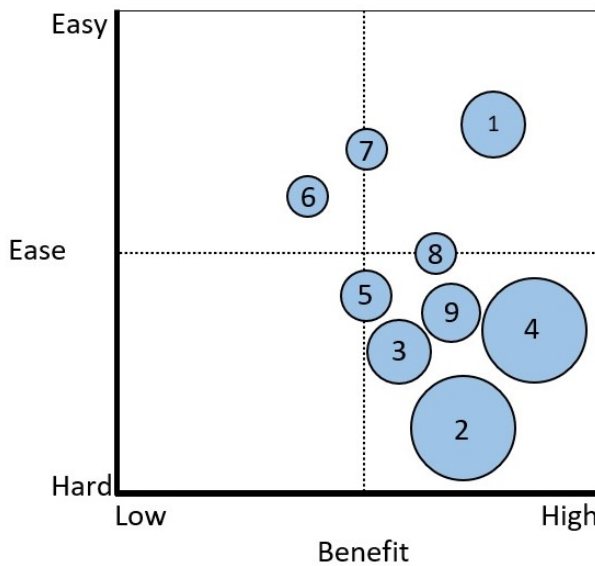


Figure 9: Project ease-benefit matrix.

The possibilities deemed to be unfeasible or undesirable were novel engine design, new engine configuration, new material application, alternative engine/fuel source and ANSYS or software optimisation. Both the novel engine design and new material application would take a large amount of resources and time due to the need for extensive testing and/or calculation required, in addition to the necessary research surrounding innovations in the areas. Pursuing these areas within the scope of the project would be futile as the energy required to produce meaningful work would require their own dedicated studies. Regarding a new engine configuration and alternative engine/fuel sources, these were additionally regarded as outwith the scope as discussed in Section 6. Finally, optimisation of the aircraft design through software was considered undesirable due to the associated costs, computational time and inability to account of the trade-offs described in the following paragraph.

Consideration was given as to the trade-offs involved with the improvement of individual aspects. The dominant areas of conflicted which had to be balanced were:

- Any changes in wing area would affect both the empty weight of the aircraft and the distribution of lift over the wings.
- Alterations of engine configuration or specification would affect the amount of thrust required for each engine and would have to be considered in weight and economic calculations.
- Optimisation of the aerodynamic performance could lead to increased structural issues. Conversely, structural changes could negatively impact aerodynamic performance.
- Optimisation of materials selection would have to be balanced with the considerations of material capabilities, cost, weight and manufacturability.
- The size of the aircraft would naturally affect the aerodynamic performance, propulsion requirements and structural capabilities, but also consideration would have to be given to the aircraft capacity and its affect on the economic analysis.

4. Taking action to bring about improvement

All changes made to the model are detailed in depth in further sections, however a brief overview of the improvements undertaken are:

- Manual optimisation of aerodynamic and structural performance through manual alterations to the wing design
- The addition of winglets to improve aerodynamic performance
- Use of Ashby's Method for consideration of optimal materials for use, with basic pursuit towards the use of composite in terms of percentage fraction of the aircraft
- Manual structural optimisation for a decrease in material to aid in aerodynamic performance and aircraft weight

2.4.3 Design Roadmap

While the SSM activity model provided a base for determining the key design architecture, it was deemed necessary to create a more comprehensive workflow in order to drive the overall process to arrive at a consistent solution. As such Figure 10 was developed detailing the various processes, design decision points and general structure for the subsequent design iteration points within the project, allowing the team to reach consensus regarding how the different departments interact with one another to produce an end design. This detailed visual figure allowed all members to easily recognise the importance of their work, who to contact for specific information and who to notify when their work would have consequential changes.

Once the process reaches the final decision point (denoted by the rhombus), the design was then assessed with regards to the requirement specifications detailed in Section 2.4.6 in order to determine whether or not a feasible design has been achieved. If not, the design then enters a process of fault analysis to determine where improvements may be made and where implemented ideas have been effective in achieving their goals.

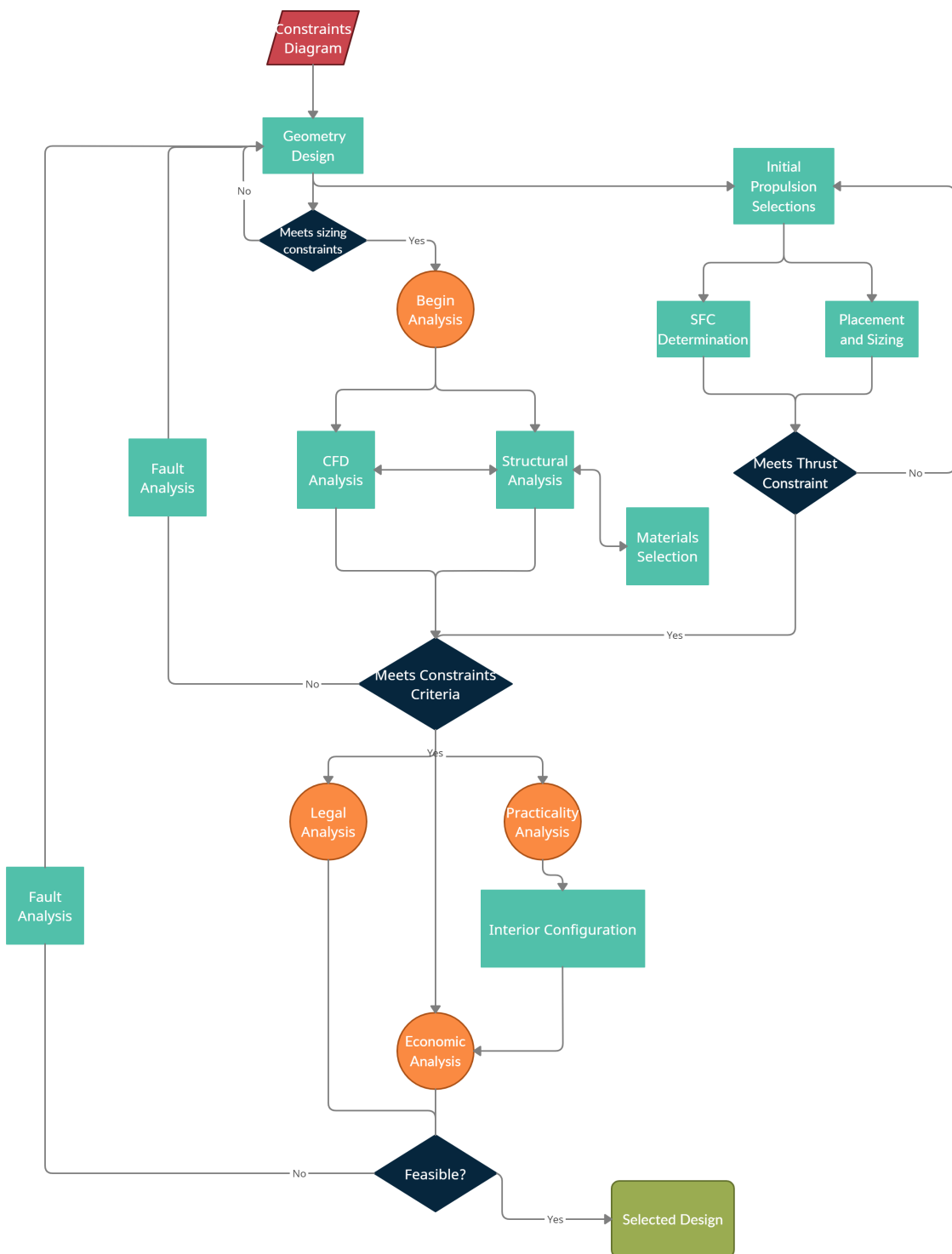


Figure 10: Design Roadmap.

2.4.4 Multi-Disciplinary Optimisation (MDO) Approach

As previously discussed, even within a relatively focused scope, the complexity and inter-reliance of sub-tasks within the overall design task demands the consideration of MDO approaches ab-initio. To ensure efficient team progress is achieved, an exploration of manual, human optimisation was compared with techniques available for automated optimisation processes.

Within the BWB literature, as well as general MDO literature surrounding similar problems, there are various approaches to optimising a design concept such as this. Some employ an approach based on engineering knowledge and the use of traditional aerospace design concepts and techniques; whereas, a component of the literature focuses primarily on shape optimisation in aerodynamics. While these have been shown to be effective design methodologies, such as in [11], [12], there is noted lack of expertise within the group surrounding this subject. The alternative approach is the implementation of manual design optimisation based on engineering judgement; which, while being potentially dangerous in the sense that poor design decisions could easily set back the project, allows the group to progress design iterations quickly without the need for further research and learning on out-of-scope materials.

Thus presenting the team with a key decision to be made in terms of the direction to be undertaken was both necessary and feasible for the progression of the project. Following discussions within the team itself and with the project supervisor, it was determined that a Manual Optimisation approach was both reasonable and sensible with respect to both the time constraints on the project and the required learning that would be necessary for several team members. Generally, it was the opinion of the team that a robust design based around sensible application of sound engineering knowledge, backed up by literature, was preferable to investing time and resources into an automatic MDO approach.

2.4.5 Design Stage Reviews

Identifying qualitative and quantitative objective functions to determine what constitutes a feasible preliminary aircraft design was vital to ensuring that the team members remained focused. As it was determined that the key competing systems were those currently available, a design would be feasible if it were to match and/or improve upon the performance of the real world comparison in the key performance indicators.

Key performance indicators (KPIs) were identified based on their relevance to the design activities and, in each case, were generally dependent on the key output of each area. Each KPI could then be compared with its real world comparative so as to assess the feasibility of the aircraft design, within the department itself and for the design as a whole. The KPIs and their dependencies are exhibited in Table 6.

Design Area	KPI	Informs	Reliant Upon
Aerodynamics	L/D	Structure & Stability	Propulsion
Structures	Maximum stresses	Materials	Aerodynamics
Stability	Static margin	Aerodynamics	Aerodynamics & Structures
Propulsion	Thrust output Weight SFC	Economics	Aerodynamics & Structures
Materials	Yield strength	Structures & Economics	Structures
Economics	Break-even model DOC	Aerodynamics, Structures, Propulsion & Materials	Aerodynamics, Structures, Propulsion & Materials

Table 6: KPIs and dependencies.

2.4.6 Requirements Definition

Having now identified the Key Performance Indicator for each design department, the next logical step was to establish a design requirement for each department, based on these indicators. The feasibility criteria for each KPI are demonstrated in Table 7.

	KPI	Criteria
Aerodynamics	L/D	\geq A380 L/D
Structures	Maximum stresses	$<$ Yield strength of chosen material
Stability	Static margin	Between 5% - 15%
Propulsion	Thrust	Meeting defined thrust requirement
	Weight	\leq A380 Weight
	SFC	Maximisation
Materials	Yield strength	$>$ Structural maximum stress
Economics	Break-even units	\leq A380 Break-even units
	DOC	\leq A380 DOC

Table 7: KPIs and feasibility criteria.

2.4.7 Fault Analysis - Non-Compliance to Requirements

Following a completion of a design loop within the roadmap, dependent on the outcome at a decision point, there was a need to perform a fault analysis so as to ascertain where the design was lacking and the specific areas where design modifications were required.

Based on an assessment of the above KPIs, with the requirements specifications, the overall design was analysed at a team level before further analysis on a departmental level. In departments where requirements were not met, for example if the L/D ratio was below the requirements, the task holder and any task owners informed by this department would meet to discuss the need for and ramifications of any changes to the design. The findings of said meetings would be reported back to the team to ensure clarity and understanding in the design before commencement of the next design iteration.

3 Literature Overview

As aforementioned, modern aircraft are typically configured with tube-and-wing (TAW) structure, where fuselage and wings are distinctively distinguished. While the wings are dedicated to lift generation with close to zero payload capability, the function of the fuselage is to carry passengers and cargo with no positive contribution in maintaining the structure in air. The conventional configuration has proved its success by constant evolution based on similar fundamental structures in the past century. However, despite the continuous focus being put on optimising the efficiency of conventional aircraft by large manufacturers Boeing and Airbus [13], the remaining capacity for sustainable development and improvement in aerodynamic efficiency is close to saturation with the current typical design [14].

During the pioneering study conducted by McDonnell, decision was made to remove the constraint of using hoop tension to maintain the structural integrity of pressurised cabin, which informed the common flatter characteristics of the fuselage in the later conceptual designs. [15]

BWB has attracted increasing number of researchers in recent decades due to the proven aerodynamic efficiency improvement of up to 25%, which historically would take over 40 years to realise for the conventional TAW structure [16]. Through a computer-based parameterisation study conducted by semi-automating design environment, Brown et al. concluded that with same top-level requirements defined by passenger capacity of between 150 and 400, BWB showed reduction in structural mass and drag, fuel consumption decreased by up to 30%. The advantage becomes more significant as aircraft size increases. However, it was remarked by the authors that certain design constraints such as stability and control were not implemented at the preliminary comparison stage, and the outcome was anticipated to change quantitatively in future comprehensive studies. [17]

Due to the lack of empirical data available for the conceptual BWB aircraft [16], current existing aircraft design programmes and models are very much restricted in the functionality of creating alternative configurations based on user input parameters [17]. Several studies have detailed their attempts in developing analytical and design modules specifically targeted at BWB sizing and layout based on performance requirements such as number of passengers, cargo weight, and range etc. According to the preliminary sizing resulted from such programme developed by Dommelen et al., BWB with 400 passengers demonstrated 44% lower wing loading compared to its counterpart jetliner A380-800, owing to its large wing surface area. [16]

4 Design Boundaries

4.1 Constraints Diagram

As mentioned previously, a constraint diagram was necessary for defining initial modelling parameters such as wing sizing. Constraint diagram plots as shown in Figure 11 were generated through equations that relate thrust-to-weight ratio and wing loading by rearranging various flight performance equations [18]. Initial parameters input to these equations as listed in Table 10 were taken from A380 specifications [19] as a preliminary guideline.

Parameters	Values
$C_{d_{min}}$	0.0265
C_l	1.5
$C_{d_{max}}$	1.7
Ma_c	0.85
Altitude	43100 ft
Maximum Banking Angle	45°
S_{wing}	843 m ²
Wingspan	79.8 m
MTOW	560000 kg
Sustained Rate of Climb	2500 fpm

Table 8: Initial input parameters for constraint diagram construction [19].

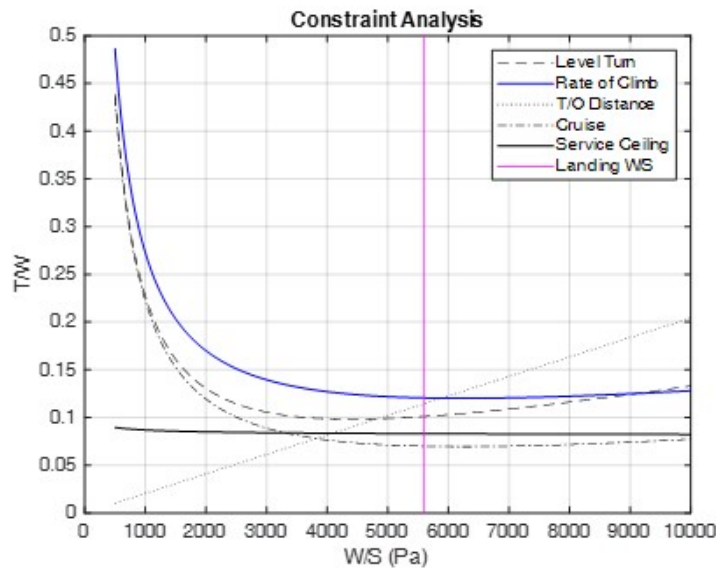


Figure 11: Constraints diagram produced based on the counterpart aircraft A380.

The acceptable thrust-to-weight ratio and wing loading combination can be selected from the region above constraint curves [18]. As shown in Figure 11, it is seen that the rate of climb and landing requirements were the major limitations for the proposed preliminary design, the optimum point of selection can be identified at the intersection between the two constraint curve and line at $W/S=5600\text{Pa}$ and $T/W=0.12$.

4.2 Regulations

In Europe, the governing body for aircraft worthiness and regulation is the European Aviation Safety Agency (EASA) and therefore, given the current location of the team, will be the regulations by which the aircraft conforms. EASA provide documents encompassing both a wide variety of air transport, from commercial aircraft to sailplanes to unmanned aircraft systems, and surrounding factors, from airworthiness to air traffic control to fines and penalties. Due to the size and purpose of the BWB aircraft, it must adhere to the criteria outlined in the Certification Specifications for Large Aeroplanes (CS-25) in order to be considered fit for purpose.

The CS-25 is a 617 page document comprising of two books: Book 1 - Airworthiness Code and Book 2 - Acceptable Means of Compliance (AMC). Due to the comprehensive nature of the specifications, much of the criteria within the document was outwith the scope of the project, given the rudimentary design process being undertaken. Regardless, knowledge and awareness of these are valuable, and select regulations would be imperative to the successful conclusion that the design would be feasible. Important criteria of note for the design process are [20]:

- The load distribution may not exceed
 - a. selected limits or
 - b. limits at which the structure is proven
- The maximum weight can not exceed
 - a. the highest weight selected by the applicant for particular conditions,
 - b. the highest weight at which the compliance with the acceptable structural loading and flight requirements is shown
- The minimum weight can not be less than
 - a. the lowest weight selected by the applicant,
 - b. the design minimum weight (the lowest weight that allows compliance with the structural loading conditions) or
 - c. the lowest weight at which compliance with each applicable flight requirement is shown

- The centre of gravity may not lie beyond
 - a. the extremes selected by the applicant,
 - b. the extremes within which the structure is proven or
 - c. the extremes within which the compliance with applicable flight requirements is shown
- Take-off climb may not be less than 1.2% for two engines, 1.5% for 3 engines or 1.7% for 4 engines
- A factor of safety of 1.5 must be applied to the limit loads

Further criteria regarding the number of cabin crew, emergency exit configurations, etc are additionally applicable to the design, but will be mentioned when of relevance in further sections.

5 The Design Process

5.1 Aerodynamics and Structures

A naturally key element of the monolithic BWB design process is the aerodynamic performance of the aircraft's structure. As an important component of the Breguet range equation, at the preliminary design stage this can be condensed fairly well to one key parameter, the L/D of the aircraft in the cruise phase of flight. This section will detail the process of obtaining this aerodynamic parameter, and the factors affecting it, for different design iterations as the global design progressed through the design road-map. As a result of their intrinsic inter-dependence, Aerodynamics and Structures may be treated as a department comprised of 2 sub-departments; this is mostly owed to the fact that any change to the aerodynamic geometry of the external surface has a direct impact on the structural aspect of the design and visa-versa, in particular alterations to wing structures must be ratified by both departments in order for design changes to be made. Overall, the Aerodynamics and Structures represent a large proportion of the work done on the project and the following section will detail this, working through each design iteration.

5.2 In the context of the Global Design

As noted above, while the Aerodynamic and/or Structural considerations of the BWB concept can and have stood alone as a project in and of itself in the literature, it is important to take the design decisions and design choices into the context of the global systems design process. In order to avoid the inconsistencies and incompatibilities that are risked when dividing the project into somewhat discrete sections, the group sought to seek the desired design consistency through defining and working to inter-dependencies between each section.

5.2.1 Inter-dependencies

Due to the nature of the design task, there exist many inter-dependencies within each section of the project. Within the Aerodynamics department, there are natural dependencies on the following departments:

- Structures: as previously noted, it informs the allowable wing geometries lifting surfaces and in general the allowable "shape" of the design.
- Propulsion: as it determines the input thrust and achievable Mach no.
- Economics: as it determines whether or not the aerodynamics performance represents an economically reasonable design.

Taking these three dependencies allowed the aerodynamics to be appropriately informed when making any design decisions. Taking an example, when altering the planform shape

of the wing to optimise for L/D, it was important to recognise the impact of this on the Structural aspect of the design and consult the task holder. In this case, in conjunction with the Structures department, the increase in area was modelled in an FEA analysis before implementing it into the more time and computationally costly CFD analysis. If the change was ratified, the analysis would then be tested in terms of aerodynamics.

Within the structural analysis the natural inter-dependencies are as follows :

- Aerodynamics: Structural design has a direct impact on the aerodynamics of the aircraft especially when considering the mass and shape of parts such as the wings.
- Materials: greatly influences the design of structures imposing hard limits to the design in terms of material limitations such as material yield strength.
- Economics: the mass and complexity of the structures have a direct impact on the economic feasibility of the design with less optimised structures requiring significantly larger quantities of material.

With these dependencies, the structures could be designed to satisfy all of these inter-dependent aspects. With the main concern of the structures initially being to ensure they allowed high aerodynamic performance within the limits of the designs being informed by materials selection. Once the design satisfied the aerodynamic targets, optimisation work could be undertaken to achieve a design that was economically feasible.

5.2.2 Inputs and Outputs

The first key design input for the Aerodynamics and Structures component, as with the majority of design fields within the project, was the initiation stage coming from the constraints diagram. Detailing the necessary wing area for the global design was essentially the starting point of the Aerodynamic design process as well as the concurrent Structural analysis.

In terms of outputs for the two departments, the KPIs served as the key values that would inform other sections of the study. For Aerodynamics, the L/D value would provide the Propulsion department the value required to perform its analysis, while the Structural department would allow the materials department to select materials based on max stresses as well as operating conditions.

5.2.3 Key Performance Indicators

As discussed in Section 2 Project Management, the driving factors for each department centred around the matching of KPIs to the pre-defined requirements of the system. In the case of Aerodynamics, this was decided to be the L/D value in the cruise portion of flight

as it provides a good indication as to the overall aerodynamic performance of the aircraft geometry and is easily related to those parameters within other departments, thus providing a value that is useful and relevant to the other project departments. Most notably, it would provide a basis for which Economic analysis of each design could be performed. While this was to be the key driving factor for the Aerodynamic optimisation process, it would be measured while varying further aerodynamic parameters, namely, the cruise Mach no. of the aircraft. In assessing a target for the L/D value, the corresponding value for the reference airframe was selected in order to meet the requirements. This value was approximately 20 based on the cruise L/D of the Airbus A380 [21].

In terms of the Structural element of the design, the KPI selected was the maximum allowable stress within the air frame, in particular on the wings as they undergo loading due to the pressure forces due to lift. In conjunction with the materials selection, this would have to fall within the operating range of the selected material for internal and external structural bodies.

5.2.4 Manual Optimisation

Manual optimisation of the aerodynamic shape of the BWB was undertaken in conjunction with the relevant departments in order to improve upon each iteration within the design process. Manual design adjustments were carried out based on a combination of background literature, best engineering judgement and CFD analysis of cruise performance. This process was heavily reliant on the Engineering judgement of the department members as previously mentioned.

The structural design relied on manual optimisation means, especially at the initial stages of design. However, when delving into the internal structures it was found to overall be inefficient for that task and more analytic means were sought after.

5.3 Literature Review

As previously noted, the concept of the blended wing body aircraft has been discussed extensively in the existing literature, with the vast majority of research looking to exploit the positive impact of the naturally high lift configuration and favourable lift distribution in order to reduce fuel burn and thus improve either economic or emissions performance. As a result, there is a reasonably strong volume of work presented on the aerodynamic and structural characteristics of this concept which was utilised in order to inform this project.

In particular, work done in the 2000s by Qin [12], [22], [23] provides a strong body of knowledge regarding the parameters affecting Aerodynamic performance of a BWB airframe. Employing the conclusions of these studies, such as the impact of sweep angle on the design, will allow for the manual optimisation process to take place in conjunction with

pre-existing knowledge of aerodynamic design. Furthermore, the existing body of work regarding the Aerodynamics of BWB configurations will provide some basis for the CFD work being completed. Specifically, the common employment of RANS models [11], [24] to determine turbulence around the airframe matches well with the proposed verification case of the ONERA M6, as well as reducing simulation times compared with a LES model.

There have been a number of studies conducted into designing BWB concepts both academic and commercial parties. In particular work by ICAS, Boeing and Chinas Northwestern Polytechnical University provide details on historical designs; design approaches and results of their own concepts which provide valuable design lessons, applicable to this projects concept[15], [25], [26]. In terms of structures, the wing structures follow typical rib and spar designs however the fuselage structure differs significantly. Most literature on BWB design reference work done by Kimmel et. al [27] on BWB fuselage structure design, with this work also being of particular focus in this paper also. Being further discussed in Section 5.6.9.

5.4 Methodology

5.4.1 ONERA M6 Flow Verification

In order to verify the flow parameters for this case, the ONERA M6 [28] wing was selected, a classic example that is often employed for studies involving cruise speed and AOA. Originally devised to study pressure distribution around a wing surface, it is useful in this case due to its similarity to the aforementioned cruise flight conditions. Table 9 details the flow parameters of the experiment:

Parameters	Values
Angle of Attack	3.06
Pressure	101325Pa
Temperature	300K
Ma_c	0.8395

Table 9: ONERA M6 Experimental Flow Parameters [28].

5.4.2 CFD Verification Problem Modelling

The problem is to be treated as steady due to the conditions of cruise flight, with the pre-processing carried out within Star CCM+. Due to the necessity for dealing with compressibility effects and highly separated flows, a coupled implicit solver was implemented due to its effectiveness in dealing with these flow parameters, employing a 3rd order Central Difference MUSCL scheme for a high accuracy simulation. Fluid properties were set to compressible ideal gas as is common to simplify problems of this class. The Reynolds

number for the simulation was 11.72e6.

Beyond the physics and solvers of the simulations, the meshing of the wing geometry was also an important consideration. From previous experience with this verification case, the majority of considerations were known and meshing the body was a simple task. Implementing an unstructured mesh with prism layers surrounding the wing surface, below are listed the various meshing parameters that were employed:

Parameters	Values
Cell Count	2619868
No. of Prism Layers	25
Near Wall Cell Distance	1e-6
Prism Layer Total Thickness	0.1

Table 10: ONERA M6 Meshing Parameters.

Figure 79 in Appendix C depicts some of the mesh characteristics, in particular the refinements around key elements such as the leading and trailing edges, the development of prism layers around the surface body, as well as the overall mesh itself.

Convergence Criteria

Three convergence criteria were established in order to ascertain when the simulation had reached a converged solution. Firstly, a lift coefficient based asymptotic criterion showing convergence when the C_L vs Iteration slope had gone asymptotic. A similar criterion for Drag coefficient was also established. Lastly, a check of the residual values to ensure each residual had tended towards a horizontal line ensure that the simulation had converged to a solution.

5.4.3 Verification Results

As can be seen from the plots depicted in Figure 12 the meshing and modelling have provided strong agreement with the experimental results for the ONERA M6 case. In terms of selection of turbulence model, the use of the k-Omega SST was chosen to be implemented due to a closer prediction of the flow field at the wingtip, an aspect that will be important as a result of the induced drag effects on the aircraft.

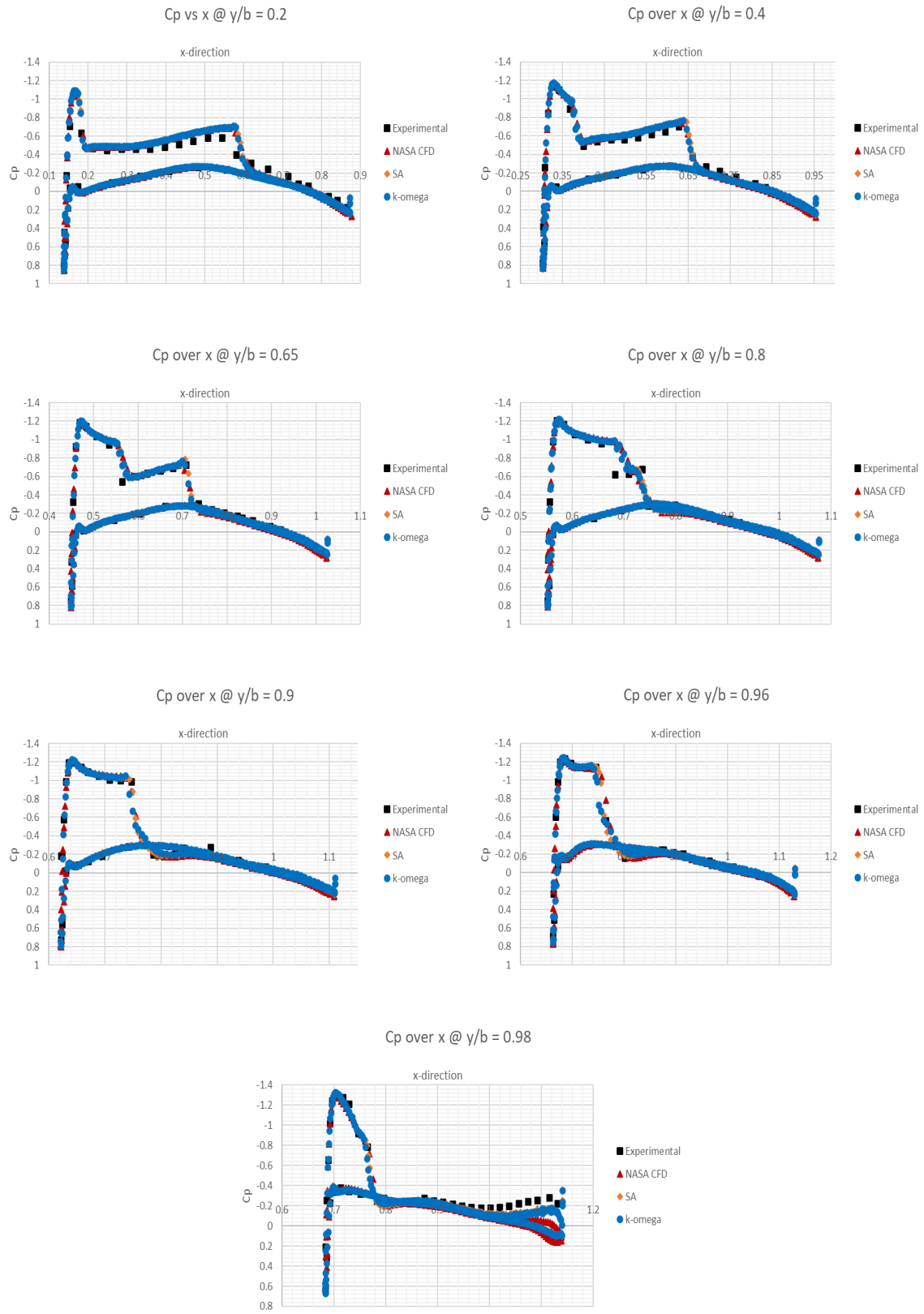


Figure 12: ONERA M6 Pressure Plot Results.

5.5 BWB Modelling

As discussed in Section 2.4.4 of this report, the key drivers for the design of the BWB geometry were based around a design to requirements philosophy. In the case of the Aerodynamics and Structures departments, the key drivers are the KPIs as previously specified.

5.5.1 FEA Modelling

For FEA analysis ANSYS 17.1 was used allowing for uncapped element counts to be used to ensure accurate results. The wing was analysed as a static structural problem with geometries using fixed supports at selected points on the model to simulate being attached to the rest of the air frame. Unstructured tetrahedral meshing was used due to the complexity of the geometries shapes coupled with limited computational resources, with more fine face sizing being applied to regions of interest.

The FEA problem was solved using ANSYS Mechanical APDL solver, using an iterative solver which provides more accurate results for such problems with the tradeoff of slightly longer simulation times.

5.5.2 CFD Modelling

Meshing

A 3D study was determined to be necessary to assess the flow field around the complex geometry. Employing similar principles from the ONERA M6 study, the meshing process for the BWB could be undertaken, using a similar approach in which boundary layers are resolved via the use of prism layers which then transition the unstructured cells up to the domain boundary. An example of one of the BWB meshes is shown in Figures 13 - 16, highlighting certain key aspects of the volume mesh.

Considering the flow domain, a spherical far-field, freestream boundary was adopted with the radius equaling 25 times the max chord length in order to ensure the pressure distribution around the airframe was fully realised. The surface of the airframe itself was set as a wall boundary to represent the BWB geometry within the problem.

An important point of note when considering the CFD modelling and meshing of the BWB geometry is that of engine placement. As determined in Section 6.2.2 of this report, the placement of the engines was likely to be toward the trailing edge of the fuselage, as opposed to the traditional under-wing arrangement seen on tube-wing configurations. As it is likely that flow interaction will occur between the flow around the airframe and the flow into the engines, a decision had to be made as to whether or not the engines should be modelled in CFD. Assessing the current literature, it is uncommon for the aerodynamic analysis to

cover these flow interactions [12], [22], [23], another study conducted by Yu in 2019 [29] stated that the effect of interactions between engine flow and airframe flow on the aerodynamic performance would be small. As a result it was decided that the airframe would be modelled without engines, also saving modelling and computational time.

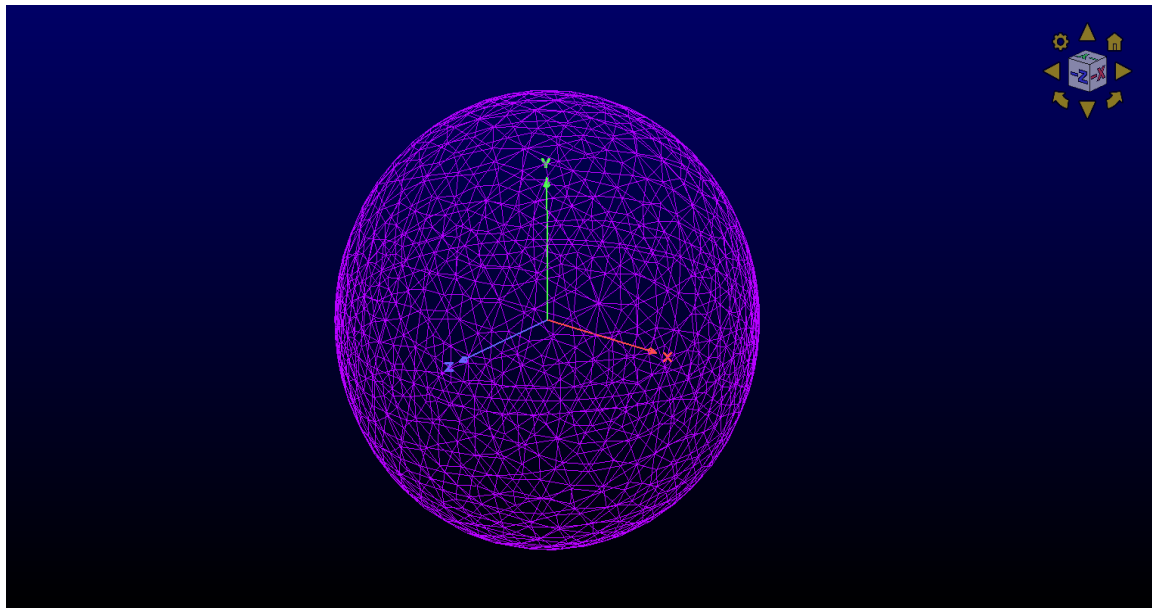


Figure 13: BWB Mesh: Fluid Domain.

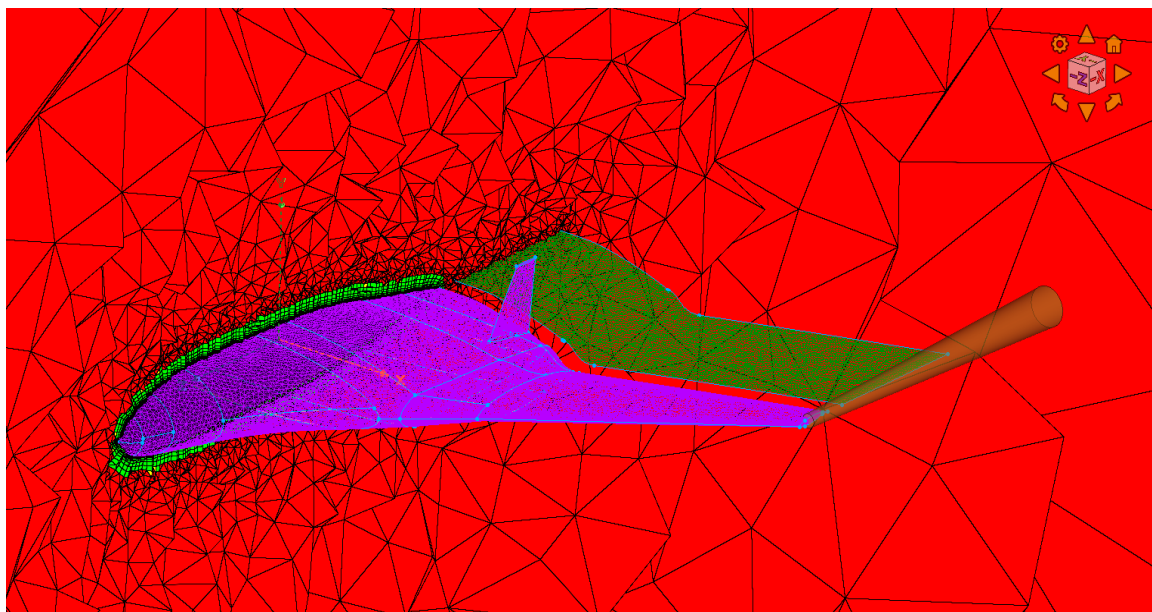


Figure 14: BWB Body Mesh.

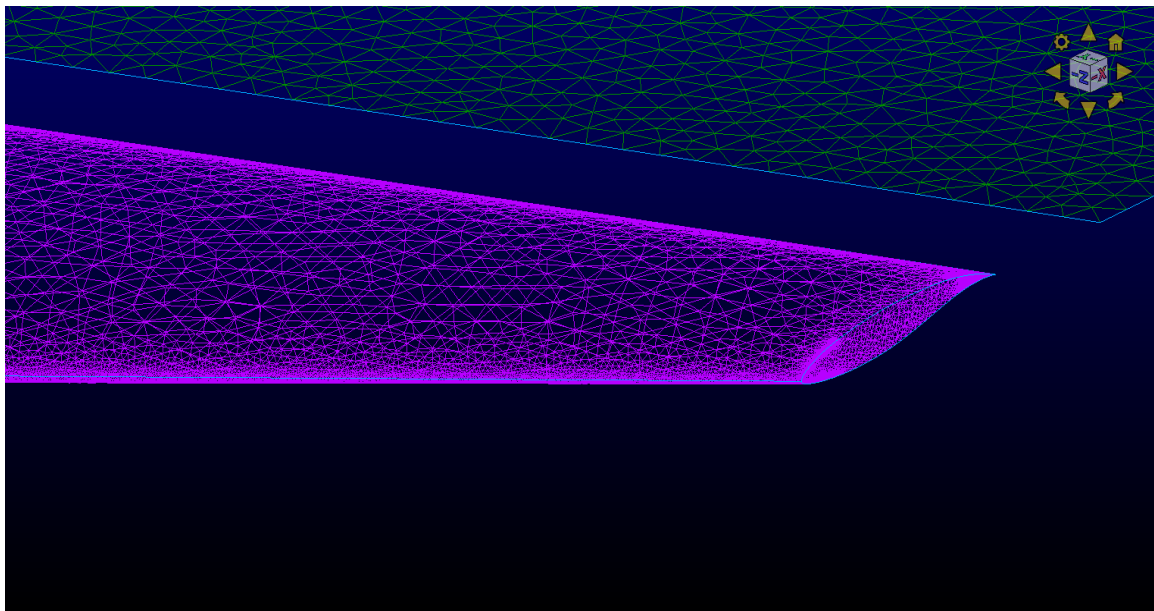


Figure 15: BWB Wingtip Mesh Refinement.

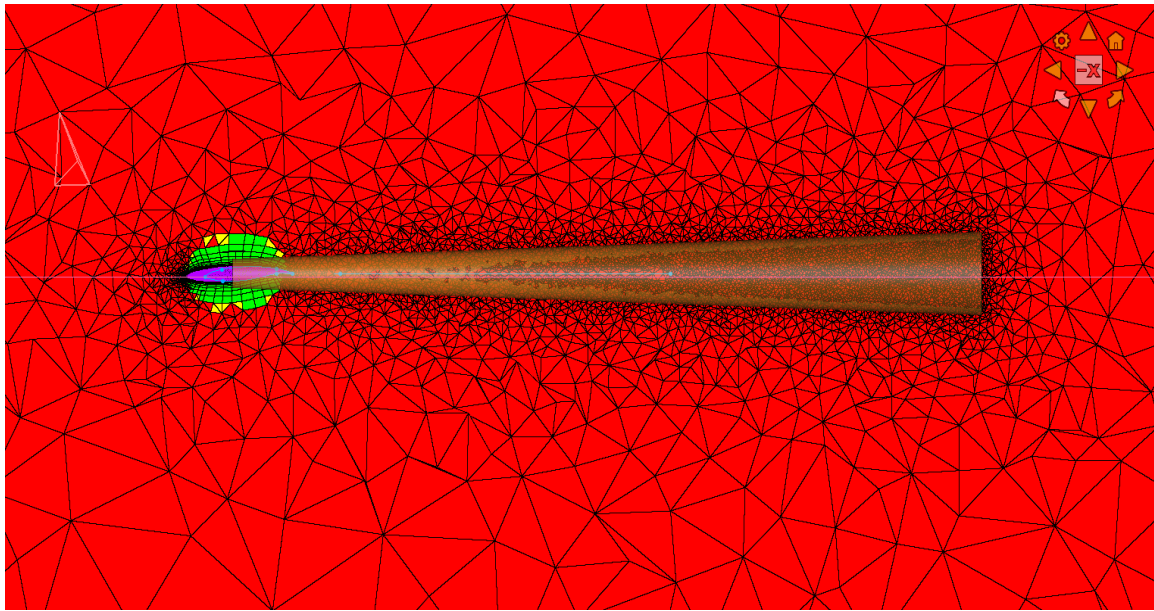
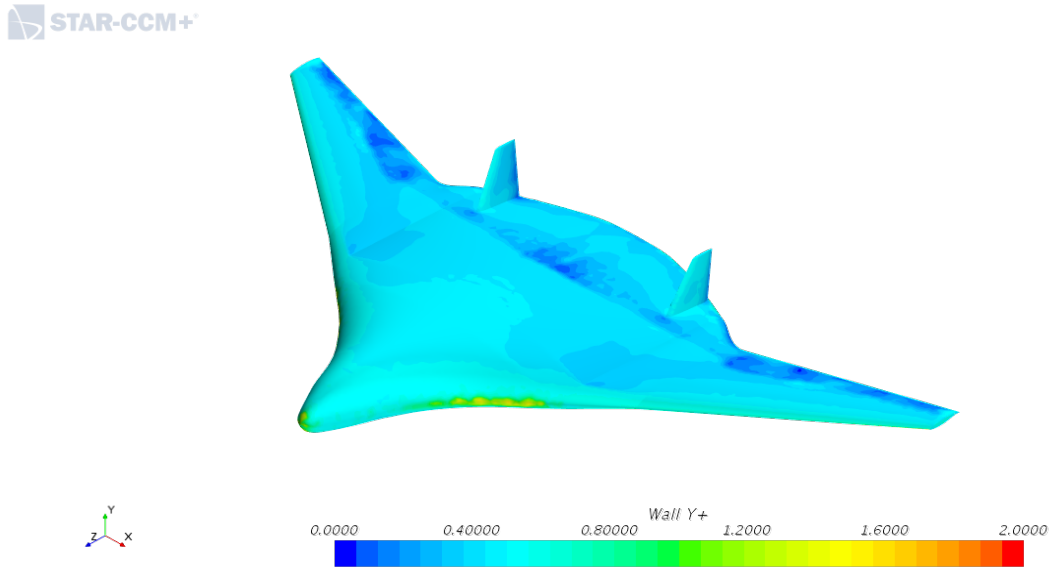


Figure 16: BWB Trailing Vortex Refinement.

The final important consideration of the meshing methodology was the $y+$ value. In order to resolve the viscous sub-layer, a $y+$ of 1 was required; for which a near wall distance of approximately $1e-6$ would be necessary. Figure 17 shows the Star CCM+ $y+$ analysis, giving a $y+ \leq 1$ across the BWB.

Figure 17: BWB Mesh $y+$.

Physical Modelling

When looking at the physical modelling of the problem, a few things had to be considered. Firstly, the selection of turbulence model for the simulation would dictate the simulation time in selecting which RANS model would be used. From the ONERA M6 study, it was clear that the k-Omega SST model, while slightly more time consuming than the Spalart Allmaras, provided better resolution in the trailing vortex region of the body. Implementation of physical conditions would follow the same process as the ONERA M6 study in order to recreate the cruising speeds that the airframe would experience. The Reynolds number for the simulations varied with Mach number, shown in Table 11.

Ma	Re
0.82	3.81e8
0.83	3.85e8
0.84	3.9e8
0.85	3.95e8
0.86	4e8

Table 11: Simulation Re Numbers.

Post-Processing

In terms of post-processing, the Lift and Drag coefficients would be calculated through determination of pressure forces on surface normals in the relevant force direction, Lift

being upwards and Drag being in the aft direction of the airframe. These forces would then be inputted to the standard lift and drag formulae as below:

$$L = \frac{C_L \rho A V^2}{2} \quad (1)$$

$$D = \frac{C_D \rho A V^2}{2} \quad (2)$$

5.5.3 Resource Cap and weeArchie HPC

As a result of the CFD Analysis process, there was a need to determine the depth of the Aerodynamic study that would be sensible and achievable within the resource and time limits. When running simulations, the weeArchie HPC was used in order to run at a high enough mesh fidelity to obtain converged solutions. Similarly, for Structural Analysis, there was necessity to determine suitable mesh size to achieve accurate FEA results while remaining computationally feasible, limited to a 6 core CPU for running analysis. A converged result was however found well within the capabilities of the system used to run the FEA analysis.

5.5.4 Mesh Convergence

CFD

A mesh convergence study was devised based on the initial startup design in order to ascertain the lower bound of mesh resolution that was required to carry out simulations that would provide a converged result. Table 12 details each iteration of the study:

Cell Count (approx.)	L/D
3000000	7.658
4500000	9.821
7000000	11.88
9000000	11.35
10000000	11.34
12000000	11.34

Table 12: Base Design Mesh Convergence Study.

From the above results it could be determined that the baseline requirement for a converged solution was approximately 10000000 cells; therefore, for any simulations carried out, this would act as a threshold value which would have to be met in order for the simulation to be uploaded to weeArchie.

FEA

A mesh convergence study was conducted for analysis in Section 5.7 and was carried out for the base wing design for design iteration 2. Using the loading conditions discussed in Section 5.7 to determine the lower bound of grid size that would provide a converged result. The results of this study are shown in Table 13.

Grid size (m)	Number of Nodes	Von mises stress result (Pa)
0.09	241823	3.1535e6
0.08	306755	3.1614e6
0.07	401289	3.2334e6
0.06	547198	3.4147e6
0.05	768495	3.6309e6
0.045	872923	3.63091e6
0.04	1204963	3.63092e6
0.03	1966238	3.63091e6

Table 13: Grid Independence study for internal structure using tetrahedral elements.

From the study, a grid size of 0.05m was selected for solid wing analysis, discussed in Section 5.7, having the same stress result as a 0.03m grid size for a fraction of the required nodes and computation time.

5.6 Iterative Results

With all of the above information, requirements, and inputs; the design iterative process could be performed in conjunction with the other departments in order to produce the required outputs from the Aerodynamics and Structures departments. The process would follow that outlined in Section 2.4.3 of this report to ensure all relevant departments were informed of the iterative process and ensure design decisions outwith Aerodynamics and Structures were well informed by the outcomes of this section.

5.6.1 Iteration 1 - Initial Design

The initial design seen in Figure 18 served as a learning exercise for dealing with problems of this class and gaining familiarity with software. This design was predicted to perform poorly but it was a jumping off point where lessons could be drawn for application to future designs while awaiting the construction of a constraints diagram.



Figure 18: Render of initial design 3D CAD model.

Following the meshing and modelling process as detailed above, a preliminary CFD study was carried out on the Base Design in order to assess the general flow characteristics of the BWB and ascertain where certain design parameters, such as wing sweep and how blended the wing structure is to the fuselage, affected the overall design performance. In doing so it would be possible to see any major changes required, as well as gain familiarity with the problem class and encounter any issues that may be prominent further in the design process.

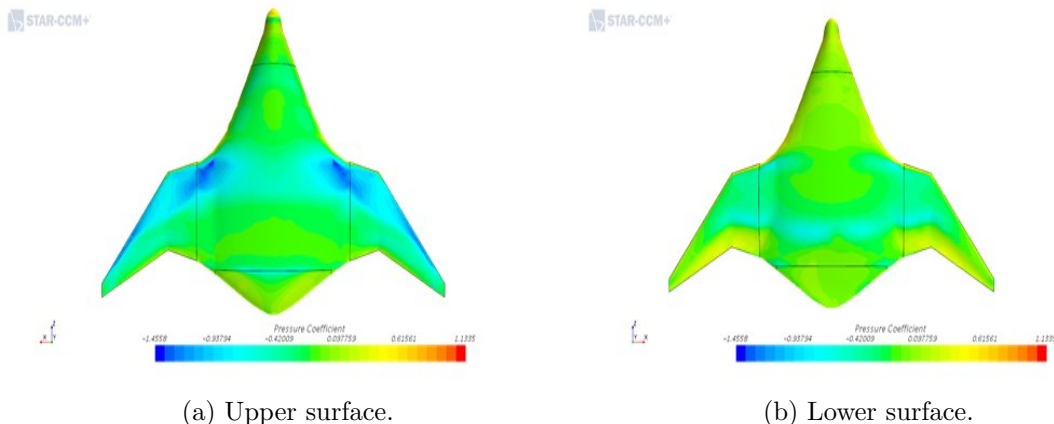


Figure 19: CFD pressure contours for base design at $\text{Ma} = 0.84$ and $\text{AOA} = 3^\circ$.

Mach No.	C_L	C_D	L/D
0.82	0.164	0.0184	8.9
0.83	0.168	0.0175	9.6
0.84	0.17	0.0173	9.8
0.85	0.163	0.0259	6.3
0.86	0.162	0.0275	5.9

Table 14: Base Design L/D for Varying Mach No.

Following this preliminary analysis, the Base Design provided an L/D ratio of 9.8 as shown in Table 14, falling significantly short of the reference aircraft at 20. While this simulation was run with a coarser mesh and would not perfectly represent the model, it was clear there were areas where the design could be altered to produce higher lift and generally better flow characteristics, as detailed in the next sub-section. The initial design of the wings also fared poorly having a maximum Von-Mises stress of almost 500 MPa as shown in Figure 20 when loaded to the equivalent pressure if the aircraft was loaded to an A380 maximum takeoff mass.

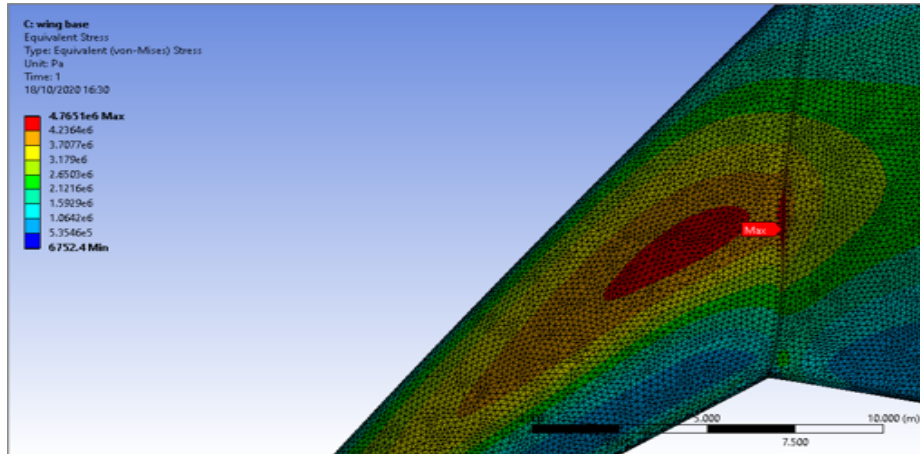


Figure 20: FEA stress analysis of initial design wing.

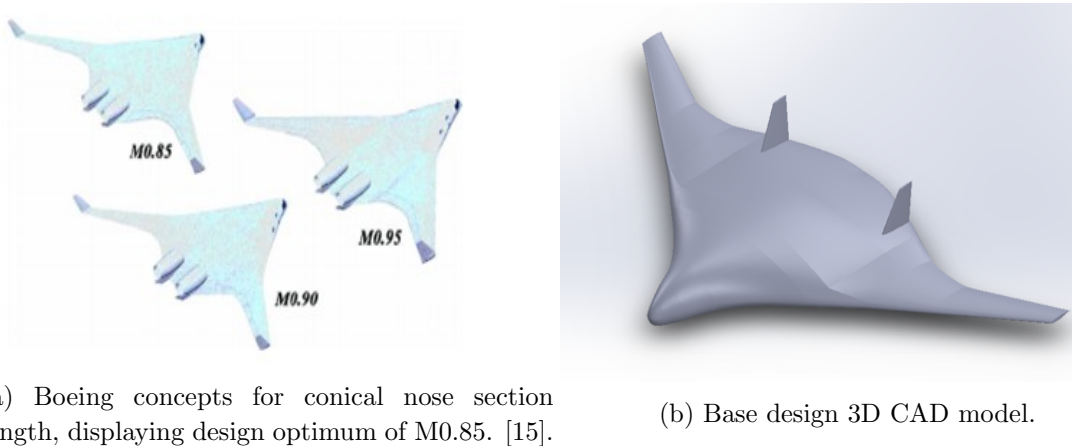
Following the devised protocol, the relevant task-holders performed an analysis of the design, arriving at the following conclusions. It can be clearly seen from the pressure contours in Figure 19 that the shock wave that would be expected in this flow type is occurring not far aft of the leading edge of the upper wing surface, thus reducing the effective lifting area of the design. Design changes at this stage would centre around the need to move this shock backwards, further aft of the leading edge. Further design changes were required in terms of Structural performance:

- Much smoother (blended) transition from body to wing required to minimise drag

- With considerations to practicality, future designs were to be sized within a standard 80m x 80m design box outlined by regulations.
- An improved aerofoil with flatter top surface was required for desired cruise conditions
- Reduce angularity in wing shape to improve both aerodynamic and structural performance
- Addition of stabilising fins to provide economical means of control

5.6.2 Iteration 2 - Basic Shape Adjustments

Incorporating the lessons learned from the initial design as well as implementing features from research and regulatory investigation, a second design was created to satisfy the value set out by the constraints diagram. An example of research implementation being shown in Figure 21b, where research by Boeing demonstrates different designs by for BWB aircraft designed to cruise at different Mach numbers[15]. This influenced the design by incorporating a blended conical like nose to the design rather than the more distinct conical section in the Mach 0.95 design in Figure 21a. This base design of the 2nd design iteration fulfilled the W/S requirements set out by the constraints diagram, being slightly lower in terms of W/S than the optimum point, suggesting that the aircraft could lift a greater load than previously designed for.



(a) Boeing concepts for conical nose section length, displaying design optimum of M0.85. [15].

(b) Base design 3D CAD model.

Figure 21: Base Design.

In terms of CFD analysis of the 2nd Design Iteration, much the same process was followed in order to attain useful results for comparison with the previous design as well as the design requirements.

Along with the 2nd design iteration, different wing shapes were analysed as solid bodies, providing basic structural performance. As the body of a BWB has good lifting charac-

teristics, the considered lifting area was assumed to consist of the wings plus the fuselage area between them. The wing loading applied to the wing design was calculated using the maximum load that an A380's wings experiences, during the takeoff phase, using the method shown below.

Using A380 max takeoff mass, $m = 550000$ kg and subsequent weight, $W = 5395500$ N

Assuming a typical take off angle of 15 degrees,

$$Maxload = \frac{W}{\cos(15)} = \frac{5395500}{\cos(15)} = 5585832.6N$$

This pressure load can be applied to provide the wing loading of the different designs, illustrated in Figure 22, depending on their respective lifting surface areas, shown in Table 15.

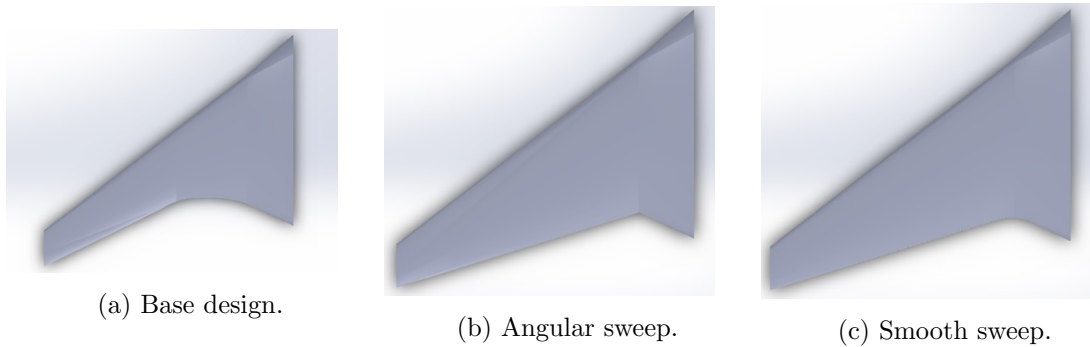


Figure 22: Wing shapes investigated.

Wing Shape	Lifting Surface Area (m^2)	W/S (Pa)
Base Design	1062.24	5258.54
Angular Sweep	1125.68	4962.19
Smooth Sweep	1126.42	4958.93

Table 15: Lifting surface area and subsequent wing loading of each design.

All designs are within the constraint diagrams wing loading limits with the potential to lift a larger maximum load. The wing loading for each design were then used to perform FEA analysis to determine the performance of in terms of stress and deformation.

For such analysis to begin, boundary conditions for the problem had to be established. As the wing and fuselage was blended into one body, the whole wing root was determined to

act as a fixed support creating a cantilever problem with the wing loading value for each design being applied to the under surface as a pressure load seen in Figure 23. The mesh was determined using the study undertaken in Section 5.5.5.

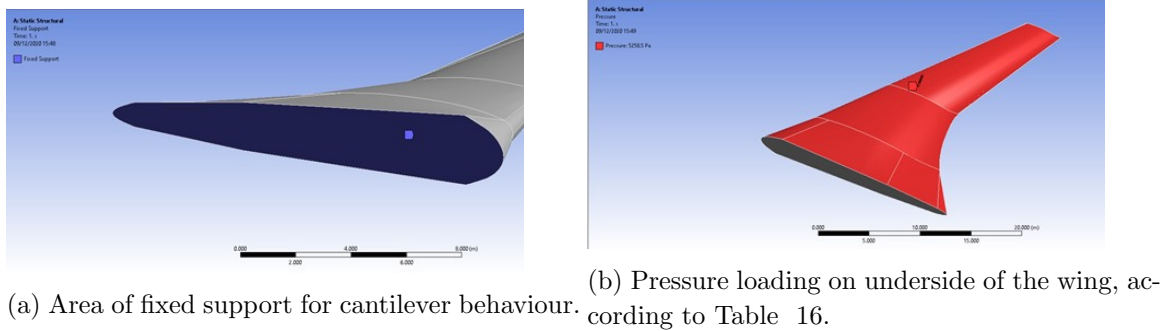


Figure 23: Boundary conditions for FEA analysis.

Table 16 displays the solid wing design results, the base design, shown in Figure 24, exhibits unacceptable stress results having a maximum Von Mises and Principal stress higher than the yield stress of most high strength aluminium alloys. The design can be seen to be suffering from a significant stress concentration between the mid and tip sections of the wing. The larger area angular sweep design shown in Figure 25 overall shows superior stress distribution; however, the stress concentration at the trailing edge where the wing transitions from the root to main section is far too angular, creating an even higher maximum stress results than the base design. This failure was expected from the analysis on the base design and served as a good means of comparison with the smooth sweep design. The small geometric change to smooth out the trailing edge corner of the angular wing significantly improved the stress within the wing, being within the range of higher-grade aluminium alloys.

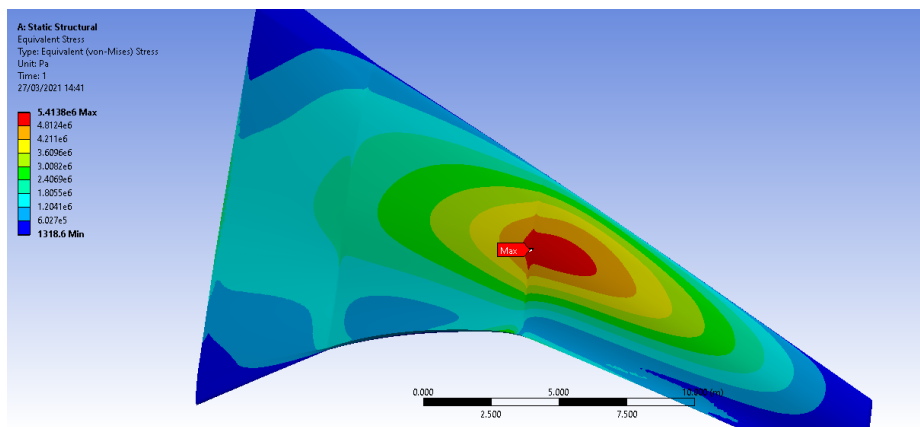


Figure 24: Ansys FEA Von Mises stress for base wing design showing with maximum stress between middle and tip wing sections.

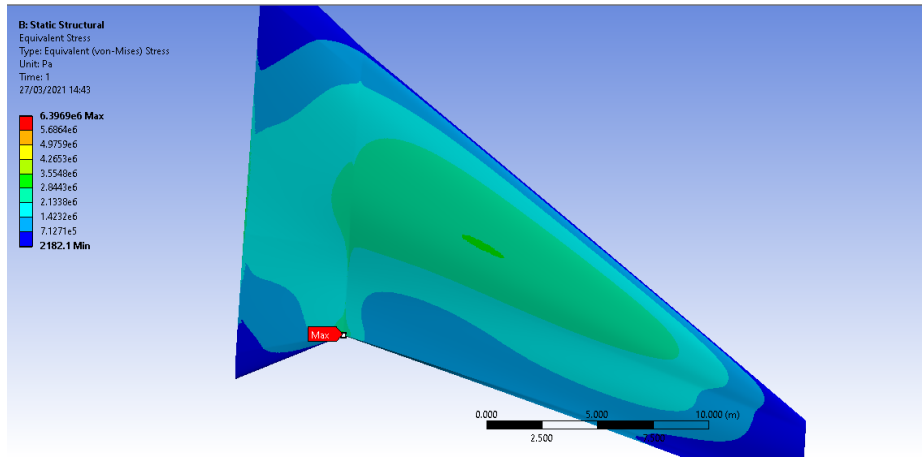


Figure 25: Ansys FEA Von Mises stress for angular sweep wing design with maximum stress at root to main wing transition.

Wing Shape	Pressure Load (Pa)	Deflection (m)	Max. Von Mises Stress (MPa)	Max. Principal Stress (MPa)
Base Design	5258.54	0.030222	5.4138	5.5309
Angular Sweep	4962.19	0.021398	6.3969	6.6223
Smooth Sweep	4958.93	0.006560	3.6309	3.9052

Table 16: Stress and deflection results of wing shapes under loading.

As the Aerodynamic department is reliant on the Structural department to essentially approve a design before simulation work is carried out, the results of the above study informed the selection of wing geometry for the simulations run for this iteration. With the smoother wing to body transition geometry yielding acceptable stresses, it would then be run through CFD analysis. Following the same approach as before, the pressure contours in Figure 26 were generated for the design iteration. The design was also run at varying Mach numbers in order to ascertain its optimum cruising speed, with the results being detailed in Table 17.

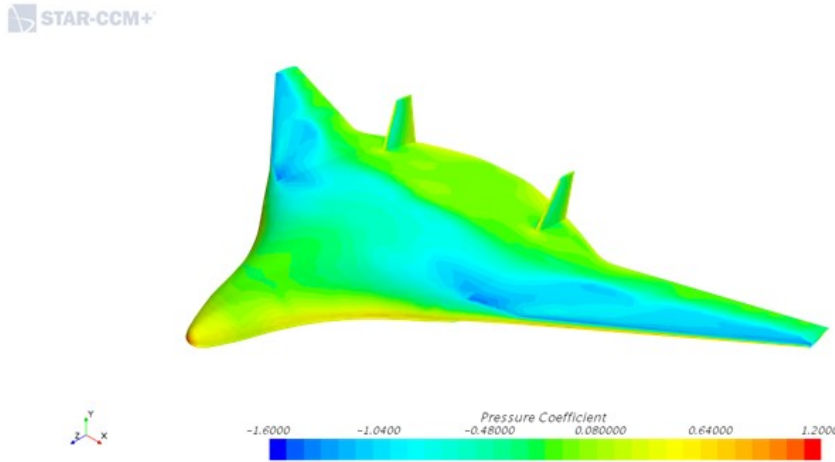


Figure 26: Mk.2 CFD pressure coefficient.

Mach No.	C_L	C_D	L/D
0.82	0.276	0.0246	11.2
0.83	0.288	0.024	12
0.84	0.292	0.0234	12.5
0.85	0.272	0.032	8.5
0.86	0.271	0.033	8.2

Table 17: Base Design L/D for Varying Mach No.

With this new model producing an L/D of 12.5 at its optimum cruise Mach no., it was clear there was a need for a change of aerofoil in order achieve the lift required by the constraint diagram design point. Some positives of note were, firstly, the movement of the shock wave further aft of the leading edge providing a greater low pressure region on the upper wing surface. Further to this, the same shock characteristic can be seen to have also moved further aft on the main body of the design, thus increasing the lifting capability of the fuselage itself, taking better advantage of the use of an aerofoil section for this part of the design.

Following the design meeting, it was clear that the structural requirements had been reasonably well met in regards to the requirements definition; however, there was still greater Aerodynamic optimisation necessary in order to attain the required L/D characteristic. The impact of Aerodynamic performance could be seen on the Economic side of the design as the increased L/D performance saw the design come closer to that of the A380 from a price per passenger standpoint, which will be further illustrated in Section 8.3.

The outcome of the design meeting had determined that the next iteration would see the selection of a new aerofoil geometry for the wings with a view to improving the lift characteristics of the global airframe.

5.6.3 Iteration 3 - Aerofoil Alterations

As a result of the findings from the previous iteration, a small study was devised in order to assess which aerofoils could see an improvement on the previous design. Alternative aerofoils were investigated to determine if any improvements in lift characteristics could be achieved. The SC(2)-0714 supercritical used in the initial design was compared with the Whitcomb integral, Eppler 417 and Eppler 403 aerofoils in Figure 27. From the website AirfoilTools.com, the following data could be compared for the selected supercritical aerofoils.

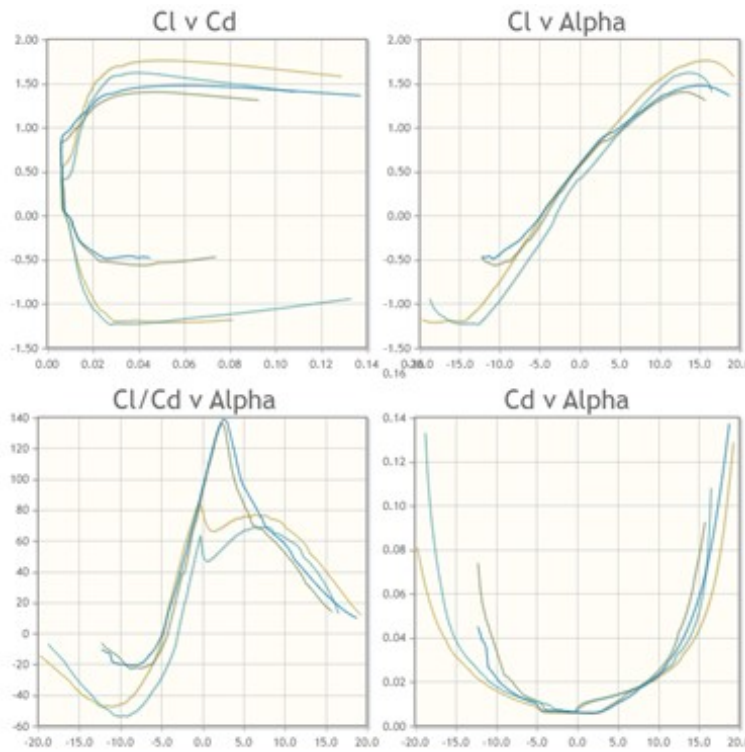


Figure 27: Aerofoil Comparison: yellow - SC(2)-0714; dark blue - Eppler 403; green - Eppler 417 and light blue - Whitcomb.

The Eppler 403 has the best L/D at optimal cruise angle, closely followed by the Eppler 417 aerofoil. However, the 403 has a rather rounded top surface, which often leads to flow shock occurrence closer to the leading edge of the wing body; therefore this leans selection towards the 417 which has a flatter top and overall shorter height coupled with its similar performance.

For analysing the Eppler wing, the boundary conditions remained the same; however, the mesh was refined to obtain a more accurate result implementing the Eppler 203 aerofoil into the smooth sweep wing shape shown in Figure 28. The mesh consisted of 2,770,661 million nodes to ensure accuracy and a stress contour was output to assess if the wing design should be taken forward for structural design.



(a) Render of Eppler aerofoil wing on smooth sweep wing design. [15] (b) Render of full design 3D CAD model using Eppler aerofoil wings.

Figure 28: Eppler 417 aerofoil design.

Figure 29 and Table 18 show that the Eppler wing provides further improved structural performance most likely due to its taller profile providing a more robust wing and smoother body. Due to this superior performance, it was taken forward to create a more realistic structure and skin model.

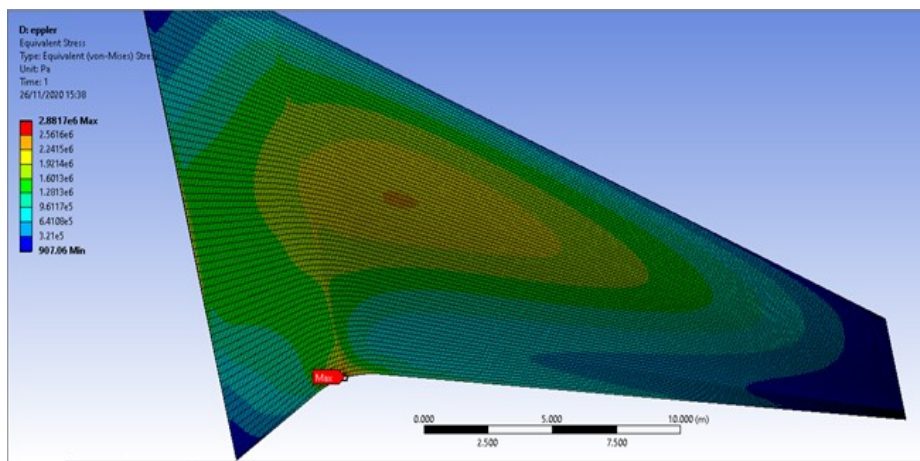
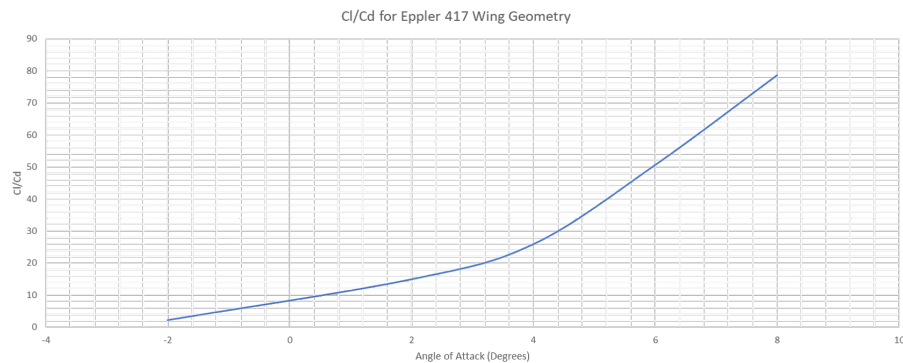


Figure 29: Ansys FEA Von Mises stress for smooth sweep Eppler wing design with maximum stress occurring as in Figure 25 to a lesser magnitude.

Wing Shape	Pressure Load (Pa)	Deflection (m)	Max. Von Mises Stress (MPa)	Max. Principal Stress (MPa)
Eppler Wing	4987.44	0.005082	2.8817	2.9665

Table 18: FEA analysis results for smooth sweep Eppler wing.

With the implementation of the new Eppler Wing it was necessary to run further simulations in order to verify its use against the data available on Airfoil Tools. A study was run on weeArchie, following a similar meshing and flow modelling procedure, varying the wing angle of attack in order to compare the data with the aforementioned Airfoil Tools data, as well as get an idea of the optimum cruise wing setting angle. The results, detailed in Figure 30, showed a general agreement with the previous data, with a high L/D also being produced by the wing in comparison with the initial geometry.

Figure 30: Plot of Lift/Drag vs AOA for the Eppler wing geometry at $\text{Ma} = 0.84$.

Also shown in Figure 31 are the pressure contours for the wing at 2° AOA, where it should be noted that the shock region, while still somewhat close to the leading edge of the wing, has been moved further aft in comparison to earlier designs, thus providing a larger effective lifting area with potential for further optimisation through taper, twist and sweep of the geometry. On the underside of the body, the large camber region effectively produces the required high pressure to generate the high lift. Now that the high lift properties of the aerofoil have been verified, it will be tested as part of the full geometry.

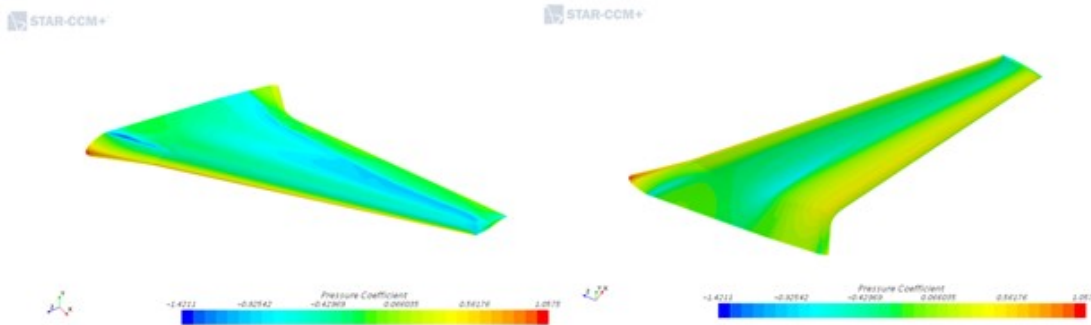
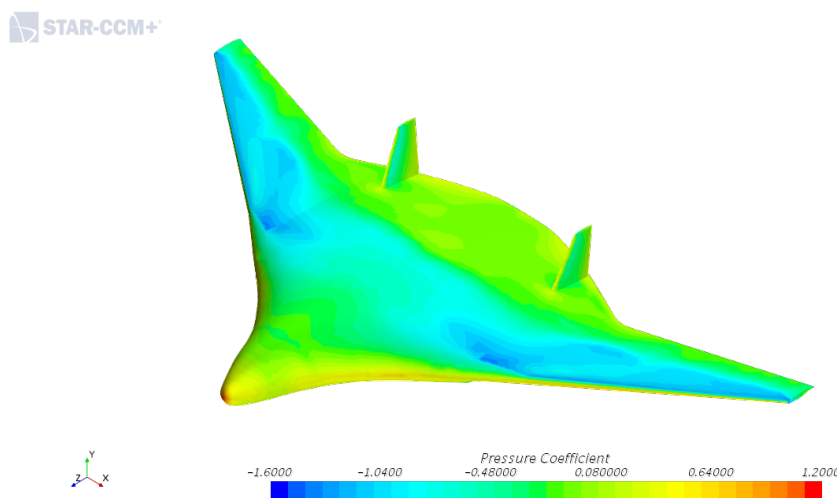
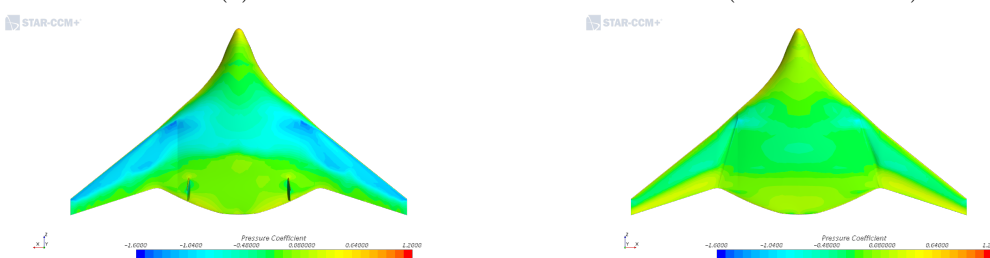


Figure 31: Pressure contours on Eppler wing geometry at $\text{Ma} = 0.84$ and $\text{AOA} = 2^\circ$.

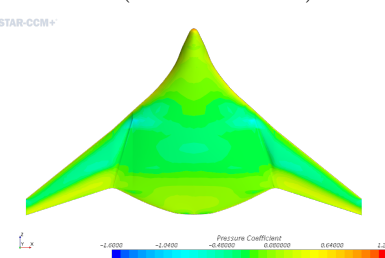
The Eppler wing profile was then incorporated into the global design and tested in Star CCM+. Following the same meshing procedure, an estimation of L/D was produced. Figure 32 shows the pressure contours around this design geometry.



(a) Pressure Contours around BWB Mk. 3 (Isometric View).



(b) Pressure Contours around BWB Mk. 3 (Plan View).



(c) Pressure Contours around BWB Mk. 3 (Undercarriage View).

Figure 32: Mk.3 Pressure Contours.

Table 19 shows the resulting lift and drag characteristics and it can be seen that even with the implementation of the Eppler wing geometry, there is still a large disparity between the reference value of 20 and the results coming from the design.

Mach No.	C_L	C_D	L/D
0.82	0.346	0.027	12.8
0.83	0.358	0.0263	13.6
0.84	0.36	0.0257	14
0.85	0.348	0.04	8.7
0.86	0.34	0.04	8.4

Table 19: Mk. 3 L/D for Varying Mach No.

In the subsequent design meeting it was noted that while the new aerofoil shape had been effective in pushing the shock further aft of the leading edge of the wings, there was still a much greater lift requirement. While it was recognised that the aerodynamic properties had not yet been fully realised in relation to the reference aircraft, the increase in L/D provided by the new aerofoil had now pushed the Direct Operating Cost below that of the A380.

It was decided that the following iteration would seek to improve Aerodynamic performance through the utilisation of wash-in at the root in order to increase the C_L , while reducing the C_D by way of approaching a more elliptical lift distribution through washout at the wing tip.

5.6.4 Iteration 4 - Wing Twist

Iteration 4 centred around an attempt to produce a more favourable lift distribution as pressure drag had become a concern with the design, a key contributor to which is induced drag. This was achieved by adding a positive twist at the root section of the wing (wash-in), increasing the lift across the larger surface area of the root section. Then adding a negative twist (washout) to the tip of the wing reducing its lift, creating a better lift distribution across the wings total length shown in Figure 33. A 1° positive twist at the root and -2° twist at the tip was applied to the design in this project to achieve this effect with the 3D CAD model shown in Figure 34.

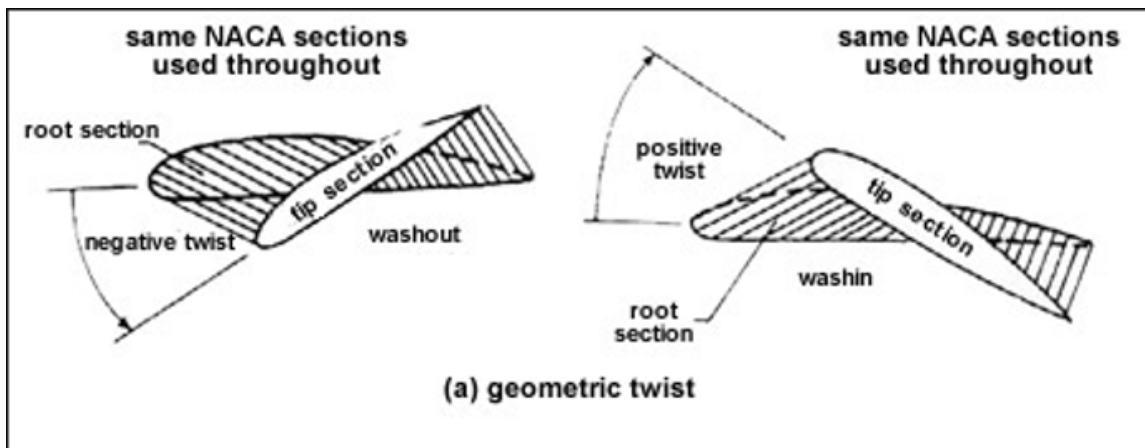


Figure 33: Diagram depicting wash in and washout on twisted wings [30].

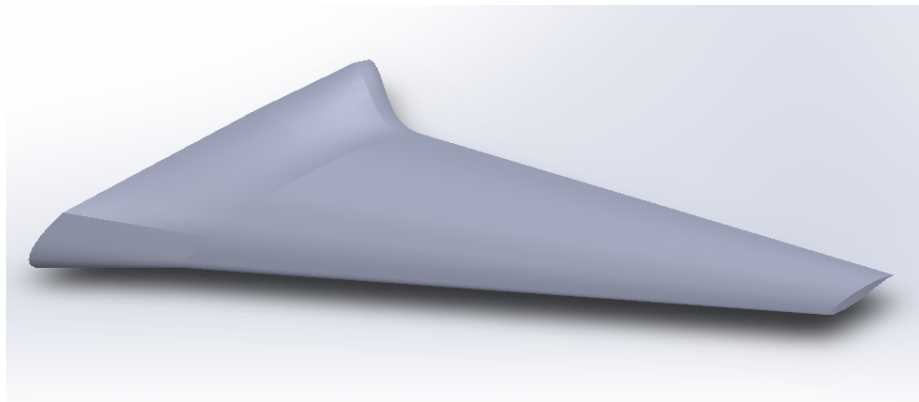


Figure 34: 3D CAD Model of twisted wing.

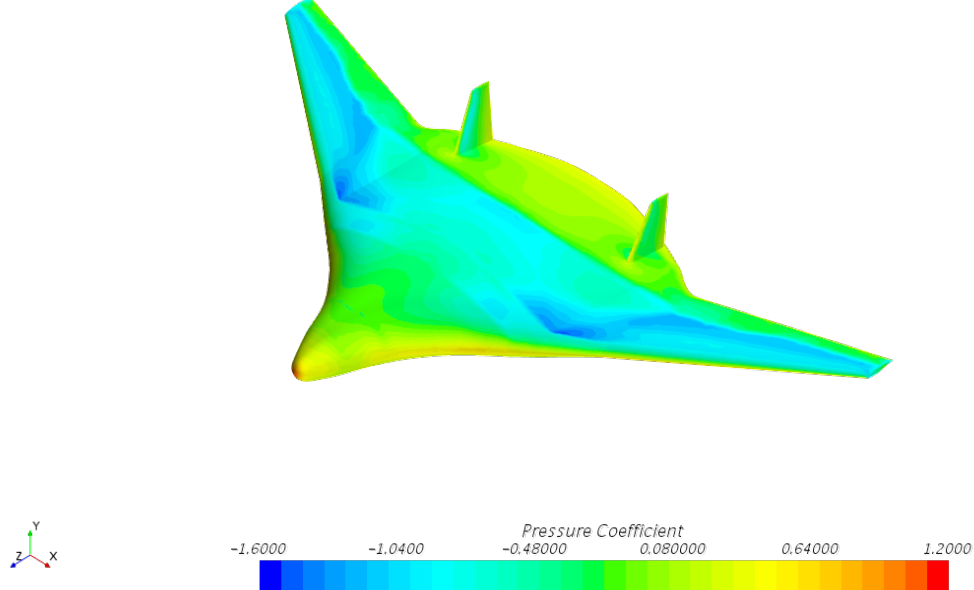
Wing Design	Deflection (m)	Maximum Von Mises Stress (Pa)	Max. Von Mises Stress (Pa)
Base Eppler	0.05082	2.8817e8	1.6394e8
Twisted Eppler	0.05246	2.94518e8	1.7845e8

Table 20: Stress results for FEA analysis of initial design with different spar shapes.

From Table 20, adding a twist to the wing does slightly increase both the deflection and stress within the wing with the area of maximum stress moving to the root section as the shape of the transition from root to wing changes. However, this is a small increase relative to the estimated aerodynamic benefits; so the design was decided to be taken forward for CFD study.

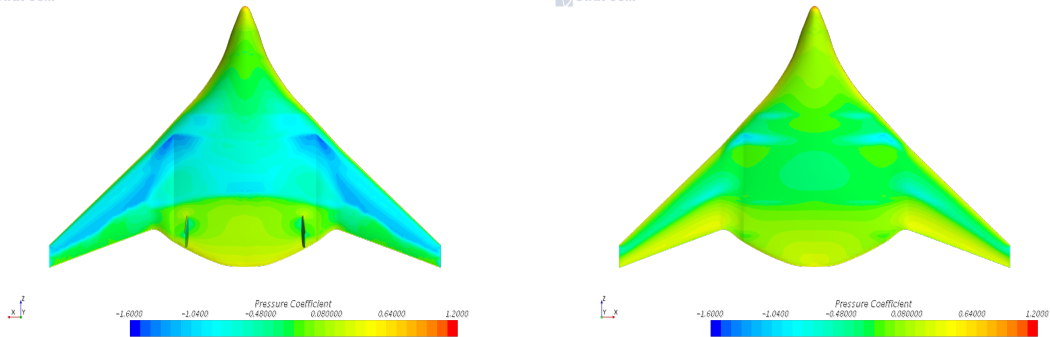
Again following the established meshing and modelling procedure the pressure contours in Figure 35 could be produced via simulation.

 STAR-CCM+



(a) Pressure Contours around BWB Mk. 4 (Isometric View).

 STAR-CCM+



(b) Pressure Contours around BWB Mk. 4 (Plan View). (c) Pressure Contours around BWB Mk. 4 (Undercarriage View).

Figure 35: Mk.4 Pressure Contours.

Table 21 details the results from each section and it can be seen that the L/D is beginning to approach the reference value of 20. Furthermore, it can be seen from Figure 35 that the shock wave occurring across the BWB upper surface has now been shifted further aft of the leading edge of the wings, thus accounting for this increase L/D profile. It should be noted however that the shock impinging on the fuselage body has begun to approach the

fin as well as where the engines were to be placed.

Mach No.	C_L	C_D	L/D
0.82	0.378	0.0224	16.9
0.83	0.385	0.0223	17.3
0.84	0.39	0.0219	17.8
0.85	0.387	0.032	12.1
0.86	0.389	0.035	11.1

Table 21: Mk4 L/D for Varying Mach No.

The design meeting for this iteration comprised mainly of aerodynamic considerations, the next design iteration looked to take the L/D up to the reference value. Now also in conjunction with the Propulsion department, it was decided that an attempt to increase the airframe's optimal Mach number to 0.85. Having been deemed reasonable based on the selection of engines detailed later in this report, this would be attained by slightly increasing the taper ratio and thus the sweep angle adopted by the wing relative to the fuselage datum. Furthermore, an attempt at winglet modelling in order to reduce the pressure drag on the body would also be implemented.

5.6.5 Iteration 5 - Taper Ratio, Sweep and Winglet Addition

The final design iteration was centred around the need to both increase the Mach number at which the design could operate, as well as further improve the lift distribution through adjustments to the wing taper. The further tapering of the wings would act two-fold as the lift distribution would further approach the desirable elliptical form, as well as slightly increasing the sweep angle, done in order to try and increase the speed at which the airframe could operate without the L/D losses that had been seen in previous iterations.

Changing the taper ratio had positive structural effects as seen in Table 22, where the taper led to a slight reduction in the wing mass reducing any occurring shearing actions on the wing, which in turn reduced the stress. The trade off of this is an increase in deflection however, this value was well within the acceptable deflection limits.

Wing Design	Deflection (m)	Maximum Von Mises Stress (Pa)	Max. Von Mises Stress (Pa)
Base Eppler	0.05082	2.8817e8	1.6394e8
Twisted Eppler	0.05246	2.94518e8	1.7845e8
Tapered and Twisted Eppler	0.05546	2.8952e8	1.6548e8

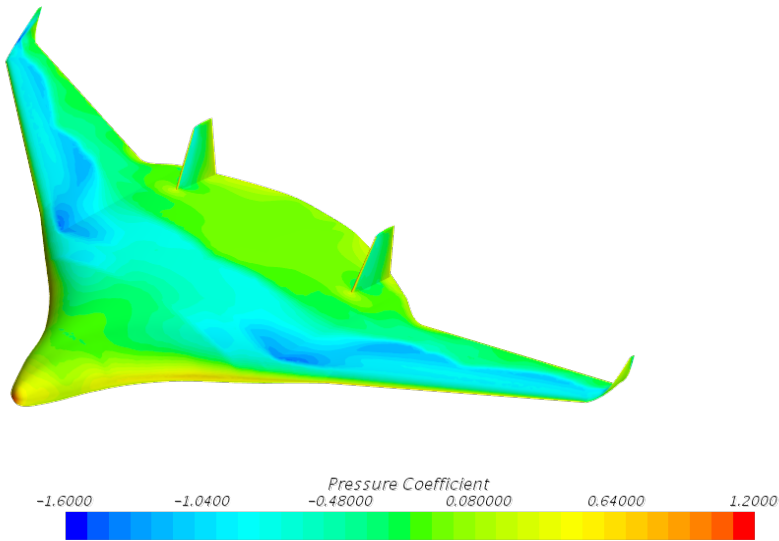
Table 22: Stress results for FEA analysis of different wing modifications.

Figure 36 depicts the pressure contours around the final iteration and some interesting points can be noted. With the sweep angle increasing, the airframe was now able to operate at a higher Mach no. of 0.85, contributing greatly to an increase in lift. Lastly, the shock across the main body of the fuselage can be seen to be slightly weaker than in previous design iterations, as evidenced by a slightly more gradual transition in colour contours. Potentially as a result of the wing body shock being shifted closer to the leading edge (as a result of the greater flow velocity), which resulted in a slight reduction in pressure drag on the fuselage. Generally the results in Table 23 show the increase in L/D that has come as a result of the increased airspeed, reaching a max value of 20.8 before dropping off as other iterations had previously done at this Mach number.

Mach No.	C_L	C_D	L/D
0.82	0.398	0.021	19
0.83	0.402	0.0207	19.8
0.84	0.403	0.02	20.1
0.85	0.432	0.02	20.8
0.86	0.401	0.029	13.8

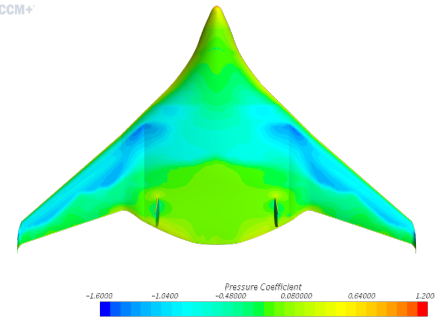
Table 23: Mk. 5 L/D for Varying Mach No.

STAR-CCM+

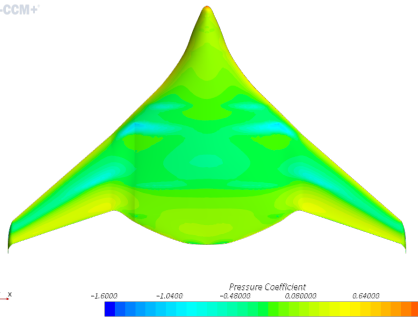


(a) Pressure Contours around BWB Mk. 5 (Isometric View).

STAR-CCM+



STAR-CCM+



(b) Pressure Contours around BWB Mk. 5 (Plan View) (c) Pressure Contours around BWB Mk. 5 (Undercarriage View).

Figure 36: Mk.5 Pressure Contours.

5.6.6 Results Overview and Discussion

Plotted in Figure 37 is the L/D for each iteration, measured against Mach Number. Here can be seen the design evolution as gradual improvements were made to the design in order to push up the L/D ratio while remaining within the stress limit.

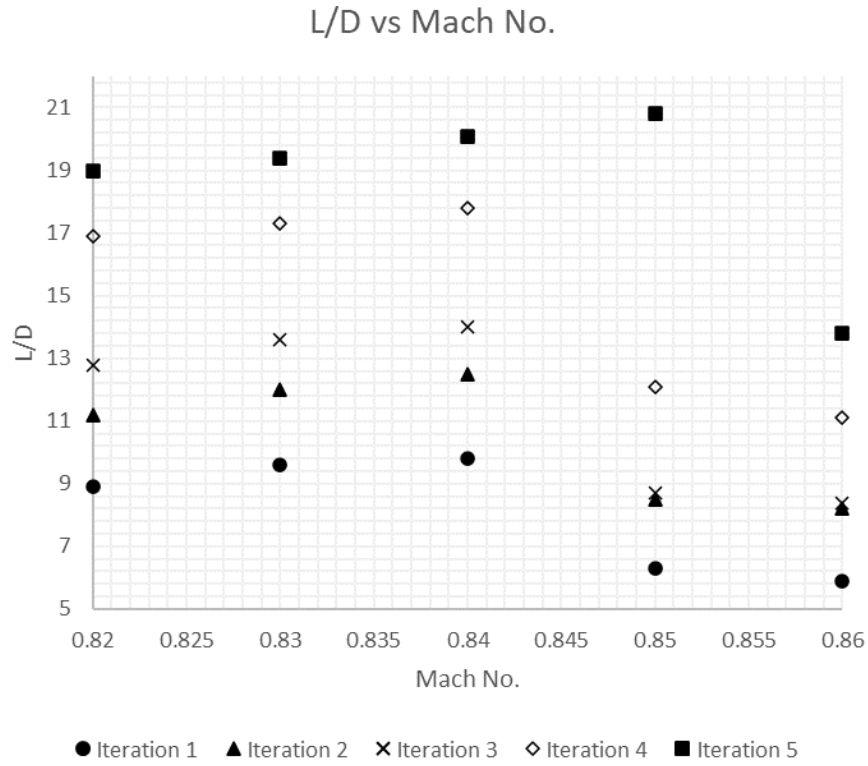


Figure 37: L/D vs Mach No. for all design iterations.

Generally, in terms of the Aerodynamic progression of the design, there were some key observations of note. Firstly, the adoption of the SSM was crucial over the course of the project to ensure that the relevant departments were consistently on the same page and working concurrently. Had it not been implemented, the prospect of all 6 departments working autonomously without clear structure of information exchange may have seen incompatibilities within the design, in particular, between Aerodynamics and Structures as they are so intertwined. Secondly, the MDO approach implemented by the group was found to be somewhat effective. It can be seen that by each iteration there had been an improvement in the aerodynamic characteristics of the BWB; however, it could be said that the autonomous shape optimisation of the airframe often seen in the literature is able to produce similar results, albeit in a slightly different shape. Overall, the decision not to go down the road of automatic optimisation had paid dividends as a successful design relative to the requirements had been achieved.

5.6.7 Ribs and Spar Internal Structure

For internal structure analysis the Eppler wing was broken into an internal rib and spar structure with a thin 5mm skin. The base Eppler design was used for this as internal structural analysis began after the base Eppler wings solid analysis, before twist or taper features were implemented. Despite this, due to the marginal deviation in stress, it serves as an acceptable simplification with any deviation in results assumed to be minor. The initial design shown in Figure 38 consisted of 0.1m thick ribs, having 2 rib spacing regimes of 1.4m at the root section and 1.8m in the main wing section. The structure was connected with two different spar shape configurations: cylindrical and, more realistically manufactured, rectangular spars.

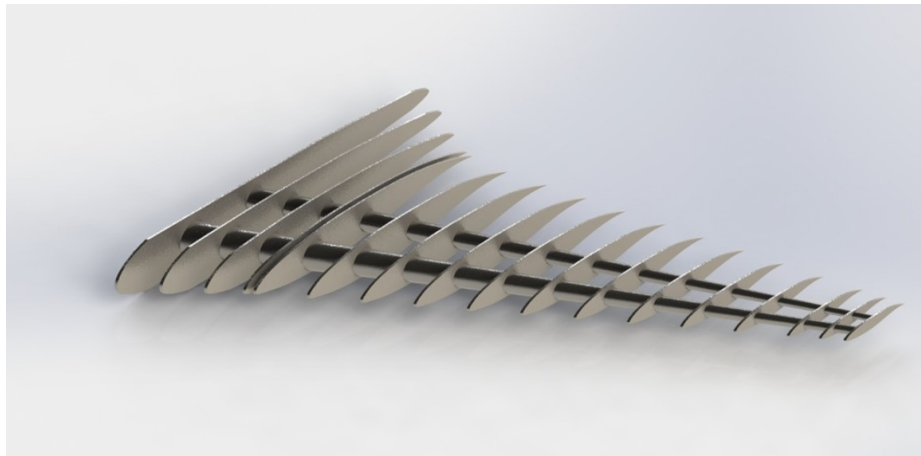


Figure 38: Render of initial rib and spar structure without skin.

To determine a suitable mesh for FEA analysis, a grid independence study shown in Table 24 was conducted ensuring both accuracy and efficient simulation time were achieved for the more complex model.

Grid size (m)	Number of Nodes	Von mises stress result (Pa)
0.5	48357	1.087e8
0.45	62589	1.234e8
0.4	77451	1.389e8
0.35	87521	1.498e8
0.30	92561	1.568e8
0.25	111676	1.631e8
0.2	161047	2.3456e8
0.15	182913	2.645e8
0.11	196681	2.8828e8
0.105	212538	2.9258e8
0.1	265704	2.9276e8
0.099	289764	2.9282e8

Table 24: Grid Independence study for internal structure using tetrahedral elements.

From the study, a grid size of 0.1m was identified to be the most optimum grid size having a 0.205 % difference in results compared to the 0.099m grid size mesh. Additionally the simulation time was halved, making it a more efficient option for the project due to time and computing power constraints. The boundary conditions for the analysis were the same as those used for the solid wing.

From Table 25, this initial structure had adequate stress results within the yield limits of high strength aluminium alloys used in the aerospace industry, especially when considering the cylindrical spars. In both cases however, the structure suffered from gross deformation, predominantly at the joint between the wing root section and the main wing area, causing the structure to fail in its required role as seen in Figure 39. After this analysis, materials for the wing were decided upon using different aluminium alloys for different components shown in Section 7, providing more absolute stress limits for future analysis.

Spar Shape	Deflection (m)	Maximum Von Mises Stress (Pa)	Max. Von Mises Stress (Pa)
Cylindrical	0.0326	2.9276e8	1.6394e8
Rectangular	0.0486	3.8252e8	2.3998e8

Table 25: Stress results for FEA analysis of initial design with different spar shapes.

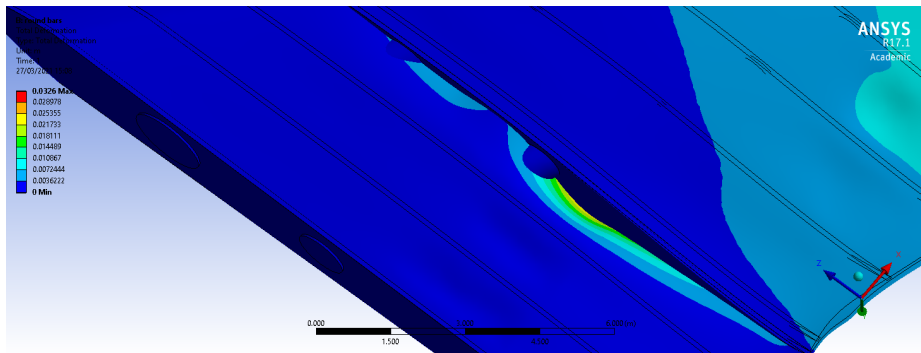


Figure 39: FEA depicting the gross deformation occurring within the root.

Further iterations were carried out to improve the wings stress results using rectangular spars while eliminating the unacceptable deformation. To achieve this, the ribs were increased in thickness to 0.16m and extra ribs were added in the area surrounding the root – main wing joint while maintaining the same spacing and loading scheme as the initial design, as can be seen in Figure 40.

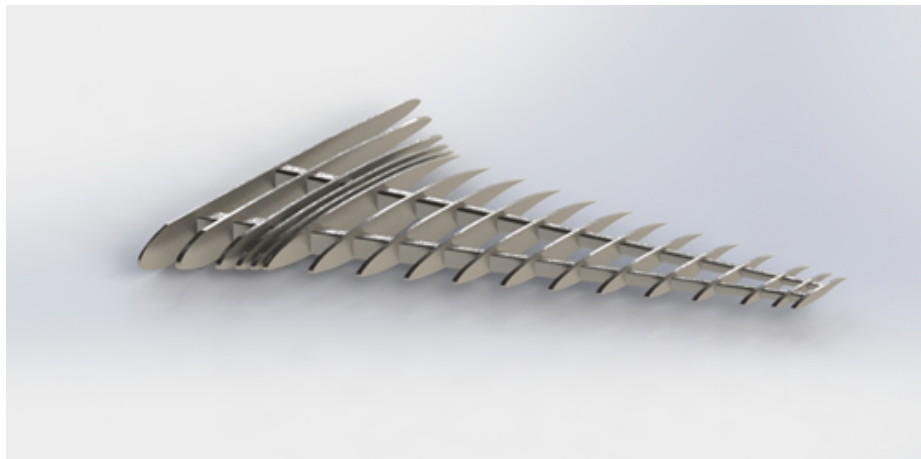


Figure 40: Improved structure with 0.16m thick ribs and extra reinforcing ribs around root-main wing transition.

As displayed in Figure 41, 42 and Table 26, these alterations eliminated the deformation issues across the length of the wing while further reducing the stresses. However, this solution had the trade-off of adding a significant amount of mass to the structure, requiring work to be undertaken with the aim of reducing the mass of the structure by removing material from the ribs.

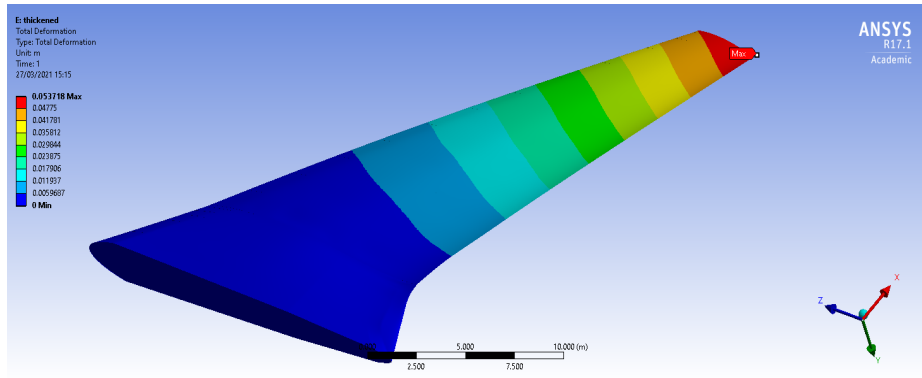


Figure 41: Logarithmic stress contour with skin stress below 100MPa.

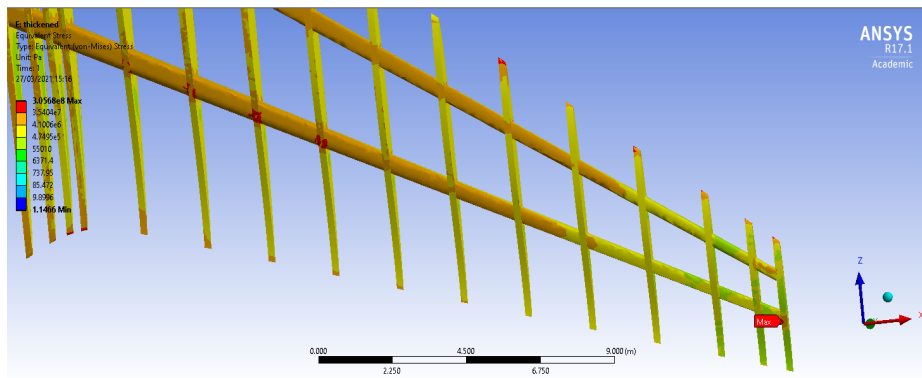


Figure 42: Internal structure stress contour with maximum stress at spar and last rib.

Iteration Number	Deflection (m)	Maximum Von Mises Stress (Pa)	Max. Principal stress (Pa)
6	0.053718	3.0568e8	2.3791e8

Table 26: Stress and deflection results for FEA analysis of iteration 6.

The initial iterations of mass reduction were achieved through manual means of removing sections of material from areas of the ribs in a trial and error manner. Although this removed mass from the structure, different configurations would cause variations in stress levels with certain designs having quite significant stress concentrations such as iteration 7 shown in Table 27.

Iteration Number	Deflection (m)	Maximum Von Mises Stress (Pa)	Maximum principal stress (Pa)
7	0.051455	2.7443e8	2.2147e8
8	0.049725	5.274e8	3.3609e8
9	0.046879	3.5687e8	3.256e8
10	0.046188	3.5366e8	3.102e8

Table 27: Stress and deflection results for FEA analysis of iterations 7-10.

Iteration 10 shown in Figure 43 has stress results that are within the selected material yield limits, although there was still room for improvement. Achieving an optimal design was proving to be ineffective and inefficient through manual means and a need for an analytical method was identified.

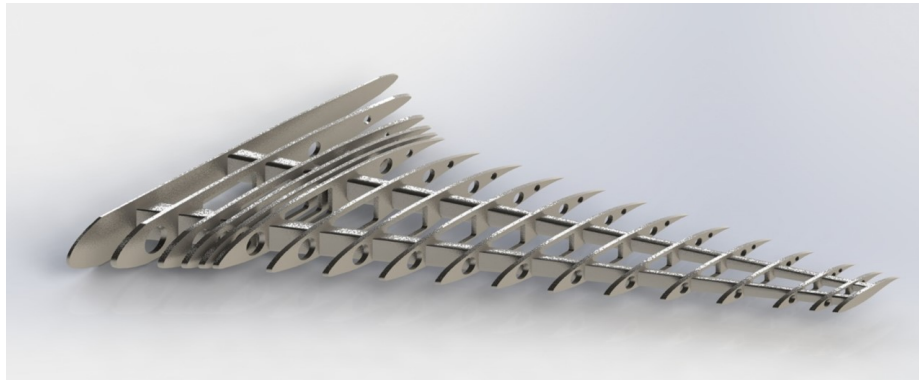


Figure 43: Render of current iteration of internal structure featuring mass saving cut outs.

5.6.8 Wing Structure Topology Optimisation

Identifying the shortcomings of manual optimisation, research was conducted into optimisation methods used for similar structures. A number of sources create their own numerical methods carry out rib optimisation [31]. Due to time constraints, topology optimisation features built into 3D CAD software were used in this case. The function solves the problem using FEA and provides a scale of what material is critical and what is not necessary to safely bear the load depending on selected material and selected goals. This output did not account for the desired shape or function of the model so had to be used as a reference. Iteration 6 was used as the base design, being loaded in the same manner as the FEA analysis with a mass reduction goal of 50% used.

Using the reference shown in Figure 44, a design was created, attempting to stay as close to the reference as possible while remaining practical in its desired function. This led to the creation of iteration 11 shown in Figure 45.

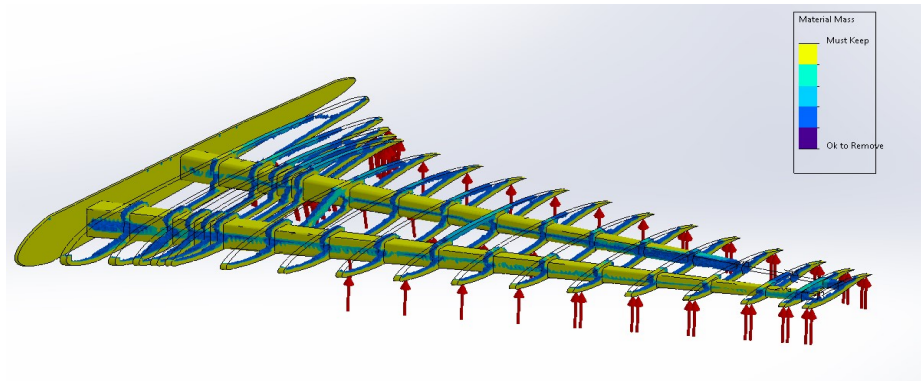


Figure 44: Output of Solid works Topology optimisation tool used as design reference.

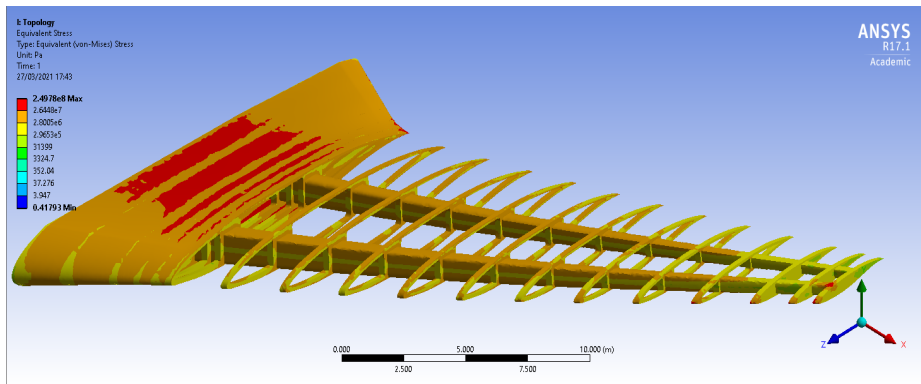


Figure 45: FEA stress contours results for the iteration 11 design.

Exhibited in Table 28, the software optimised design far outperforms the manually optimised design reducing the stress by over 100 MPa while significantly reducing the mass of the structure. Iteration 11 reduced the mass from the original iteration 6 by around 24 tonnes; however, this only considered the ribs and not the solid spars.

Iteration Number	Max. Von Mises Stress (Pa)
10 (manual)	3.5366e8
11 (topology)	2.4978e8

Table 28: Stress results comparison of manual optimisation vs using topology function.

Further iterations aimed to hollow out the spars and remaining rib material to further reduce the mass, coupled with the choice to only use the slightly lighter AL-2024 alloy for the whole structure. This allowed the final iteration to have a bar thickness of 40mm and

a total structure mass of 63.2 tonnes, including the skin.

From Table 29, it is seen that the mass of the structure has been reduced significantly by over 100 tonnes while also reducing the stress acting on the structure. The spars, having to support lighter ribs, reduce any shearing actions on the joints. Furthermore, with stress in the wing remaining under the yield limits of the chosen materials being below the 90% yield criterion, high fatigue life was ensured for the structure.

Iteration Number	Mass (Tonnes)	Deflection (m)	Maximum principal stress (Pa)
6	170.43	0.053718	3.0568e8
11	139.54	0.058441	2.4978e8
12	97.995	0.068915	2.3497e8
13	63.2	3.5366e8	2.2584e8

Table 29: Mass, stress and deflection results for FEA analysis of iterations 11 - 13.

5.6.9 Fuselage Structure

The fuselage structure of an aircraft is an essential component given the difficult task of having to withstand high loads while remaining relatively light and thin. The dominating force that it has to deal with, especially when regarding the skin, is differential pressure loading at altitude as seen in Figure 46. Internal pressure is generally set between 10.5-11.2 psi for ensuring passenger comfort, whereas the external pressure decreases as altitude increases; this induces an increased differential pressure at high altitude, which ultimately increases the load acting on the skin and pressurised structures.

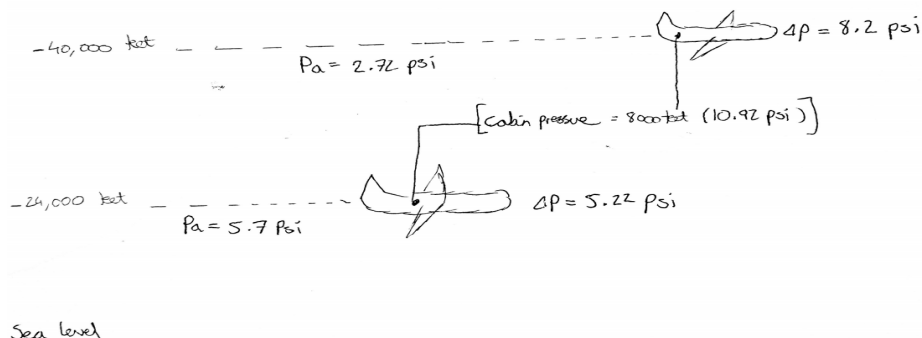


Figure 46: Sketch illustrating the increase of differential pressure as altitude is increased.

These problems can be further exacerbated when it comes to BWB design which loses the pressure bearing strengths of a cylindrical fuselages. There are a number of structure design schemes when it comes to conventional aircraft design such as: monocoque; the more common semi-monocoque, or the more modern lattice design. These design concepts are difficult to apply to BWB designs due to modelling complexity from the irregular non-cylindrical geometry, but also the large area of skin that is wrapped over a geometry inefficient at being pressurised, causing it to fail unless it is much thicker than standard designs. Research has been conducted to counter act this problem such as [27] which presents the concepts in Figure 47.

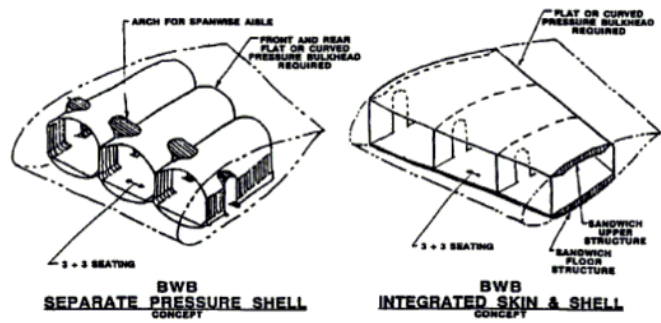


Figure 47: Structural concepts for BWB designs [27].

An initial design for pressure loading was created using the cylindrical pressure shell concept where due to time constraints only a section of the fuselage was analysed. The design consisted of interlinked quasi-cylindrical shells reinforced by rigid frames shown in Figure 48. This design meant that there would be an internal shell for the internal pressure, leaving a much thinner outer skin that only had to consider external loading, thus removing the differential pressure loads. This initial iteration of the design failed significantly when loaded to the internal pressure alone, with the shells having stress resultants several orders of magnitude greater than the desired material yields.

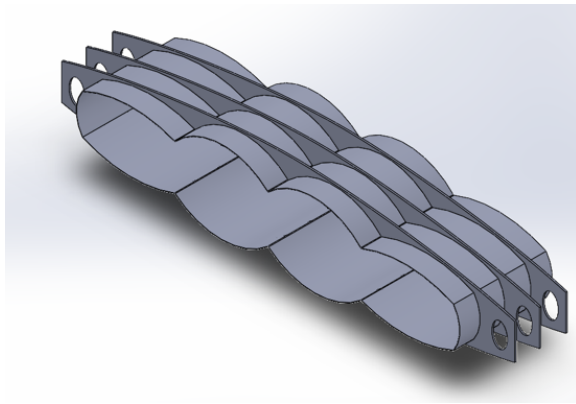


Figure 48: 3D CAD Model of initial fuselage structure section design.

Despite the early setbacks, it was thought that this design would have promise if reworked and was improved over several iterations. This process involved thickening the pressure shell significantly to 20 mm and adding additional reinforcement in the lengthwise direction to add additional support, as shown in Figure 49. Although these improvements brought the structures stresses down significantly, the design was still over the yield stress of the desired aluminium alloys due to significant stress concentrations in less rounded areas of the structure.

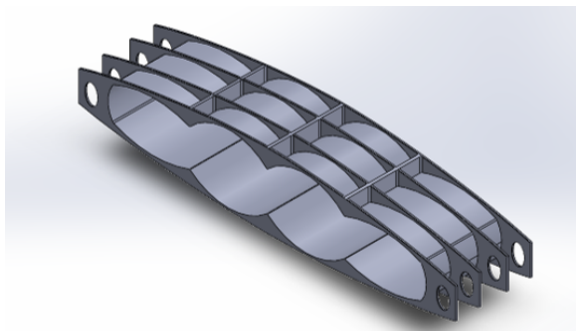


Figure 49: 3D CAD model of fuselage section iteration 6 showing design improvements.

The final iteration, shown in Figure 50, focused on eliminating or mitigating these stress concentrations, rounding out features while reducing mass by hollowing the frames and shell. Producing a final iteration that satisfied the loading conditions while being within the yield limits of selected materials.

From Table 30 the stress reduced significantly between iterations 6-12 to around 386 MPa. The frames having low values of stress, feasibly being made of the light AL-2024 alloy. When looking at areas of the shell, the contour results were within the yield especially for the higher strength variants of AL-2024. However, the results were concerning in terms of fatigue life, which approached the 90% yield criterion of that alloy; so the higher strength

but slightly heavier AL-7075 was considered to be the better option for the shell.

Iteration Number	Max. Von Mises Stress (Pa)
6	6.721e8
12	3.9863e8

Table 30: Stress results comparison between different iterations.

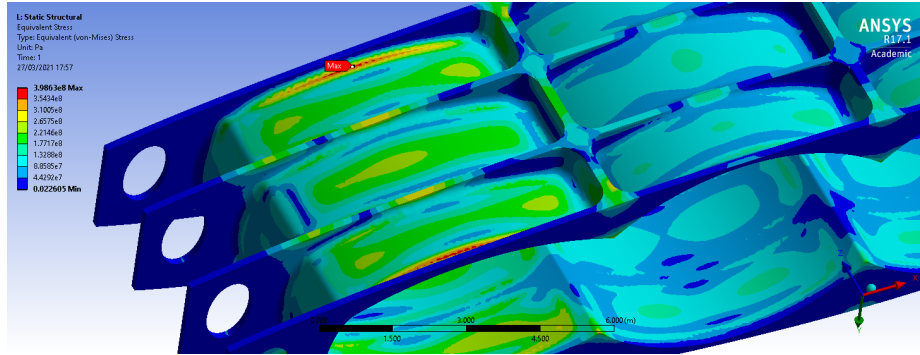


Figure 50: FEA stress Analysis of iteration 12.

5.7 Stability and control

5.7.1 Static Stability

Static stability is the ability of an aircraft to return to its original state when disturbed, for example if a statically stable aircraft's nose is pointed up due to a disturbance it will immediately lower its nose to return to the original state. This project only considers longitudinal stability as it is the most important stability direction for large aircraft.

An essential component used in stability analysis is the centre of gravity (c.g.). For brevity, only the key components and where they were located in the x-axis were used to determine this. All components were simplified to point masses with the landing gear and fixed equipment mass being taken from a paper which used a similarly sized BWB aircraft[32]. The other masses were taken from the weight estimation method discussed in Section 6.3, assuming a 3-engine configuration. These masses and their location are as detailed in Table 31 and Figure 51.

Description	Mass (Tonnes)	location	x distance (m)
Fixed Equipment	73.315	A	10
Landing Gear	46.246	B	32
Wing	128	C	33
Payload	63.470	D	27.4
Fuel	121.930	E	33.5
Propulsion	24.846	F	38.25

Table 31: Point masses and their locations.

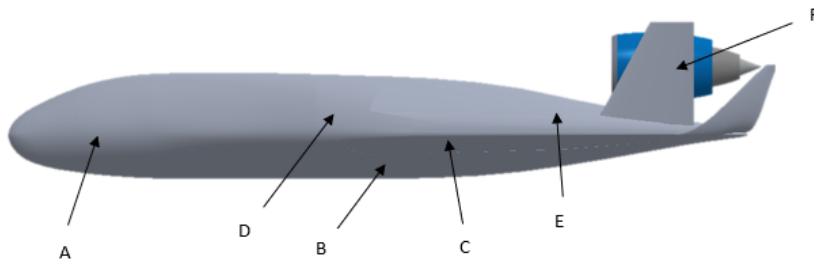


Figure 51: Locations of point masses on aircraft in longitudinal direction.

Using the values in Table 31, the centre of gravity was determined for different loading scenarios:

1. Empty Weight = 27.1189m
2. Empty weight + payload = 27.1909m
3. Empty Weight + fuel = 29.092m
4. Empty Weight + Payload + Fuel (MTOW) = 28.8713m

5.7.2 Static Margin

The static margin is an indicator of aircraft stability, calculated using the Mean Aerodynamic Chord (MAC) of the aircraft, which is the average of the wing and tail chords; Neutral Point (NP), which is the centre of mass point where the aircraft would be neutrally stable; and c.g. The MAC and NP are calculated using the characteristics of the wings and tail. However, in the case of a BWB aircraft there is a number of design elements that do not allow the traditional calculations to be undertaken, so some large assumption were needed to be made to allow their deployment. The BWB design has no distinct tail section, so it was assumed part of the tail section was representative of a tail plane. The half span

of the aircraft was assumed to include the body of the aircraft, hence the value of 40m was taken; however, the rest of the wing parameters were kept the same as a conventional aircraft. With these assumptions, the MAC of the aircraft was calculated to be 13.63m and the NP was found to be 11.48m aft of the wings leading edge. Using these 3 parameters the static margin was calculated for each loading case using Equation 3.

$$\text{StaticMargin} = \frac{NP - CG}{MAC} * 100 \quad (3)$$

The c.g is the only parameter that changes per case so for each case was represented in its relation to the wing leading edge to remain consistent with value of the NP.

C.g aft of leading edge for each case was 8.217m, 8.29m, 10.19m and 9.968m respectively, therefore the Static Margin (SM) for each case is:

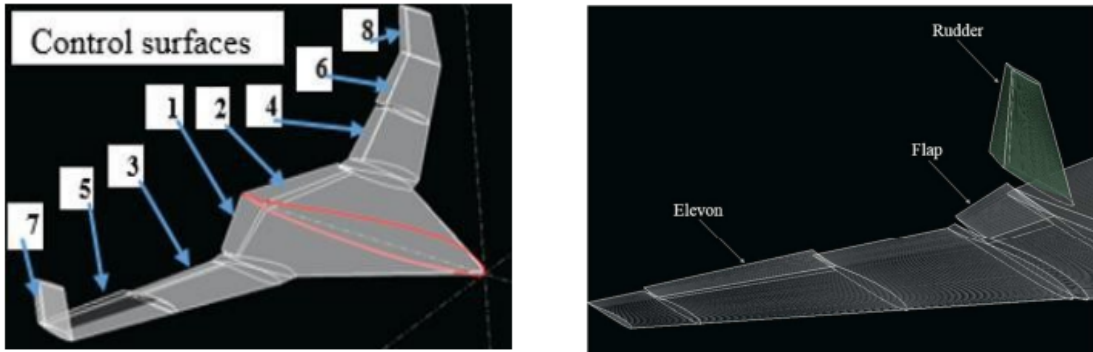
1. SM-Empty Weight = 23.9 %
2. SM-Empty Weight + Payload = 23.4 %
3. SM-Empty Weight + Fuel = 9.5 %
4. SM-Empty Weight + Payload + Fuel (MTOW) = 11.1 %

The typical range for desirable static margin is 5%-15% with a lower static margin indicating a less stable aircraft and a higher margin indicating a more stable aircraft. However, the aircraft becomes too nose heavy with possible elevator stall occurring on takeoff if SM exceeds 15% by a significant amount. The empty weight and payload laden aircraft cases were found to be nearing too stable, requiring control surfaces and systems to work harder. Although the aircraft would normally not fly under these conditions except for possibly during initial flight testing. At the end of cruise the aircraft may have a nose down tendency on descent where only a small amount of reserve fuel remains; even so, the SMs in these cases were deemed to be within the reasonable range for airworthiness. When the aircraft is at its maximum fuel capacity, it was found to be at its least stable configuration with the most manoeuvrability, trending towards the stability of the empty aircraft as fuel is burned. When looking at the aircraft in realistic flying configurations for service, the aircraft was stable being closer to the upper end of the desired range with capabilities of performing essential manoeuvres. This was considered suitable for passenger aircraft where comfort is a priority and aerial acrobatics are not required. If the 4-engine configuration was considered, the centre of gravity would be brought slightly further back with minor decrease in stability.

5.7.3 Control Surfaces and Dynamic stability

Control surfaces and dynamic stability are important areas in aircraft design. Due to the time frame and the scope of the project, these areas were not specifically investigated. In terms of control surfaces, the BWB concept is well suited to implementing control surfaces

having very similar placements to conventional aircraft, notably when looking at the wings. Figure 52 shows control surface layout for similarly sized designs.



(a) Full control surface layout for BWB concept [32]. (b) Sectioned control surface layout for BWB concept [33].

Figure 52: Example control surface layouts from different projects on similarly sized BWB concepts.

From Figure 52, a combination of flaps and elevators may be placed along the trailing edge of the wings with elevators implemented on the tail section of the BWB aircraft. Rudder control may be handled by the existing vertical stabiliser but could also be included into the winglets to provide greater lateral control.

Dynamic stability is how an aircraft responds over time to a disturbance, where positive dynamic stability means the disturbed aircraft will oscillate damping out over time to its original state which is desired for large aircraft. The opposite is the case for negative dynamic stability where these oscillations grow in size over time. Dynamic stability is complex and was considered not feasible in the time frame of the project; however, research by Paudel et al. into the dynamic stability of a similarly sized design was dynamically stable in the phugoid, dutch roll, roll and spiral modes using eigenvalue analysis, so it can be assumed that such concepts can be dynamically stable also [33].

5.8 Interior Layout

In order to estimate the passenger capacity of the final design of the BWB aircraft for informing direct operating cost calculation, the seating layout in the main cabin area was modelled by considering three separate configurations: 1-Class (Economy), 2-Class (Business and Economy), and Cargo only. The passenger-cargo configuration was also further investigated for its capability in temporarily transporting cargo without the necessity to convert the passenger aircraft to a freighter in the event of a heavy aviation hit, such as an

ongoing pandemic. Relevant regulations as stated in CS-25 for airworthiness were examined, with designs and calculations carried out in adherence. Emergency egress procedure for such aircraft was also investigated.

5.8.1 Cabin Layout Methodology

Based on the final exterior model and the fuselage structure of the designed BWB aircraft, the cabin floor was first modelled according to the width of different sections, and aft sections where the height was low were excluded from the cabin area. The final cabin sizing and placement is shown in Figure 53.

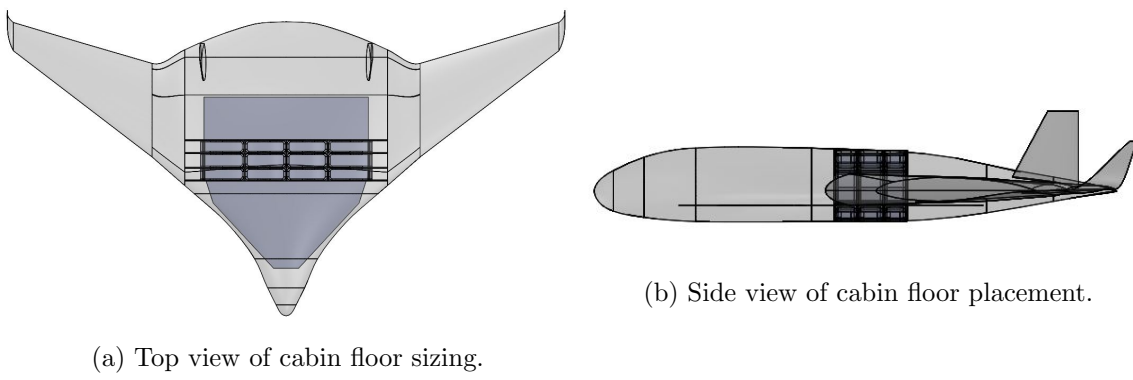


Figure 53: Cabin floor placement.

Passenger Configuration

Seating widths and pitches for economy and business classes were decided based on typical dimensions listed by Raymer [34] as shown in Table 32. Lower to medium range of the dimensions were chosen for more economical solutions with reasonable passenger comfort. The seats were modelled as boxes in Solidworks assuming same length and width, then assembled into groups of 2 and 3 for business and economy arrangements respectively.

	First Class	Economy
Seat pitch (in.)	38-40	30-36
Seat width (in.)	20-28	16-22
Chosen Seat pitch (in.)	38	32
Chosen Seat width (in.)	21	18

Table 32: Typical seating dimensions and chosen dimensions, adapted from [34].

Standard certifiable emergency exits were modelled according to CS-25, 5 Type A and 3 Type B exits were placed on each side of the cabin floor, with distance between any 2 adjacent exits being less than 60 feet [35]. A preliminary single class seating arrangement was first considered for estimating possible maximum passenger capacity, as shown in Figure

54, where economy seating groups were linear patterned covering the cabin floor. Passages leading up to the exits were kept at least 36 inches wide [35]. Dimension for one lavatory was taken as 40" x 40" shown in green [34] and galley areas shown in orange colour were roughly evaluated based on current commercial aircraft British Airways A380 [36].

Initial layout estimated a maximum passenger count of 639, which was used for a more detailed sizing of galley and wardrobe floor space using Equations (4)-(5) [37].

$$S_{galley} = 41 * \frac{n_{pax}}{1000} + 0.5m^2 \quad (4)$$

$$S_{ward} = 0.03 * (1 - 3 * \frac{n_{aisle}}{n_{pax}}) * n_{pax}m^2 \quad (5)$$

Where n_{pax} and n_{aisle} are number of passengers and aisles respectively.

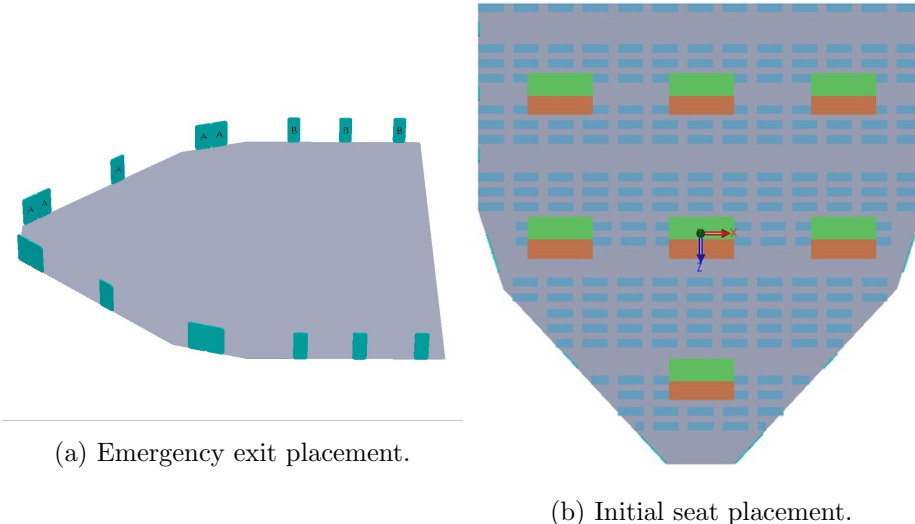


Figure 54: Initial layout design.

Lavatory space was decided according to the number of passengers as stated in Table 33.

	First Class	Economy
Passengers per lavatory	10-20	40-60

Table 33: Typical lavatory count, adapted from [34].

Cargo Configuration

Available height between the cabin floor and the fuselage structure was measured, allowing most suitable commercially available cargo containers to be decided, such that the container height did not exceed maximum available space while the unutilised space was kept at minimum. Due to the restricted vertical space below the cabin floor, customised cargo

containers were designed with standard width and depth, but reduced height. All containers were modelled in Solidworks with dimensions shown in Table 34 and assembled with the fuselage structure for evaluating the cargo carrying capability of the aircraft.

Container Code	Width (in)	Depth (in)	Height (in)	Volume (m^3)
LD-1(AKC) [38]	92	60.4	64	5
M-1H(AMD) [38]	96	125	118	21.2
Customised	92	125	40	6

Table 34: Cargo container dimensions.

5.8.2 Consolidated Layout Design

Passenger Configuration

Following the methodology as stated previously, spacing between rows of seats were further tuned for uniformity. Passageways leading to emergency exits were kept at 36" to meet the minimum requirement. Additional lavatories were placed for 2-class configuration to meet the typical industry standard. The consolidated layouts and their capacities compared to that of A380 are as shown in Figure 55 and Table 35.

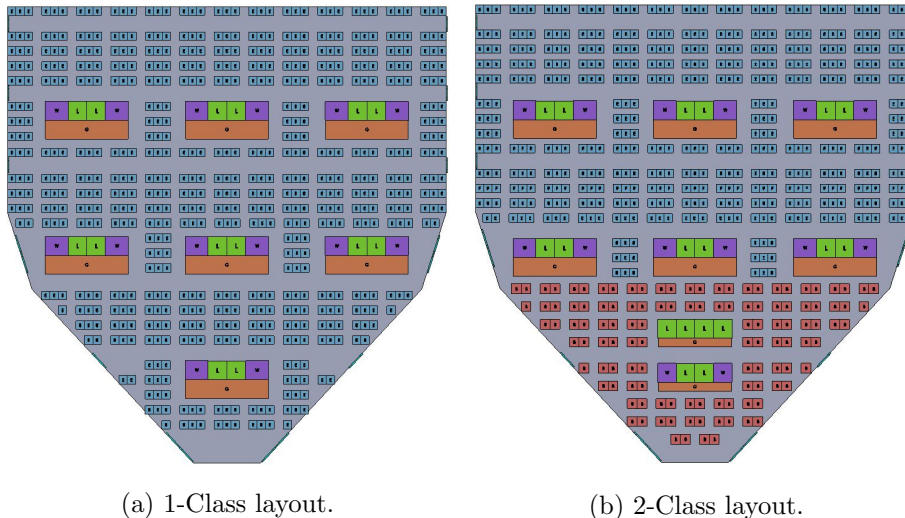


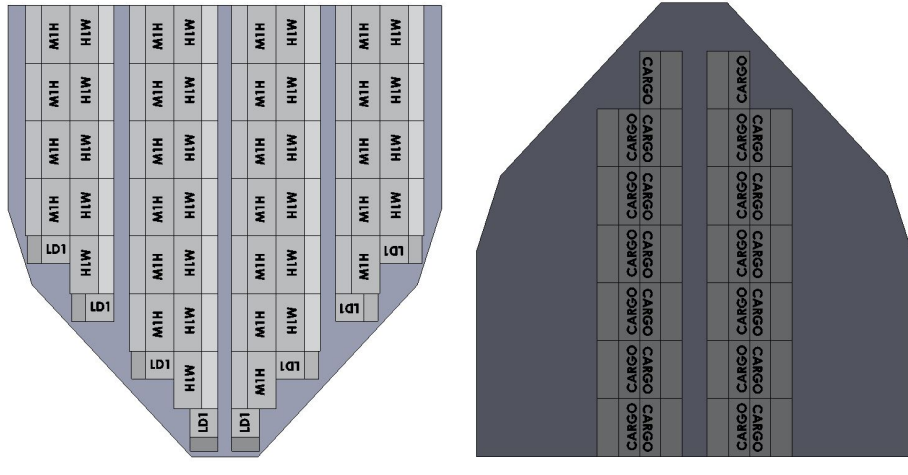
Figure 55: Cabin layout - passenger.

	A380 (1-Class)	BWB (1-Class)	A380 (2-Class)	BWB (2-Class)
Pax. No.	868	604	555	562
Lavatory No.	-	14	17	18
Galley Area (m^2)	-	31.5	-	31.5
Wardrobe Area (m^2)	-	17.5	-	17.5

Table 35: Passenger capacity comparison between A380 and BWB.

Cargo Configuration

As the studied counterpart freighter variation of A380 never entered production, the current freighter aircraft with the largest cargo capacity B747-8F was used as comparison. The total cargo volumes for the two aircraft are listed in Table 36, the BWB was found to hold up to 31.8% higher capacity compared to B747-8F. 13.6% higher if only standard containers were used. It should be noted that the landing gear space was not deducted from the BWB lower hold volume; however, the additional available space on the two sides of the lower compartment was also excluded in this case due to the lack of suitable standard containers. The said space may be utilised with other forms of storage, hence offsets the room occupied by landing gears. The cargo placement is shown in Figure 56.



(a) Cargo layout - top view.

(b) Cargo layout - bottom view.

Figure 56: Cabin layout - cargo.

	B747-8F[39]	BWB
Main Deck (m^3)	692.7	972.8
Lower Hold (m^3)	164	156
Total (m^3)	856.7	1128.8

Table 36: Cargo volume comparison between B747-8F and BWB.

5.8.3 Evacuation Considerations

Unlike conventional tube-and-wing aircraft with comparatively narrow fuselage designs, the wider BWB fuselage design requires a majority of passengers to traverse the aircraft in order to reach an emergency exit at the fuselage periphery. To date, the aviation industry has no physical experience dealing with concerns surrounding emergency egress for such an aircraft design [40]. CS-25 Appendix J requires that all passengers must be able to be safely evacuated in under 90 seconds while using no more than 50% of the available emergency exits [20].

Previous work by D’souza discusses the difficulties in emergency exit placement for a BWB design, with limitations imposed by the reduced ratio of accessible wall surface to aircraft volume [41]. D’souza suggested utilising tunnels to allow emergency exits to be accessed from the rear of the aircraft, however admitted this approach does not meet FAA regulations [*ibid.*]. Galea *et al.* performed a computer simulated evacuation of a 1000 seat BWB design to explore evacuation difficulty and fire hazard. Galea *et al.* consider a single class configuration with 20 emergency exits, however no consideration is given to the feasibility of these exits.

This section proposes an alternative passenger evacuation model. It aims to assess the feasibility of the proposed interior layout in a worst-case scenario. An initial validation study is performed considering the floorplan of a single-class Airbus A380 with 868 seats. All exits on one side of the aircraft are closed to mimic Airbus’ 2006 evacuation test where all passengers were successfully evacuated in 78 seconds [42]. Following this, the single class BWB interior layout proposed is simulated for two cases: first, with all exits available, and second, with only fore aircraft exits available. This second case is considered a ‘worst-case’ scenario, where only 50% of exits are available and a majority of passengers must traverse the entire length of the plane to reach an exit.

Methodology

In absence of open source modelling software uniquely suited to this type of simulation, a model was created in Python. The model makes use of three connected environment models:

- Aircraft layout map

- 2D Occupancy grid
- Weighted bidirectional graph network

The layout map is a 2D array representing a discrete component model of the aircraft, including walls, isles, seating, and internal structures; for example, toilets and galleys. The layout map is static, and is used to seed the remaining environment models. The 2D occupancy grid serves to track the position of each occupant throughout the simulation, while the graph network is used to model the relationship between elements in the environment and to allow individuals to select paths through the aircraft interior. This is achieved by modelling each discrete point in the layout map as a node, and connecting all adjacent nodes. The weighting of edges between nodes is updated to reflect their relationship: all edges connecting to walls have a weight of infinity, to prevent occupants moving through walls, while edges between isles have a low weight to facilitate movement along anticipated pathways. This approach allows individuals to identify optimal pathways to emergency exits by using Dijkstra's algorithm to identify the shortest paths between two nodes.

The simulation is temporally discretised into 0.5 second timesteps, with an initial delay of 11.1 seconds for cabin attendants to open the emergency exits [43]. Each individual requires time to decide how to move, taking between 0 and 15 seconds before making an initial move. During this time each individual evaluates a number of possible routes to emergency exits using Dijkstra's algorithm. Each individual selects their initial route using a weighted random selection where probabilistic weights are assigned by applying the softmax function to the path lengths; in this way individuals are more likely to select shorter exit paths. As the simulation progresses, it is likely for individuals to become stuck in exit queues. Individuals will re-assess their selected route in this situation, dependent on how long they have waited since last moving and if there is an alternative path available. The period of time individuals are willing to wait decreases as the simulation continues. The complete code for this simulation is given in Appendix K.

Results

An initial validation study was performed considering a single class A380 configuration (868 seats), with an expected egress period of roughly 80 seconds when using exits on only one side of the aircraft. In Figure 57 we see the locations of all remaining individuals at $t = 0$ and $t = 50$ seconds. For the case shown, when only 50% of exits are available, evacuation was completed in 73 seconds on average, considering 10 simulations. This is close to the time encountered during Airbus' physical test [42], indicating the model is a good approximation of a real emergency egress situation. When all exits were available, evacuation was performed on average in 44 seconds.

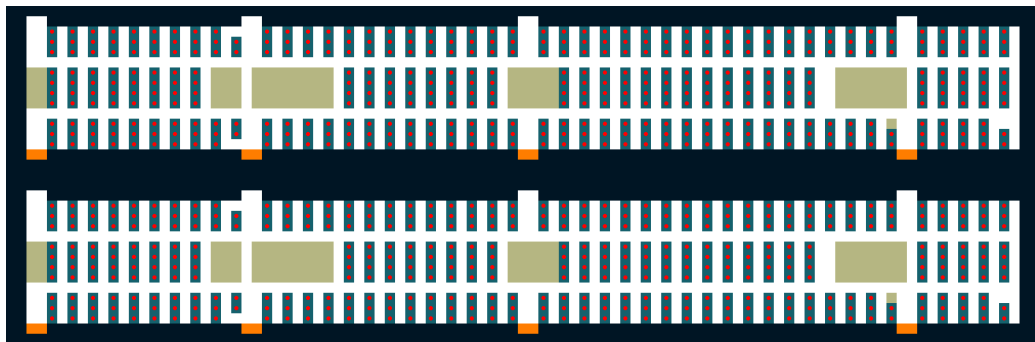
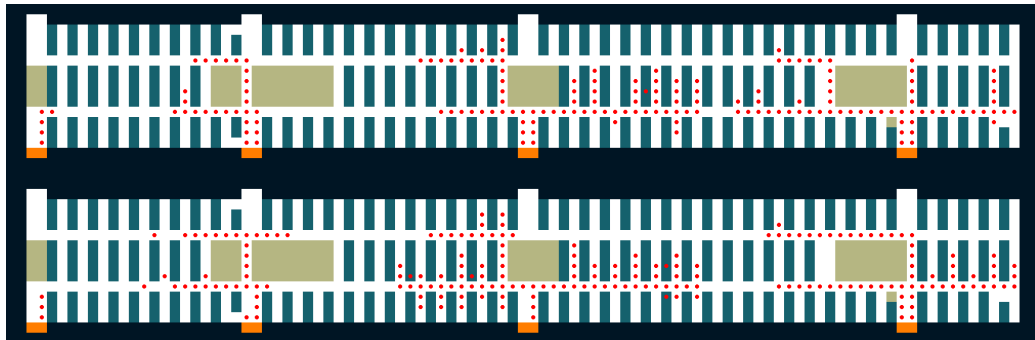
(a) A380 simulation. $t = 0$ seconds.(b) A380 simulation. $t = 50$ seconds.

Figure 57: A380 validation simulation. Red dots indicate individuals. Blue areas represent seating and orange areas represent emergency exits.

Applying the simulation to the proposed single-class BWB configuration (604 seats), complete egress is observed to be achieved on average in 55 seconds. This is significantly below the requirements of CS-25, but is longer than the egress period for the larger 868 seat A380. This reflects the difficulties anticipated when evacuating a wider-bodied aircraft. The worst-case emergency exit scenario, where all rear exits are unavailable, is shown in Figure 58. In this case, complete egress requires 98 seconds on average. Although this is greater than the 90 second requirement, it is noted that individuals in the simulation tend to favour closer exits as opposed to quiet exits (due to the softmax probability function), and as such the suggested egress time may be inflated. In a real emergency situation where cabin staff assist in directing occupants to quiet exits it is likely that the evacuation time would fall below the mandated 90 seconds. Additionally, when using a 2-class configuration the capacity of the aircraft will be reduced and egress will be faster.

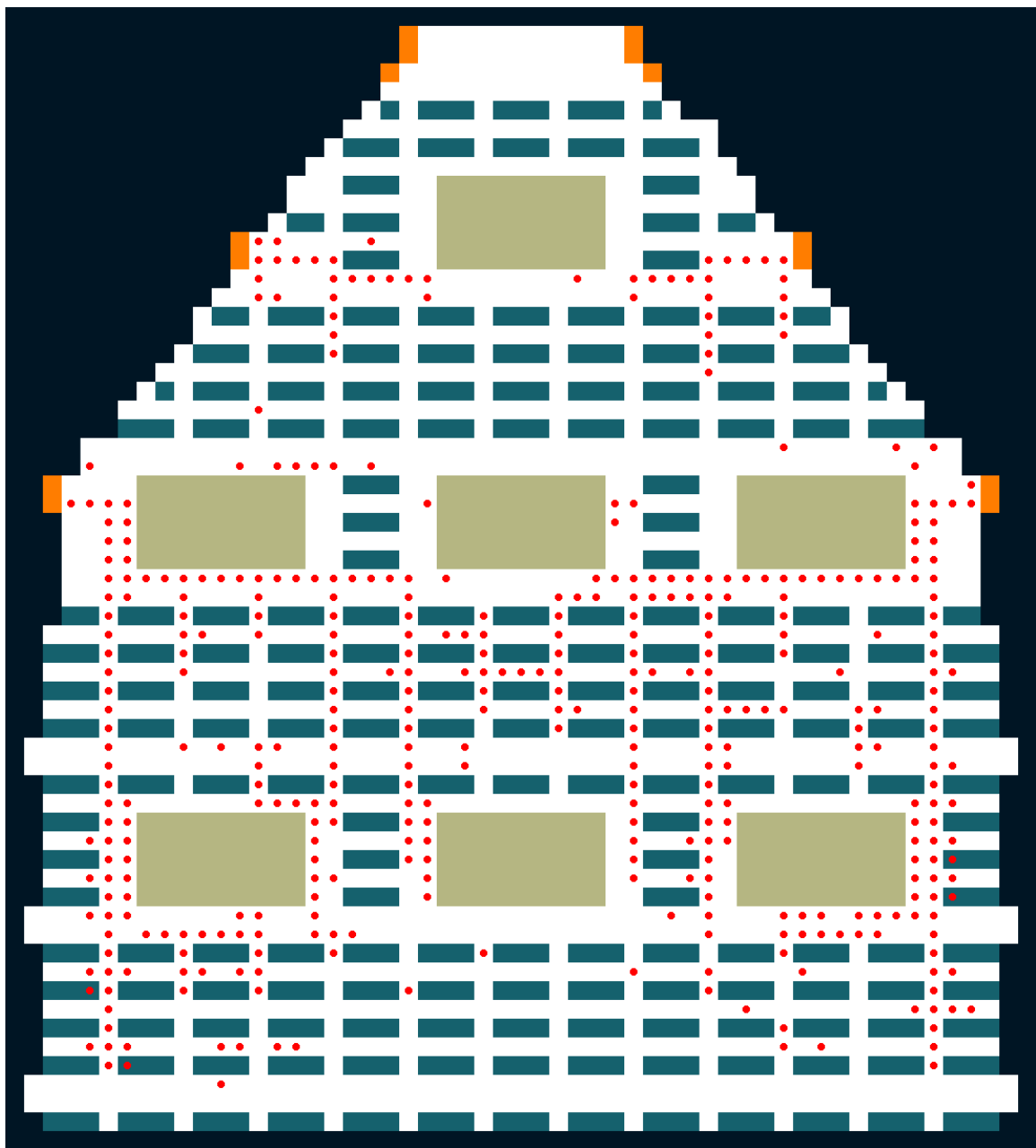


Figure 58: BWB single-class simulation. Worst-case: all aft exits unavailable. $t = 50$ seconds. Red dots indicate individuals. Blue areas represent seating and orange areas represent emergency exits.

5.8.4 Cargo-Passenger Configuration

Due to current global and industry circumstances, consideration was given to the benefit of the BWB design should it be directly introduced to the world. Presently, due to the travel restrictions induced by the Covid-19 pandemic, most commercial aircraft have been grounded. In response, EASA released a new guideline (Transport of Cargo in Passenger Compartment - Exemptions Under Article 71(1) of Regulation (EU) 2018/1139) regarding the use of the grounded passenger planes for cargo transportation during the duration of the pandemic, to aid in the continual supply of "*critical products such as food, medical supplies and personal protective equipment (PPE), and other products [44]*". By guideline definition [44]

"The exemption should allow, on a temporary basis and as applicable or necessary, the transport of cargo and a limited number of occupants in the passenger cabin, if justified by a fire risk assessment. Cargo items may be installed on seats, with adequate restraint systems/means, or, if seats are removed, directly attached onto the aircraft floor by using the available seat tracks."

As a result of the novel shape, the BWB design allows for a wider floor plan, which was initially considered an advantage over traditional aircraft in the transportation of pallets of essential items and additional cargo.

Regulations

Building upon the existing guidelines regarding stowage in standard operations (CAT.OP.MPA.160) [45] and adherence to the new EASA guideline [44], further new operational aspects must be considered in the preparation and operation of the aircraft for such a configuration, and should be included in the estimation of available cargo volume. The most prominent aspects of which are detailed in Appendix D.

In preparation for loading, the passenger convenience systems and automatic supplemental oxygen systems must be deactivated. Besides conforming to cargo restraint specified by CS-25.561 and aircraft structural requirements [35], the cargo loading should ensure[44]:

- A minimum of one longitudinal aisle meeting the minimum dimensions of at least 0.51m width is present
- When the cargo is loaded on the floor
 - Height of the cargo should not exceed 1.27m
 - Volume should not exceed $3.54\ m^3$
 - Access must be available fore and aft of each loading area where aisles must be at least 0.51m width, access of at least 0.38m width and no obstructions in pathways

BWB Cargo Capabilities

To conclude whether the BWB configuration would prove an advantage in this use, brief calculations for total cargo loading volume of the A380 and BWB were calculated. For a fair comparison of cargo holding capability, the following aspects were assumed for both:

- 1-class economy layout
- Seats would be 17.5" (44.45cm) in width - as is the standard economy width in multiple A380 configurations [46] [36] [47] and so as to allow for parity and 0.51m regulation aisle width in the BWB configuration
- Regulation access of 0.38m allowed fore and aft of each loading area
- Loading area is defined as an individual area of maximum regulation load volume within an aircraft section
- Passenger seats would be removed for floor cargo storage so as to maximise loading capabilities
- Loading areas only within the current seating areas to ensure compliance with spacial regulations and aid in aircraft stability and safety
- Loading areas of aircraft sections would not exceed the current seat track width so as to allow for easy and robust securing of the cargo by nets attached to the seat tracking

For the calculation of the A380 cargo volume, the interior layout for economy seating, exit routes and facilities of a Malaysia Airlines aircraft [48] was used as a basis for determining the available cargo area. As the emergency exit widths are given, which can not be obstructed, and the area unavailable due to the placement of the facilities can be calculated in terms of corresponding rows of seats, the available cargo area can be calculated for each lettered section (Figure 59) by subtracting the unavailable area from the total deck length. Due to the 1-class economy assumption, the seating configuration of the sections can be assumed to be continued along the entire deck length.

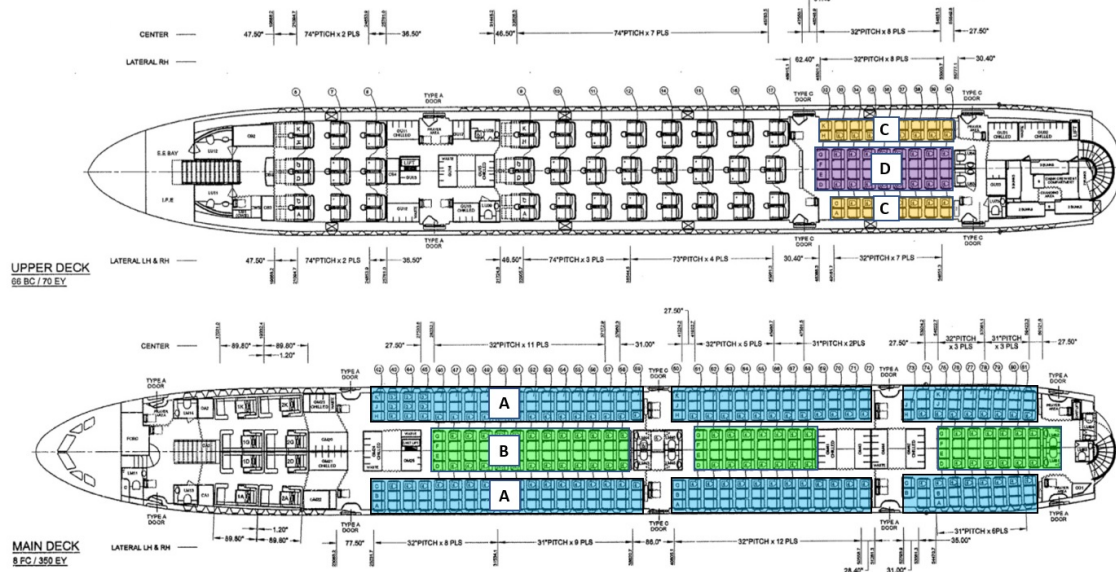


Figure 59: Colour coded A380 layout for seating formations considered.

In reference to the available length of each deck for a corresponding section, the width of the exit paths will be referred to as the length for ease of comprehension. For the main deck, based on the interior layout shown in Figure 59 (larger image in Appendix C), in section A it was assumed that there were 3 exit paths of 0.787m (31") length and 2 exit paths of 1.969m (77.5") length which would be unavailable, and in section B, this plus an additional 12 seat rows (due to space taken by the facilities) would be unavailable. Each seat row is equivalent to 0.699m (27.5"). For the upper deck, the same logic is applied hence in section C and section D it was assumed that 2 exit paths of 1.969m (77.5") length, 2 exit paths of 1.334m (52.5") length and 7 seat rows are unavailable. Where the main deck total length is 49.9m (1965") and the upper deck total length is 44.93m (1769"), the available lengths for each section are given in Table 37.

Section	Total Length (m)	Unavailable Length (m)	Available Length (m)
A	49.9	6.3	43.6
B	49.9	14.68	35.22
C	44.93	12	32.93
D	44.93	12	32.93

Table 37: Available cargo loading lengths for each section.

Each section is required to have designated loading areas within so as to not exceed the maximum volume limits and to make securing of the cargo simpler. Therefore, with a limited volume size, height and width, the length of each loading area (l) can be calculated

from a basic volume formula. Allowing for 0.38m fore and aft of the area, the available length of the section is divided by the loading area total length (l_{lat}) to determine the number of loading areas (N_{la}) achievable. The number of loading areas is then multiplied by volume limit to calculate the loading volume of the section (V_{sect}). Full calculations for each section can be found in Appendix D. The total loading volume of the A380 was determined as 265.5m^3 and the breakdown of section volumes can be seen in Table 38.

Section	Quantity	Section Volume (m^3)	Total Volume (m^3)
A	2	53.1	106.2
B	1	53.1	53.1
C	2	28.32	56.64
D	1	49.56	49.56
Grand Total			265.5

Table 38: A380 loading area volumes.

For the calculation of the BWB cargo volume, all dimensions of the seating areas are clearly shown on the interior layout drawing, hence calculations to determine available area were not necessary. The seating areas were grouped depending on their arrangement and length as is displayed in Figure 60.



Figure 60: Colour coded BWB layout for seating formations considered [48].

Sections B, C, D and F would exceed the volume limit if considered as 1 loading area themselves, therefore, after deducting 0.38m from their length for an access, the lengths were halved so that each section would have 2 loading areas. Knowing the length, width and height, the volume of each section (V) was calculated from the basic volume equation. To get the total volume of the sections (V_{sect}), the calculated volume was then multiplied by the number of section areas. Full calculations for each section can be found in Appendix E. The total loading volume of the BWB was determined as $208.16m^3$ and the breakdown of section volumes can be seen in Table 39.

Section	Quantity	Section Volume (m^3)	Total Volume (m^3)
A	30	0.78	23.4
B	31	4.26	132.06
C	4	4.36	17.44
D	4	3.74	14.96
E	2	3.47	6.94
F	2	5.64	11.28
G	4	0.36	1.04
H	2	0.52	1.04
Grand Total			208.16

Table 39: BWB loading area volumes.

6 Propulsion

Propulsion is an essential component of any commercial aircraft. The differing geometry of the BWB in comparison to the classic tube and wing geometry allows us to explore different methods of propulsion outwith the status quo of wing mounted engines. These are explored through two main areas: a) The type of engine(s), and b) The placement of the engine(s). Different engine placements are investigated along with the effects of the type of engine used, in order to provide the BWB with an efficient and effective propulsion system using engines that are currently operational and in mass production.

6.1 In the context of the Global Design

Similar to the Aerodynamics and Structures departments, the work undertaken in the Propulsion department could itself have been the focus of a study in itself. Therefore, it was necessary to keep the work within a scope sensible for the project. Based upon the following inter-dependencies and the required outputs for progress in the other departments, work was limited to the calculation of these outputs with considerations given to areas requiring further depth of investigation.

6.1.1 Inter-dependencies

For adequate selection of appropriate engines and placement, thrust calculations had to be performed in order to define thrust parameters for flight requirements. Within the various aspects of propulsion, there are natural dependencies on:

- Aerodynamics: as it informs the aerodynamics properties required for thrust calculations
- Structure: as it informs the aircraft size and loading for thrust calculations, as well as constraints on engine placement
- Economics: as the fuel consumption characteristics from propulsion systems directly impact the DOC

Iterative changes in aerodynamics or structure were considered and accounted for in the calculations to provide optimum engine selection and placement. Propulsion updates were reviewed by the team, with new data forwarded on to the relevant design areas.

6.1.2 Inputs and Outputs

Creation of the propulsion iterative cycle identified the main inputs which would influence the propulsion requirements, and subsequently led to the development of the weight estimation method. To form a propulsion process which informed the greater iterative design process, consideration was given to the basic formulae which would provide key values for

propulsion and comparative purposes. For an encompassing yet simple overview, basic parameters were decided upon - displayed in Table 40.

Parameter	Equation	Reference
Take-off weight	Weight estimation method in following section	Bradley [49], Kroos [50], Kumar [51], Tulapurkara [52]
Total empty weight	Weight estimation method in the following section	Bradley [49], Kroos [50], Kumar [51], Tulapurkara [52]
Stall speed	$V_{stall} = \sqrt{\frac{2W}{\rho S C_{Lmax}}}$	Afsar [53]
Lift-off speed	$V_{lift-off} = 1.1V_{stall}$	Gudmundsson [18]
Take-off speed	$V_{take-off} = 1.2V_{stall}$	Gudmundsson [18]
Cruise speed	$V_{cruise} = M_{cruise} \sqrt{\gamma R T_a}$	Taylor [54]
Take-off distance	$(\frac{T}{W}) = \frac{1.1^2}{C_{Lmax} \rho g (\frac{T}{W})} (\frac{W}{S})$	Gudmundsson [18]
Climb thrust at 10°	$T = W(\frac{\cos(10)}{\frac{L}{D}} + \sin(10))$	Taylor [54]
Climb thrust at 15°	$T = W(\frac{\cos(15)}{\frac{L}{D}} + \sin(15))$	Taylor [54]
Cruise thrust	$T_c = \frac{W}{\frac{L}{D}}$	Taylor [54]

Table 40: Propulsion parameters.

An iterative cycle for propulsion optimisation, see Figure 61, was realised where all related equations were found to be dependent on the aircraft weight and/or aerodynamic properties (maximum lift coefficient and the lift to drag ratio). Another major influence is the wing area which, coincident with the weight, changes throughout aerodynamic optimisation. The main inputs of the propulsion were therefore concluded as the lift-drag ratio (L/D), wing area (S) and maximum lift coefficient (C_{Lmax}), as weight is additionally dependent on these.

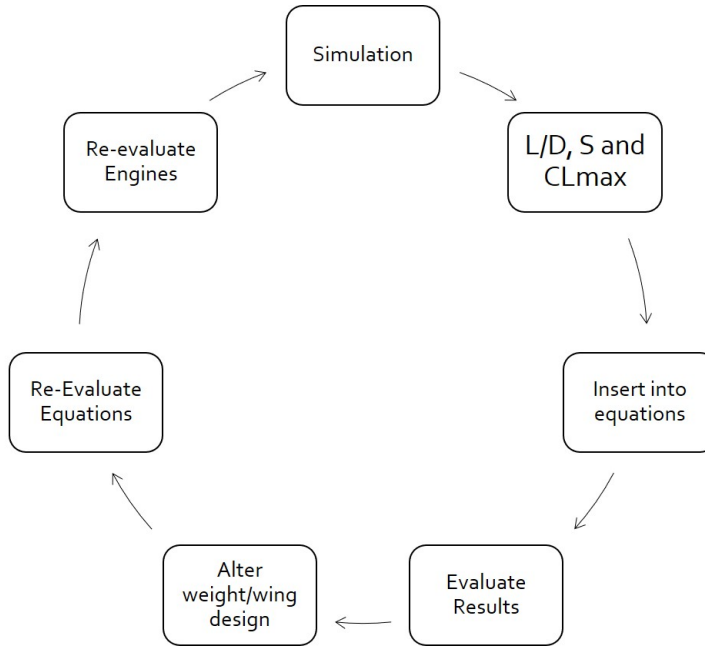


Figure 61: Propulsion Iteration Cycle.

Initially values from the A380 design were input to provide a preliminary idea of expected results, replaced in the future iterations by values obtained through simulations. From these results, a selection of engines were investigated for use for the engine placements considered, which converged upon final selection as the design was fine-tuned through use of a civil turbofan/turboprop database. Aircraft aerodynamic properties, size and loading allowed for the engine selection, placement, aircraft weight, thrust and speed parameters to be calculated. These outputs were relayed to the Aerodynamics, Structures and Economic departments for their consideration in both design and economic feasibility.

6.1.3 Key Performance Indicators

The primary KPIs are the required thrust and aircraft thrust which would determine engine selection and economic considerations. However, a secondary KPI is the aircraft weight as empty weight savings can have positive economic effects, potentially providing an advantage over conventional design. A tertiary KPI to consider was the SFC of the engines being used as these would drive the SFC and emissions emitted by the aircraft, this was an area that also limited our selection of engines.

6.2 Literature Review

6.2.1 Weight Estimation

Despite available literature regarding BWB aircraft with focuses encompassing design, aerodynamics and configuration of propulsion systems, there was limited information regarding the weight estimation of a concept BWB design. As such, the limited literature available was required to be supplemented by that regarding the weight estimation of conventional commercial aircraft. These married well together to provide, what was considered, an accurate estimation as any aspect in relation to the shape of the aircraft was derived from BWB specific literature. Estimations taken from literature, with respect to conventional aircraft, were regarding internal systems and items which could be largely assumed to remain the same between concepts, as the shape should not have a substantial impact.

Bradley produced a sizing methodology for the conceptual design of BWB transports [49] to improve NASA's Flight Optimisation System (FLOPS). While focusing primarily on the ease of sizing the aircraft for multiple passenger loads and the effects of the methodology implementation into the FLOPS system, weight estimation equations of the aircraft body structure were developed through the use of FEA. The equations were developed from a variety of models accounting for passenger capabilities ranging from 200 - 450. From regression analysis, accounting for material and aerodynamic considerations, generic equations were attained which, when implemented into FLOPS, calculated a weight to within 4% of the value measured from previous studies [49].

Estimations accounting for the internal systems and considerations were sourced from Kroos online textbook detailing the design process of a conventional aircraft [50], inclusive of the necessary steps and topics of interest. Kroos, a prolific academic at Stanford University, compiled the textbook from comprehensive industry knowledge to provide a handbook to be referenced for aircraft design. All weight estimations detailed in the textbook were developed by NASA or Stanford University, having been confirmed with reasonable accuracy in preliminary design.

6.2.2 Engine Placement and Configuration

The placement of the engines on the main aircraft body are one of the design points carrying significant importance. Different geometries allow for different propulsion methods to be used. There are two main placements to consider for the BWB, a) Aft-mounted engines, and b) Under-wing mounted engines. In the traditional tube and wing design of aircraft, the engines are mounted on the underside of the wings. This being the preferred placement for the tube and wing geometry primarily due to factors such as better accessibility for maintenance and reduced cabin noise.

The BWB allows for different, less traditional methods of propulsion to be proposed for the design of an efficient propulsion system. A study conducted by Dommelen and Vos [16] on the conceptual design and analysis of the BWB compared the aft-mounted and under-wing mounted engine configurations. The study found that the aft-mounted placement of the engines gave rise to greater aerodynamic performance compared to the under-wing mounted configuration. Specifically, for the same geometry, the aft-mounted engine placement had a greater than 10% average and maximum L/D in comparison with the under-wing mounted design. This is due to the aft-mounted engines decreasing the frontal area of the overall geometry rather significantly and hence decreasing the overall aerodynamic drag of the design and positively impacting the lift distribution of the design. In addition to this, many conceptual and early-stage development designs of the BWB utilise the engines in an aft-mounted placement. These include the Airbus BWB design, named the MAVERIC [6], which is currently being developed and tested through implementation of a 2m x 3.5m scale model. This model utilises 2 engines aft-mounted on the fuselage and it is claimed it can reduce fuel consumption by “up to 20%”, at the time of writing it is still currently in testing therefore data is not yet available. A NASA [4] prototype named the X-48B, superseded by the X-48C BWB also utilised the aft-mounted engine placement through 3 engines. Among many others there is also a study conducted by Li Peifeng et al. [55] which found that another benefit of mounting the engines on the upper surface of the trailing edge of the aircraft can act to reduce the noise level of the BWB. This is due to the forward radiated fan noise being shielded and also avoids exhaust noise reflecting off the lower surface of the BWB.

The above research findings combined with the generally adopted industry consensus that aft-mounted engines are the preferred propulsion configuration to provide the BWB with an efficient propulsion system, hence only aft-mounted engines were considered for the design in this project. Under-wing mounted engines could have been investigated further, however this was deemed unnecessary.

There is also the possibility to utilise the effect of Distributed propulsion for our system. Distributed propulsion utilises the implementation of a larger number of smaller engines. The exhaust of these engines exit out along the trailing edge of the aircraft. This method serves to increase the Aerodynamic performance of the BWB as found in the Kumar and Khalid [51] BWB propulsion study by reducing the frontal area of the aircraft, reducing the drag. The engine exhausts exiting along the trailing edge also allows for the trailing edge jet to ‘fill in’ the wake of the aircraft and furthermore decrease the overall drag of the aircraft. The reason this was not implemented into the design is that the smaller engines that are required to utilise this effect are typically used on short haul journeys and therefore have higher SFC, compared to the GE-90 series and other larger engine types. This is due to the fact that in short haul flights the engines are used in such a way that most of the fuel is burned in takeoff, climb, descent and landing due to the nature of the flight.

Whereas in longer haul flights like the BWB in this project from London to Shanghai, cruise performance is much more important and is where most of the fuel will be used as cruise constitute a larger portion of the flight time due to the nature of the flight path. Therefore, in order to use these smaller engines, they would either have to be re-designed completely or their SFC drastically improved with developments in technology. Accordingly, it was logical to opt for the larger GE-90 series engines that are more specifically designed for long haul flights, until future developments in the industry may allow for the implementation of a larger amount of smaller engines to be used.

6.2.3 Alternative Engines and Fuel Sources

The implementation of alternative fuel sources and engines was considered as an opportunity for the BWB configuration to outperform conventional aircraft in use. The primary option explored was conversion from traditional fossil fuel engines to electric or hydrogen powered engines. Flight has been achieved in aircraft utilising each type of engine, with ambitious plans for the future, although the scale is limited.

The first, and so far only, hydrogen engine commercial grade aircraft, by ZeroAvia, to take flight occurred on 24th September 2020. The 6 capacity plane was in flight for 8 minutes, reaching a height of 1.000ft and a speed of 185km/hr [56]. This was a momentous milestone for aviation, and zero-carbon aviation, proving the viability of hydrogen powered flight. Furthering their success, ZeroAvia have intentions of producing 10-20 capacity commercial planes ready for 500 mile aircraft within three years and 50-100 capacity aircraft by the end of the decade. Additionally, they claim that aircraft with capacity of 200 and a range in excess of 3000nm could be developed by 2040 without any technological breakthroughs [57]. Earlier in June, they also completed a test flight of a 6 capacity battery powered electric aircraft, making it Europe's largest zero-emission plane currently flying [57].

Major aviation company Airbus have also released concepts for their hydrogen powered ZEROe range (Figure 62), due for release at the earliest of 2035, of reduced capacity short range aircraft. The concept range consists of a turbofan (150-200 capacity with 2000nm range), a turboprop (100 capacity with 1000nm range) and BWB (200 capacity with 2000nm range) aircraft [58]. The challenge which arises with hydrogen as a fuel is that it requires a larger storage area on the aircraft, which would favour the shape of a BWB configuration [58]. Due to this complication, it is estimated that there could be an upper limit of an A320-sized aircraft with 1500-2000nm range before the weight of the cryogenic tanks makes the operation unprofitable [58]. There is scope for capacities greater than 200, however this would be highly unlikely to be achieved in the first iteration of commercial aircraft. Airbus did explore the possibility of electric hybrid engines with the E-Fan X, but the research program was terminated in April 2020 without any engine ever having been successfully trialed in an aircraft [59].



Figure 62: Airbus ZEROe concept range [58].

Secondary contemplation was given to sustainable aviation fuel (SAFs). While there is no singular definition for what constitutes a SAF, they can be considered as bio-based fuels which reduce greenhouse gas emissions, as well as other environmental and social aspects such as biodiversity, land use, water use and labour standards, and support the socio-economic development of the communities involved in the production [60]. Fuels must be certified before usage in commercial flights and the American Society for Testing and Materials International (ASTM) have developed standards for approval of bio-based aviation fuels, with six pathways currently certified for SAFs to be blended with conventional fuel [60]. SAFs are compatible with standard aviation engines as they are produced to the same chemical composition and blended with fossil-based aviation fuel at ratios dependent on their manner of production. While SAFs are used on regular flights and being produced in Europe, at present capability, at maximum production, the fuel output would only account for only 4% of the EU aviation fuel demand [60], exhibiting the small scale of the operation. A major factor in the slow growth of the industry is the price of SAFs relative to kerosene. Excluding the market volatility, the typical price for kerosene is around £517/tonne (€600/tonne) whereas SAFs, produced from cooking oil, range from £818-£874/tonne (€950-€1,015/tonne) [60]. Therefore, despite the advantage of carbon footprint offset, economic effects and supply stability would have to be accounted for in the determination of its use.

6.2.4 Experimental Propulsive Technologies

An effect that could be extensively utilised on the BWB is an effect called Boundary Layer Ingestion (BLI), this remains a highly experimental area within industry. The most notable experimental work in the area comes from NASA's Glenn Research centre [61]. They

acknowledge that the idea isn't a new concept, however they are testing new technologies that can derive the benefits of Boundary Layer Ingestion. Every aircraft or object moving through a fluid develops a layer of slower moving air close to the surface of the moving object. This is due to the fact the molecules moving right next to the surface stick to the surface, slowing down the molecules just above these stuck molecules due to them colliding with each other. Hence, the further you move away from the surface, the less collisions occur and the airflow is faster than at the surface. The result of this is that a thin layer of fluid is formed near the surface in which the velocity changes from zero at the surface, to the free stream value away from the surface, it is given the name the boundary layer [62] as it occurs on the boundary of the fluid.

This boundary layer builds up along the skin of the fuselage of the aircraft and wings and hence increases the overall drag of the aircraft. Engines on currently operational commercial aircraft are designed to not ingest this boundary layer as the boundary layer airflow is highly distorted and that affects the performance of the fan. The design of a BLI system therefore requires a full re-design of the engine. The new engines must have a much stronger fan to overcome the constant pounding force that it will experience as a result of ingesting the highly distorted air flow, along with a specialised inlet to help straighten out the flow before it reaches the fan itself.

The ingestion of this slower moving boundary layer will accelerate the slower moving air through the engines and thus works to decrease the total drag of the aircraft. The BWB is the perfect geometry for this design to be utilised as the air must be ingested at the rear of the aircraft in order to maximise the positive effects. The reduction in drag in turn means the engines require less thrust to propel the aircraft forward at a given velocity and hence do not need to work as hard. As the engines do not need to work as hard, they do not need to burn as much fuel, aiding the SFC of the aircraft. It is estimated by NASA that this effect can reduce fuel burn by 8.5% [61] in comparison to aircraft flown today. Jim Heidmann [63] of the Advanced Air Transport Technology Project at NASA's Glenn Research Centre claims, "It all works out very nicely on paper, but there is still an engineering challenge to overcome", in relation to the production of distortion tolerant fans required for BLI. Therefore, it is clearly a very exciting area in terms of propulsive systems for use on the BWB, however significantly more research is required before it can be properly implemented into the real world and hence could be identified as an area of future work if further technological advances prove its feasibility. Therefore due to this, BLI will not be utilised in the propulsion system.

6.3 Weight Estimation and Propulsion Parameters

After initial propulsion calculations using A380 data, a weight estimation method was devised with reference to previous BWB research [51], [49], [50]. The weight estimation method produced values for the take-off weight (TOW) and the empty weight, coded into a MATLAB script to allow ease of calculation and use in the iterative process. Once values for the BWB design were calculated, these replaced the initial A380 propulsion calculations to provide a more accurate result. The weight breakdown for the estimation is as displayed in Table 41.

Component	Equation	Reference
Wings	Approximate at 128000kg total	FEA study
Propulsion	$m_{prop} = 1.6m_{eng-dry}$	Bradley [49]
Cabin	$m_{cabin} = (5.698865)0.316422TOW^{0.166552}S_{cabin}^{1.061158}$	Bradley [49]
Aft	$m_{aft} = (1 + 0.05N)0.53S_{aft}TOW^{0.2}(\lambda_{aft} + 0.5)$	Bradley [49]
Landing Gear	$m_{gear} = 0.04TOW$	Kroos [50]
Surface Controls	$m_{sc} = I_{sc}0.33S_{wing}$	Kroos [50]
Auxiliary Power Unit (APU)	$m_{APU} = 0.454(7N_{passengers})$	Kroos [50]
Instruments and Navigational Equipment	Constant at 544.32kg	Kroos [50]
Electrical and Electronics	$m_{elec} = 0.454(13N_{passengers} + 1500)$	Kroos [50]
Hydraulics and Pneumatics	$M_{HP} = 0.65S_{ref}$	Kroos [50]
Furnishings	$m_{furn} = 0.454(101.6N_{passengers})$	Kroos [50]
Air-conditioning and Anti-icing	$m_{AA} = 0.454(15N_{passengers})$	Kroos [50]
Operating Items	$m_{opi} = 0.454(40N_{passengers})$	Kroos [50]
Payload	$m_{payload} = 110(555 + 3 + 12)$	Kroos [50], Tulapurkara [52]
Fuel	$m_{fuel} = T_{cs}fct$	Kumar et al [51]

Table 41: Weight component breakdown.

A review was also conducted into current performance of the A380 aircraft, the real world comparative, such as key speeds, thrusts, and engine configurations. Designing towards

the A380 aircraft flight profile would allow for the BWB to be able to integrate into the real world more effectively. These values were used as points of comparison against which to measure potential improvements and judge credibility of the calculated values from the weight estimation. The values are shown in Table 42.

A380 Values	
Take-off weight (tonnes)	560.2
Total empty weight (tonnes)	274.9
Stall speed (m/s)	79.03
Lift-off speed (m/s)	86.93
Take-off speed (m/s)	94.84
Cruise speed (m/s)	250.79
Take-off distance (m)	3047.19
Climb thrust for 15° (kN)	1687.77
Climb thrust for 10° (kN)	1224.9
Cruise thrust (kN per engine)	68.7

Table 42: A380 performance values for comparison [54].

During calculation of the parameters, the following assumptions were made:

- Air density $\rho = 1.225 \text{ kg/m}^3$
- Cruise height of 11,000m
- Cruise Mach number of 0.85
- $\gamma = 1.4$
- $R = 0.287 \text{ kJ/kgK}$
- Engine inlet air temperature $T = 216.66\text{K}$

The weight values of the final design calculated for the 3- and 4-engine configurations are displayed in Table 43, alongside their corresponding propulsion parameters.

	3 Engine	4 Engine
Take-off weight (tonnes)	430.43	440.64
Total empty weight (tonnes)	245.03	255.24
Stall speed (m/s)	124.1	125.57
Lift-off speed (m/s)	136.51	138.12
Take-off speed (m/s)	148.92	150.68
Climb thrust for 10° (kN per engine)	311.05	238.82
Climb thrust for 15° (kN per engine)	429.65	329.89
Take-off distance for 10° (m)	2363.05	3221.5
Cruise thrust (kN per engine)	67.67	51.96

Table 43: Thrust requirements for engine configurations.

6.4 Engine Selection Process

The type and number of engines used depends on the performance requirements of the aircraft itself, these are outlined in Table 43. Using these requirements for the maximum thrust required per engine, typically when the aircraft is climbing at 15 degrees, the thrust requirement per engine were able to be found and hence engines for the BWB design could be specified. 3- and 4-engine configurations in an aft-mounted placement were considered to be the focus of this project due to their unique performance in two key areas: specific fuel consumption (SFC) and maximum take-off weight (MTOW).

A study conducted by Kumar and Khalid [51] on propulsion systems of a BWB for a constant geometry identified the 3-engine aft-mounted configuration to give the maximum take off weight, which is highly desirable for commercial aircraft as it potentially translates to higher revenue per flight. The 4-engine aft-mounted case showed the best performance in terms of SFC, another extremely important trait for a commercial aircraft in order to meet future guidelines on emissions and to maximise the profitability of the aircraft.

Given the decided number of engines, the required thrust per engine was then used to select specific engines from a civil turbojet/turbofan database [64]; the engines that met the thrust requirement with the lowest SFC were selected, these are shown in Table 44 along with their performance characteristics. The data comes from an embedded datasheet in the database for the GE90 series of engines published by the European Union Aviation Safety Agency [65].

	4 Engine	3 Engine
Engine Selected	GE90-77B	GE-90-110B1
Sea Level Static Thrust (kN)	363.42	492.68
Maximum Continuous Thrust (kN)	335.53	489.30
Specific Fuel Consumption	0.545	0.545
Weight (kg)	7893	8762
Range (km)	11169.09	11500.32

Table 44: Selected engine performance characteristics.

One of the main drivers of the selection was to use an engine that is already in mass production and widely used within the industry. This would mean the BWB could again, integrate into the real world with more practicality and ease, as opposed to designing a whole new engine at significant time and expense. As you can see from table 40, different versions of the GE-90 engine are selected for both the 3 and 4 engine cases. Another performance criteria that had to be met was the 9197km range from London to Shanghai. This can be calculated through Breguets range equation [66] shown by Equation 6 below:

$$S = \left(\frac{vL/D}{gSFC} \right) \ln\left(\frac{W_{end}}{W_{start}} \right) \quad (6)$$

Using Equation 6 and the relevant values from our final iteration of the BWB design we can work out the total range the aircraft will be able to operate, this for both cases as seen in Table 44 is well above the required operational range for London to Shanghai, therefore the range criteria is met. Finally, the GE-90 engines selected will be superseded by the GE9X [67] in the industry, however, the later was decided not to be taken forward as it only gained its Federal Aircraft Administration (FAA) certification in September 2020 and is not currently in mass production and therefore does not meet the criteria of currently mass produced and operational engines. Therefore it can be concluded that the selected GE-90 series engines provide the design with a sufficient propulsive system that satisfies all of the design requirements.

7 Materials

In context of this project, materials selection aims to assess whether a given structural design is feasible with current generation aerospace materials, to inform future structural design iterations, and to select optimal materials for a subset of main components. This is achieved through close coordination with structural design, and by applying Ashby's method of materials selection to a database of aerospace materials.

7.1 In the context of the Global Design

7.1.1 Inter-dependencies

While materials selection is inter-dependent with all areas of aircraft design [68], in this project structural design was identified as the sole internal factor dependent on materials selection. This decision was made based on reasoning that considering the impact of materials selection on financial, logistical, and operational design aspects requires a more complete materials selection assessment for the entire aircraft, which was deemed out of scope of this project. While this section does not consider the impact of materials selection on economic feasibility, this is considered generally in Section 8.2.

Materials selection and structural design are tightly coupled. In general the iteration cycle between both departments was as follows:

1. Get maximum component stress values from structural design.
2. Perform materials selection to identify suitable material.
3. Return optimal material to structural design.

7.1.2 Inputs and Outputs

The primary input to the materials selection process considered was the structural design from the current design iteration. Additionally, technical requirements for components based on their intended function were considered. The output of the materials selection process was the selected optimal material, which was returned to structural design.

7.1.3 Key Performance Indicators

The primary KPI for materials selection was whether a material was able to meet the operational requirements imposed on it. Operational requirements included yield strength, temperature, and durability. Beyond this, materials selection then became a multi-objective optimisation problem, with a secondary KPI being to best select an optimal material based on the objective of a given component.

7.2 Literature Review

Materials significantly affect aircraft throughout their life: from preliminary design, to construction, operation, maintenance, and end of life [69]. Therefore, the selection of optimal materials is of critical importance; however, for each project and component the definition of optimality may differ. In general, optimality is concerned with the balancing of factors including:

- Material performance
- Availability
- Cost
- Manufacturability
- End of life disposal

In aerospace design, minimising mass and maximising strength or stiffness are common objectives [18]. However, these objectives must be considered in the context of constraints imposed by difficult operating conditions. In light of this, materials such as advanced aluminium alloys, CFRP, and thermoplastics are commonly used in aircraft construction. Thermoplastics and CFRP in particular offer significant weight saving opportunities over conventional alloys, being up to 10 times lighter [70]. Thermoplastics are not able to offer the same strength as CFRP or alloy components, but are cost effective, extremely durable, and easy to manufacture to high tolerances [71]. For these reasons thermoplastics are commonly used for body fairing and leading edges, as well as internal components [72]. CFRP has similar, and often higher, strength than traditional aerospace alloys however can be considerably expensive and difficult to manufacture into large components. These barriers are, however, slowly being overcome with manufacturing cost decreasing and manufacturing complexity increasing [72]. The aerospace industry is justifiably slow in adopting new materials, particularly for safety critical applications. For this reason, CFRP has slowly been increasing in adoption: from contributing less than 10% of aircraft components until the 90s to up to 50% in current generation commercial aircraft [73]. The airbus A380 for instance uses CFRP in the construction of the wing box, empennage assembly, and some body panelling [72], while the recent Boeing 787 has made use of CFRP for wing spars and panels, allowing greatly increased structural flex [74]. While CFRP and thermoplastics are increasing in popularity, advanced aerospace aluminium such as AL 2024 and AL 7075 remain popular due to their ease of manufacturing, low cost, and high strength [69].

In order to compare and select optimal materials, a robust materials selection methodology is required. In general, materials selection can be broken down into two main steps:

1. Identification of the desired material attribute profile.

2. Comparison with real materials to find the optimum selection.

Ashby's method of materials selection [75] describes four tasks which provide a robust framework to achieve this (Figure 63).

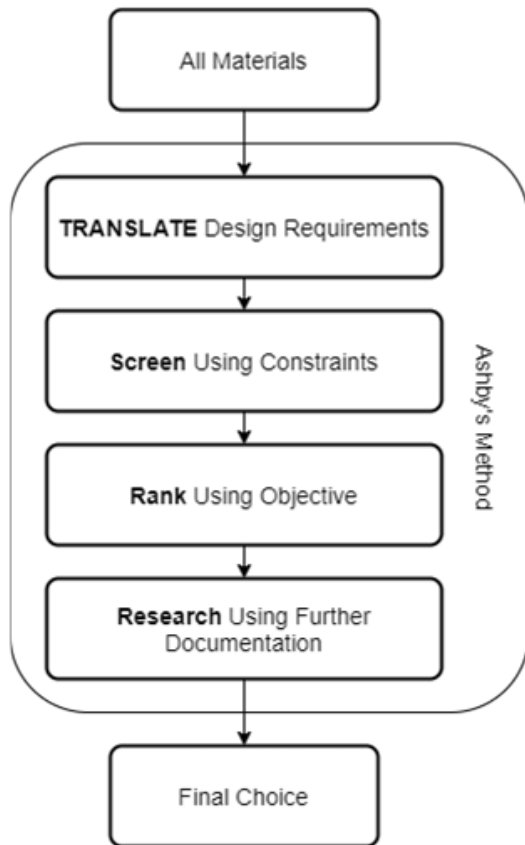


Figure 63: Ashby's method of materials selection. Adapted from [75].

The first step, translation, aims to clearly identify the function of a component as well as imposed constraints, its objective(s), and any free design variables. Each element is explained in Table 45. Translation is required to identify the desired material attribute profile. Screening then aims to identify the domain of all feasible solutions by excluding non-suitable materials. Ranking then aims to identify optimal selections based on an objective criteria - referred to as a material index. Finally, supporting documentation must be consulted to explore qualitative material attributes and select a final material [75].

Translated Component	Explanation
Function	What the component does.
Constraint	The required or desired operating conditions.
Objective	That which is to be optimised. E.g., mass, strength, cost, etc.
Free Variable	Non-fixed component parameters, typically dimensions.

Table 45: Explanation of each output from the translation stage. Adapted from [75].

Material Indices

Material indices are some combination of material properties which, when maximised or minimised, allow optimal materials to be identified for a given function and objective. For simple material selection processes, a material index may consist of one value: for example, unit cost or density. However, more complex selection processes require a combination of desirable properties. In these cases, the following process is used to derive material indices.

1. Identify the performance equation which defines the objective.
2. If there is a free variable:
 - 2.1. Identify the limiting constraint.
 - 2.2. Use this to eliminate the free variable.
3. Generate the material index from the remaining material properties in the performance equation.

7.3 Methodology

Materials selection was performed for four integral aircraft components. These components constitute the primary considerations of structural design.

- Wing spars
- Wing skin
- Fuselage frame
- Fuselage shell

Ashby's method was applied to each component in turn. The fundamental function of each component was identified, as were operating constraints and relevant objective. From these, material indices for each component were generated and compared with available literature [75]. Allowable operating temperatures were considered, with constraints of $\text{MinServiceTemperature} < -100$ and $\text{MaxServiceTemperature} > 100$ being imposed on all components. This was identified as above the maximum expected take-off temperature for commercial aircraft and below the minimum operating temperature of commercial

aircraft in flight (Appendix L). However, most materials identified have operating temperature ranges significantly greater than this range. Granta Edupack was used to provide a comprehensive and easily searchable materials knowledgebase [71]. Edupack also allowed the stages of screening, ranking, and supporting research to be applied; allowing optimal materials to be identified which were then returned to structural design.

7.4 Results

7.4.1 Wing Spars

In conventional designs, the wing carries the greatest aerodynamic lift of any substructure. The wing spars provide the primary load path for the wings and are designed to withstand high bending and shear loading [18]. Wing spars should be light, to increase efficiency, while also being able to flex under load to reduce the structural loading at the wing root and to better handle turbulence during flight. These considerations were used to inform the translation given in Table 46. Initial structural design required a minimum yield strength of 280MPa, however this was reduced to 224MPa for the final design iteration.

Wing Spar Translation	
Function	Cantilever beam
Constraints	Non-ferrous alloys or composites $\sigma_{yield} > 224\text{ MPa}$ Min Service Temperature $<-100^\circ$ Max Service Temperature $>100^\circ$ Non-flammable Resistant to light acids, alkalis, and sunlight
Objective	Minimise mass
Free Variable	Material choice, cross-section area

Table 46: Translation for wing spars.

Material Index

Equation 7 gives the performance equation for the mass of a beam of free-variable area, A . Area can be related to the maximum internal stress due to bending through Equation 8. The resulting Equation 9 can then be grouped by functional and geometric constraints, allowing for the identification of the material index ρ/σ_y . Thus, selection of a material for a light, strong beam loaded under bending can be performed by maximising σ_y/ρ , represented by a line of gradient 1 on a log-log plot of yield strength to density (Figure 64).

$$m = AL\rho \quad (7)$$

$$\frac{M}{I} = \frac{\sigma}{y}; I = \frac{by^3}{12} = \frac{Ay^2}{12} \Rightarrow A > \frac{12M}{\sigma_y y} \quad (8)$$

$$m > (12M) \left(\frac{L}{y} \right) \left(\frac{\rho}{\sigma_y} \right) \quad (9)$$

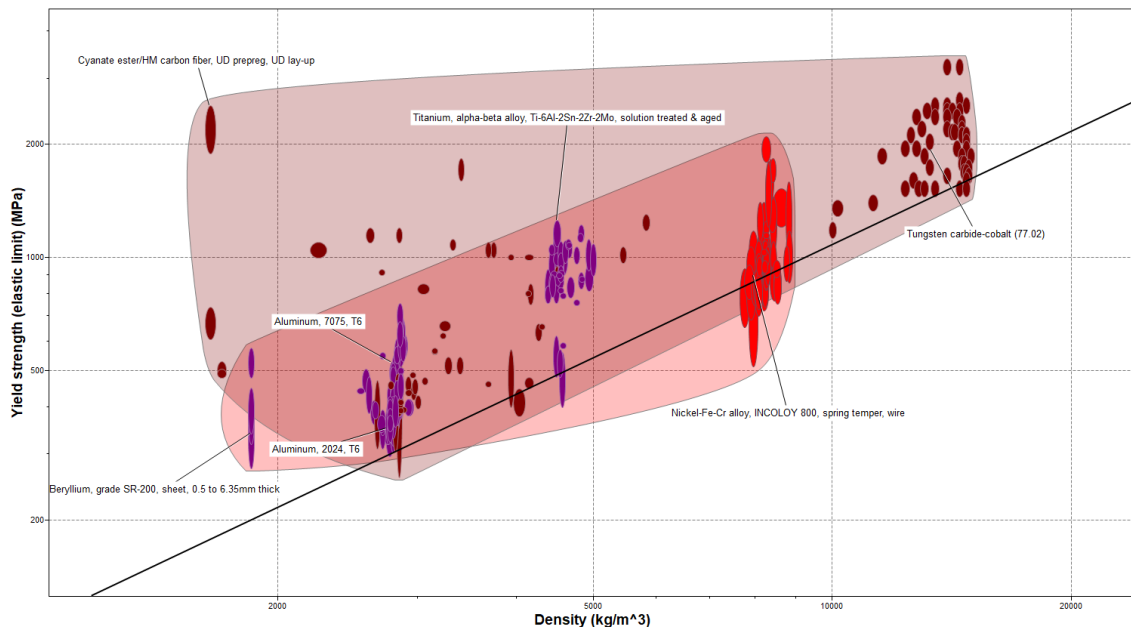


Figure 64: Materials selection chart for wing spars [71].

Selection

Considering the material property chart above, several material families can be identified, for each of which supporting documentation was consulted (Table 47).

Material Family	Positives	Negatives
Tungsten carbide-cobalt ceramics	-	High excess strength High density: $>10000\text{kg/m}^3$ Expensive: £57 - £100 / kg
Nickel alloys	High fatigue strength	High excess strength High density: 8000kg/m^3 Expensive: £20 - £25 / kg
Titanium alloys	Good fatigue strength	Moderate excess strength High density: 4500kg/m^3 Expensive: £20 - £25 / kg Susceptible to stress-corrosion cracking
Advanced Aluminum alloys	Good fatigue strength Acceptable price Good fatigue life Acceptable strength Low density	Slightly susceptible to stress corrosion cracking
Carbon Fibre Reinforced Composites	Low density Very strong	Expensive Difficult to manufacture large components
Beryllium	Low density	Expensive Carcinogenic

Table 47: Assessment of supporting documentation for possible materials families.

While materials occupying the upper left portion of Figure 64 may be considered ideal in terms of density and strength, consultation of supporting documents identifies that Cyanate Ester based CFRP is very expensive and can be difficult to manufacture. For this reason, advanced aluminium alloy AL 2024 T6 was chosen for use in the wing spars. This family of aluminium alloys already has a proven history of usage in safety critical aerospace components [18][76].

7.4.2 Fuselage Frame

The function of the fuselage frame is to support the pressurised inner fuselage shell. The fuselage shell is loaded under internal pressure, and as such the fuselage frame is simplified to that of a thin cylinder under internal pressure loading. Initial structural design identified maximum stress values for this component to be 380 MPa, however this was reduced to 310MPa after subsequent iterations. The fuselage frame must also be capable of operating in similar conditions to that of the wing spars, leading to the translation given in Table 48.

Fuselage Frame Translation	
Function	Cylindrical pressure vessel
Constraints	Non-ferrous alloys or composites $\sigma_{yield} > 310 \text{ MPa}$ Min Service Temperature $<-100^\circ$ Max Service Temperature $>100^\circ$ Non-flammable Resistant to light acids, alkalis, and sunlight
Objective	Minimise mass
Free Variable	Material choice, cross-section area

Table 48: Translation for fuselage frame.

Material Index

As before, the performance equation to minimise mass is given by Equation 10, with the compatibility equation for strength-limited design given by Equation 11. Rearranging allows for the performance equation shown in Equation 12. The material may be optimised for strong, light design by maximising $\frac{\sigma_y}{\rho}$ - note, this is equivalent for the index previously derived for a strong, light beam loading in bending (Equation 9).

$$m = AL\rho = 4\pi rtL\rho \quad (10)$$

$$\sigma_y > \frac{Pr}{t} \quad (11)$$

$$\Rightarrow m > (4\pi P)(r^2 L) \left(\frac{\rho}{\sigma_Y} \right) \quad (12)$$

Selection

Due to the equivalent constraints and material indices, the selection process yielded identical results to that of the wing spar (Figure 64). For this reason, Aluminum 2024 T6 was also selected for use in the fuselage frame.

7.4.3 Fuselage Shell

As discussed above, the function of the inner fuselage shell is to withstand the internal pressure of the cabin. The shell is a complex shape, consisting of many panels contributing to a generally elliptical shape. This structure is required to be light and stiff in response to internal pressure, and also any in-plane loads the shell panels may be subject to. Two material indices were considered: one for a stiff, light cylinder with internal pressure and another for a stiff, light plane compressed in-plane. From structural design, the initial required yield stress was identified as 872 MPa but this was revised to 399 MPa. These considerations were used to develop the translation given in Table 49.

Fuselage Shell Translation	
Function	Cylindrical pressure vessel / Plate loaded in-plane
Constraints	Non-ferrous alloys or composites $\sigma_{yield} > 399 MPa$ Min Service Temperature $<-100^\circ$ Max Service Temperature $>100^\circ$ Non-flammable Resistant to light acids, alkalis, and sunlight
Objective	Minimise mass
Free Variable	Material choice, cross-section area

Table 49: Translation for fuselage skin.

Material Index: Light, Stiff Cylindrical Pressure Vessel

As before, the performance equation to minimise mass is given by Equation 13, with the compatibility equation for stiffness-limited design given by Equation 14. Rearranging allows for the performance equation shown in Equation 15. The material may then be optimised for light, stiff design by maximising $\frac{E}{\rho}$.

$$m = AL\rho\pi(4rt + t^2)L\rho \approx 4\pi rtL\rho \quad (13)$$

$$S = EI = E\left(\frac{1}{2}\pi((r+t)^4 - (r-t)^4)\right) \geq S^* \quad (14)$$

$$\Rightarrow m \geq (8S^*)\left(\frac{rtL}{(r+t)^4 - (r-t)^4}\right)\left(\frac{\rho}{E}\right) \quad (15)$$

Material Index: Light, Stiff Plate Loaded In-Plane

As before, the performance equation to minimise mass is given by Equation 16, with the compatibility equation for stiffness-limited design given by Equation 17. Rearranging allows for the performance equation shown in Equation 18. The material may then be optimised for light, stiff design by maximising $\frac{E^{1/3}}{\rho}$.

$$m = AL\rho = bhL\rho \quad (16)$$

$$S = \frac{C_1 EI}{L^3} \geq S^*; I = \frac{bh^3}{12} \quad (17)$$

$$\Rightarrow m \geq \left(\frac{12S^*}{C_1 b}\right)^{1/3}(bL^2)\left(\frac{\rho}{E^{1/3}}\right) \quad (18)$$

Selection

The resulting materials selection chart is shown in Figure 65. Due to the smaller size of the individual panels which make up the shell, CFRP materials were considered more feasible for use. For an equivalent volume, CFRP materials are approximately 1kg lighter - leading to considerable performance gains. However, this comes at the cost of price with Cyanate Ester CFRP being as much as £100 more expensive per kg [71]. As a result of the higher yield stress requirements, Aluminium alloy 7075 T6 was selected for manufacturing the fuselage shell.

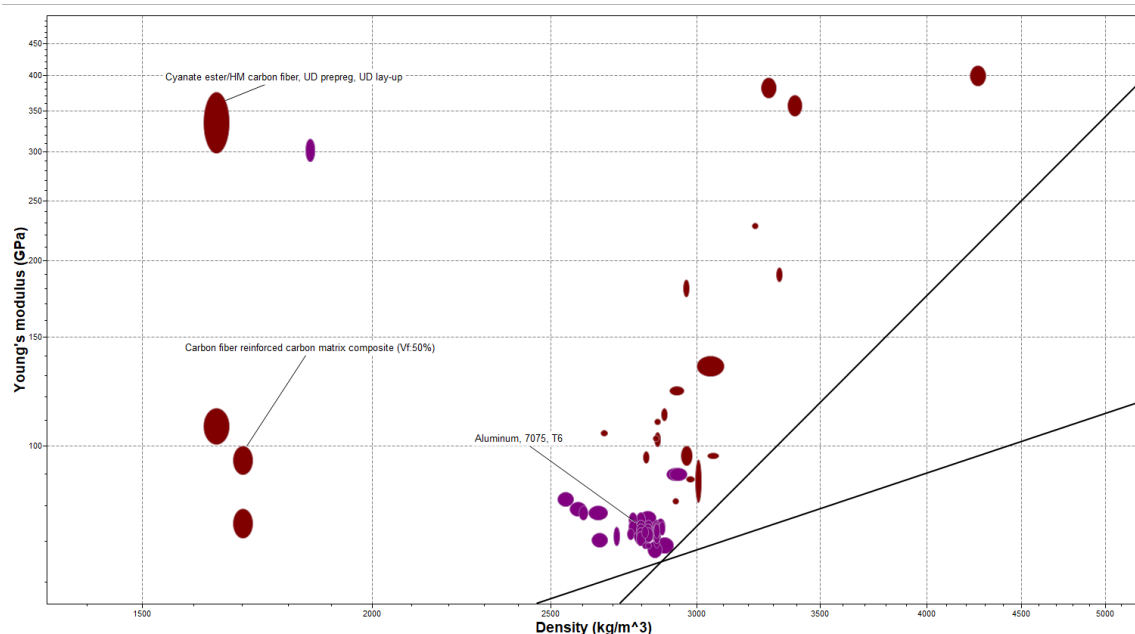


Figure 65: Materials selection chart for fuselage shell [71].

7.4.4 Wing Skin

Unlike the fuselage shell, the wing skin is not intended to withstand any internal pressure but will flex significantly during use. The skin must be light, and should be able to withstand continuous exposure to rainfall and sunlight. The wing skin is comprised of multiple smaller panel sections which may be considered as being loaded in-plane. Initial structural design identified maximum panel loading as 60MPa, however this increased to 128MPa for the final design. These considerations were used to perform the following translation (Table 50).

Wing Skin Translation	
Function	Plate loaded in-plane
Constraints	Non-ferrous alloys or composites $\sigma_{yield} > 128 MPa$ Min Service Temperature <-100° Max Service Temperature >100° Non-flammable Resistant to light acids, alkalis, and sunlight
Objective	Minimise mass
Free Variable	Material choice, cross-section area

Table 50: Translation for wing skin.

Material Index

For a strong, light plate loaded by a central point force, the material index to be maximised is $\frac{\sigma_y^{1/2}}{\rho}$ [75]. This can be represented by a line of gradient 2 on a chart of yield strength to density. This is shown on a materials property chart of yield strength against density in Figure 66.

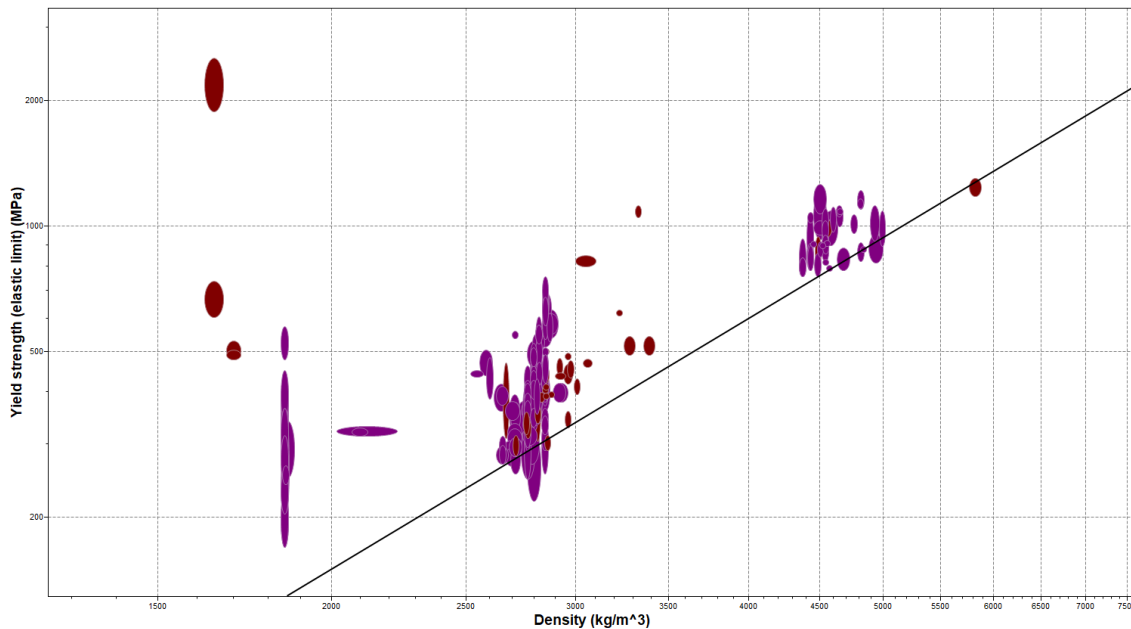


Figure 66: Materials selection chart for wing skin [71].

Selection

From Figure 66 it can be seen that the optimal materials are similar to that previously identified. Similarly to before, while Cyanate Ester based CFRP is optimal in terms of

density, it is again rejected because of its high cost [71]. Aluminium 2024 T6 is again selected for use in the wing skin.

8 Economics and Environmental Impacts

Continuous technology development in the commercial aviation industry is largely driven by economic profitability [1]. With the emerging goal of carbon neutrality by 2050 across the globe, various power and transportation sectors have shifted towards cleaner technology solutions [77], as have been explored previously in Section 6.2.3. However, developments of revolutionary technology in the aviation industry generally requires substantial amount of time and cost with great uncertainties in policies and fuel prices across years-long project durations. Hence, economic viability analysis is considered necessary at the conceptual or preliminary design stages of such technologies to reduce the risk of unsustainability and unprofitability. The two main factors relevant to aircraft performance characteristics that contribute to airline direct operational costs are fuel costs and emissions taxation [1]. Fuel cost accounts for up to 40% of the total operational costs for an aircraft [78]; while commercial aircraft operations contribute only 2.4% to the global carbon dioxide emissions from fossil fuel combustion [79], with possible carbon tax increase from future policy makers, this can translate to high operating costs for airlines. In a simple sense, if the cost for implementing new technologies is outweighed by the increasing expenses for keeping the conventional aircraft in fleet, then the technology is deemed economically feasible.

The economic analysis for the BWB aircraft was mainly evaluated in two stages:

1. Development and manufacturing cost per unit.
2. The DOC per nautical mile per passenger.

As the BWB aircraft development is currently still in the conceptual stage, the acquisition cost information that is required for the DOC evaluation must be estimated using empirical relationships stated in literature using the design parameters determined from other departments. The output development cost from the first stage was used to inform the second stage as the acquisition cost for a complete cost evaluation. Number of sold units for break-even was investigated for different listed prices, the minimum selling price required to reach break-even for an assumed number of production units was calculated.

Two different DOC models were implemented and compared for the initial calculation; the more comprehensive model was then chosen for all other design iterations. The DOC per nautical mile per passenger determined for each iteration of the BWB design was compared to the A380 and B747 to gain an overview to the economic implication of the design. The estimated DOC for the A380 was validated against literature. The carbon emission characteristics were also evaluated at the end.

8.1 In the Context of the Global Design

The economics in this project specifically refers to the cost for manufacturers to develop and produce the designed BWB aircraft as well as the direct operating cost for airlines to own and operate such aircraft. The indirect operating cost such as marketing and administration fees were considered out of scope. The cost evaluation integrates all of the design choices stated in the previous sections, any changes made throughout the design iterations had impacts on the development costs and DOC. The economic analysis hence plays an important role in this project for quantifying the feasibility of the designs in a commercial sense. With the possibility in carbon taxation policy introduction to the aviation industry in the future for environmental benefits, CO_2 emission was also considered as a key parameter for instigation.

8.1.1 Inter-dependencies

As the final step of investigation for each design iteration, the economic analysis is strongly dependent on all other technical departments; out of these, the inter-dependencies that directly impact the economic outputs are:

- Propulsion: as it provides the thrust performances and engine SFCs for fuel consumption requirements
- Structure: as it informs the airframe mass which affects development and maintenance costs
- Materials: as it informs the fraction of expensive materials (e.g. CFRP) used which affects manufacturing costs

However, due to the complexity in determining detailed material choice for the entire aircraft as aforementioned in Section 7.1, a comprehensive cost analysis associated with materials at component levels was deemed out of scope.

8.1.2 Inputs and Outputs

For development cost consideration, the major inputs required from other departments are airframe mass, composite material fraction, number of engines, and thrust per engine. Up to 18 input parameters were identified necessary for DOC evaluation, which may be grouped into categories: flight definition, variable rates (such as fuel price and labour rates), engine properties (such as mass, thrust, SFC, overall pressure ratios, etc.) and weight properties (empty weight and MTOW).

The outputs would consist of development cost for each aircraft, production units for break-even, DOC and carbon dioxide emission. These parameters would inform other departments at the start of each iteration for further reduction in structural mass and thrust requirements. The information flow structure will be explored in detail in the following sections.

8.1.3 Key Performance Indicators

The KPIs identified from the overall output parameters through economic analyses are: development and manufacturing cost, which was used as acquisition cost for DOC evaluation; DOC and CO_2 emission per nm-pax, which act as indicators for parallel comparison between different iterations as well as the commercially available aircraft.

8.2 Development Cost

With the ultimate aim of evaluating the DOC to operate the designed BWB aircraft, it was found that the information on acquisition cost was necessary for proceeding with such goal. While rough listing prices for current passenger aircraft are available from relevant companies, no simple judgement can be made for approximating the pricing of a conceptual aircraft. Therefore, cost models from the point of view of an aircraft manufacturer were searched to fulfil the requirement.

One of the most commonly used aircraft development cost models is the latest DAPCA IV model, which was developed largely dependent on military aircraft acquisition cost from the Department of Defence database. However, due to the expensive nature of aircraft developed for military use, the DAPCA IV model tends to over-predict the acquisition cost by up to two times higher than the list price for general aviation aircraft, hence it is considered unsuitable for civilian aircraft cost estimation. [80]

A new model has been developed in the 1990s based on the original DAPCA IV model by Eastlake and Blackwell [18], with additional weighting factors implemented to differentiate the cost disparities between military and civil aircraft [80]. The author of literature [18] has since adjusted the constants in the Eastlake model to the most recent market outlook, with Consumer Price Index (CPI) also implemented in relation to the year 2012 taking into account of the inflation rate. The latter was deemed the most reasonable model to be applied for the purpose of this project.

8.2.1 Methodology

Eastlake Model

The total development cost calculated using Eastlake model is constituted of development labour, flight test, development support, quality control and material costs. Each part of the costs depends on the input from the structural weight and other design decisions such as percentage of composite material, number of production units in a period of 5 years, certification type (i.e. CS-25 in this case) and etc. as illustrated in Figure 67. All equations stated in Tables 51 - 53 were implemented in MATLAB scripts for easier plotting automation and change of input parameters through different design iterations.

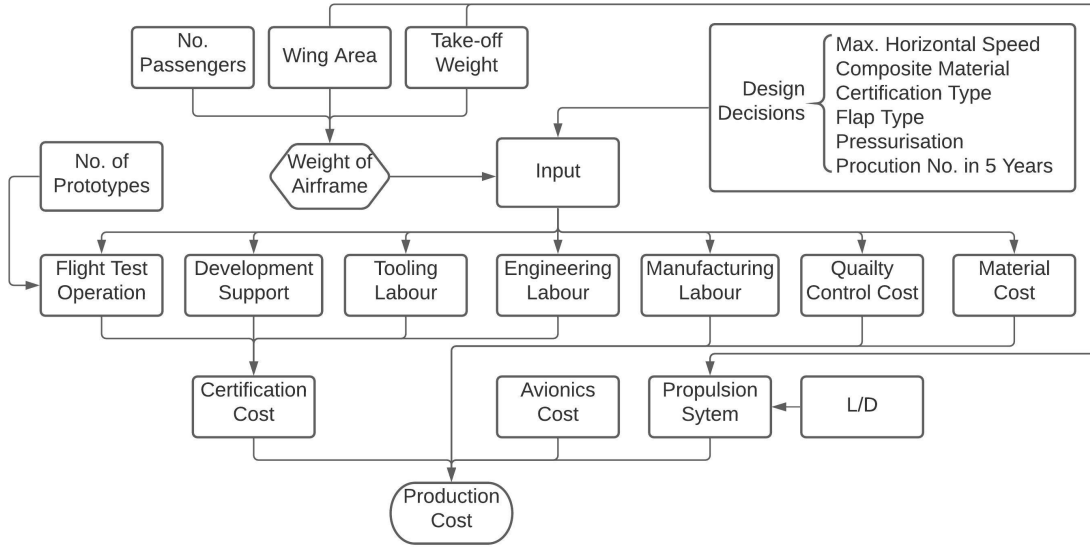


Figure 67: East-Lake production cost flow diagram, derived from equations [18].

Labour Cost (\$)	
Man-Hours (hr)	
Engineering	$H_{ENG} = 4.86 * W_{airframe}^{0.777} * V_H^{0.894} * N^{0.163} * F_{CERT} * F_{CF} * F_{COMP} * F_{PRESS}$
Tooling	$H_{TOOL} = 5.99 * W_{airframe}^{0.777} * V_H^{0.696} * N^{0.263} * F_{CERT} * F_{TAPER} * F_{CF} * F_{COMP} * F_{PRESS}$
Manufacturing	$H_{MFG} = 4.86 * W_{airframe}^{0.777} * V_H^{0.894} * N^{0.163} * F_{CERT} * F_{CF} * F_{COMP} * F_{PRESS}$
Total Labour Cost (\$)	
Engineering	$C_{ENG} = 2.0969 * H_{ENG} * R_{ENG} * CPI_{2012}$
Tooling	$C_{TOOL} = 2.0969 * H_{TOOL} * R_{TOOL} * CPI_{2012}$
Manufacturing	$C_{MFG} = 2.0969 * H_{MFG} * R_{MFG} * CPI_{2012}$

Table 51: Development Labour Cost. [18]

Other Costs (\$)

Development	$C_{DEV} =$
Support	$95.24 * W_{airframe}^{0.63} * V_H^{1.3} * CPI_{2012} * F_{CERT} * F_{CF} * F_{COMP} * F_{PRESS}$
Flight Test	$C_{FT} = 2606.51 * W_{airframe}^{0.325} * V_H^{0.822} * N_P^{1.21} * CPI_{2012} * F_{CERT}$
Quality Control	$C_{QC} = 0.133 * C_{MFG} * F_{CERT} * F_{COMP}$
Materials	$C_{MAT} = 23.066 * W_{airframe}^{0.21} * V_H^{0.621} * N^{0.799} * CPI_{2012} *$ $F_{CERT} * F_{CF} * F_{PRESS}$
Avionics	\$100,000 per airplane for 14 CFR Part 25 Certification
Power Plant	$C_{PP} = 1035.9 * N_{PP} * T^{0.8356} * CPI_{2012}$

Table 52: Other Development Costs. [18]

Total Development Cost (\$)

Certification	$C_{CERT} = C_{ENG} + C_{DEV} + C_{FT} + C_{TOOL}$
Production	$C_{PROD} = C_{CERT} + C_{QC} + C_{MAT} + C_{AVIO} + C_{PP}$
Liability	$C_{LIAB} = 0.17 * C_{PROD}$
Total Cost (\$)	
Total	$C_{TOTAL} = C_{PROD} + C_{LIAB}$

Table 53: Total Development Cost. [18]

The minimum selling price was determined from Equation 19:

$$P_{MINSELL} = \frac{C_{TOTAL}}{N} \quad (19)$$

Where N is the total number of production in 5 years, which was taken the value of 67 based on the number of delivered A380 within 5 years since it first entered into service [81]. The minimum selling price of an A380 was first estimated using parameters in Table 54 for numerical verification. The parameters were subsequently varied through each design iteration with all results recorded for comparison. The effect of produced number of units on minimum sales price was plotted, the production cost distribution was also investigated.

Parameters	Value
$W_{airframe}$	396955 lbf
V_H	550.83 KTAS
N	67
f_{comp}	0.25
N_{pp}	8
T	$4.74 * 10^4$ lbf

Table 54: Used parameters for A380 development cost analysis.

Break-even Analysis

Break-even analysis estimates the minimum number of aircraft required to be produced and sold to reach profitability. Based on different anticipated unit sales price, the break-even number of units can be found using Equation 20.

$$N_{BE} = \frac{\text{TotalFixedCost}}{\text{UnitSalesPrice} - \text{UnitVariableCost}} \quad (20)$$

Where the reasonable range of Unit Sales Price was determined based on the minimum sales price calculated from the previous section. The Total Fixed Cost and Unit Variable Cost are defined by Equations 21 - 22.

$$\text{TotalFixedCost} = C_{CERT} \quad (21)$$

$$\text{UnitVariableCost} = C_{MFG} + C_{QC} + C_{MAT} + C_{AVIO} + C_{PP} + C_{LIAB} \quad (22)$$

The development costs and revenue were plotted against number of produced aircraft with three different listing prices being considered, the corresponding numbers of units for break-even were compared between each aircraft configuration.

8.2.2 Results

Due to the final decision of excluding composite materials from materials selection as stated in Section 7, the development cost for A380 with 0% composite material was considered as the base of comparison despite up to 40% of the A380 weight is consisted of composite materials [82]. This was to make sure the costs differences were due to the changes in geometric and performance characteristics rather than material choices.

The minimum sales price at different production capacities are shown in Figure 68, the price drops significantly as number of production increases. With the assumed 67 units of production in a 5-year period, the last BWB design iteration with 4 engines shows 6% decrease in the selling price. Table 55 shows the minimum selling price calculated for each design iteration, a slight increase in price was found between iteration 1 and 2, with a significant drop in price between iteration 2 and 3, and between 4 and 5. The 3-engine

configuration of the last design iteration showed further decrease in price, up to 9% less compared to the A380.

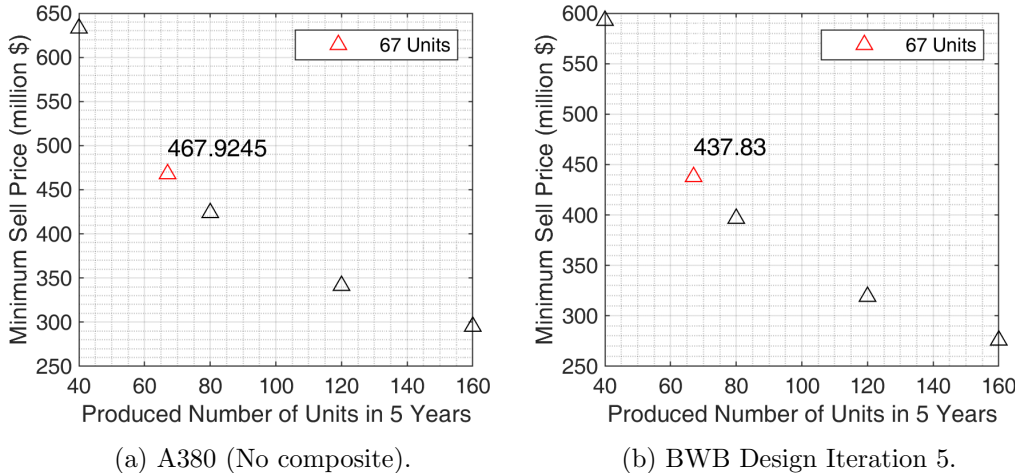


Figure 68: Minimum list price per unit for different produced units in 5-year period.

	A380	A380 (No Comp.)	Iter1	Iter2	Iter3	Iter4	Iter5	Iter5 (3-Engine)
List Price (\$m)	533.8	467.9	458.0	458.1	445.6	445.6	437.8	423.5

Table 55: Minimum list price for break-even assuming 67 units produced in a 5-year period.

The distribution of each part of the overall development costs are shown in Figure 69, no major differences are seen between the BWB and A380, the materials cost accounts to a fifth of the total cost.

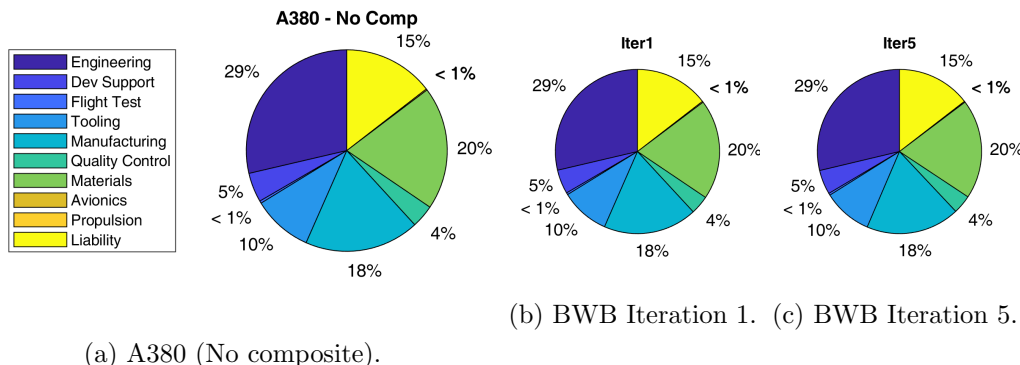


Figure 69: Development cost distribution.

Detailed breakdown of costs is demonstrated in Table 56, the most significant decrease was found in the cost of engines (C_{PP}) at 10% and 16% for 4-engine and 3-engine configurations respectively. Second to that is material costs with decreases of 7% and 11%. Full breakdown for each iteration can be found in Appendix G.

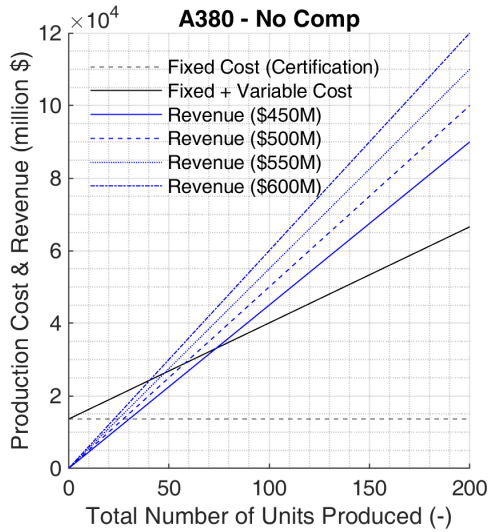
	C_{ENG} (\$b)	C_{DEV} (\$b)	C_{FT} (\$b)	C_{TOOL} (\$b)	C_{MFG} (\$b)	C_{QC} (\$b)	C_{MAT} (\$b)	C_{AVIO} (\$k)	C_{PP} (\$m)	C_{LIAB} (\$b)
A380 (No Comp.)	8.98	1.48	0.12	3.02	5.79	1.15	6.20	100	60.45	4.56
Iter1	8.80	1.45	0.12	2.96	5.66	1.13	6.05	100	63.28	4.46
	-2%	-2%	-1%	-2%	-2%	-2%	-2%	0%	5%	-2%
Iter5	8.43	1.41	0.12	2.83	5.41	1.08	5.75	100	54.12	4.26
	-6%	-5%	-3%	-6%	-6%	-6%	-7%	0%	-10%	-6%
Iter5 (3 Engine)	8.16	1.37	0.11	2.74	5.23	1.04	5.53	100	50.62	4.12
	-9%	-7%	-4%	-9%	-10%	-10%	-11%	0%	-16%	-9%

Table 56: Breakdown development costs for each analysed aircraft using the Eastlake model.

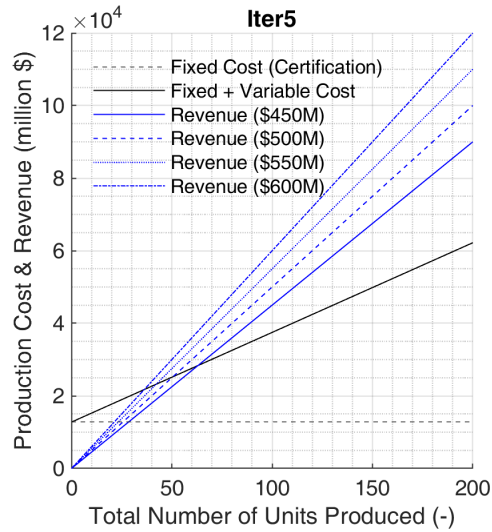
From break-even analysis, 3-engine configuration requires 14 and 7 less units sold for break-even at the list prices of \$450m and \$600m respectively compared to the no composite version of A380 as listed in Table 57. Figure 70 shows production costs and revenue with respect to produced units, higher list prices generate higher revenue at the same number of units, the lower gradient of Variable Cost plot for the BWB compared to A380 illustrated in Figure 70b shows lower production cost per unit, which translates to higher profits.

List Price (\$m)	A380 (No Comp.)	Iter1	Iter2	Iter3	Iter4	Iter5	Iter5 (3-Engine)
450	101	73	70	66	66	63	59
500	77	58	55	52	52	51	47
550	63	48	46	44	44	42	40
600	53	41	39	37	37	36	34

Table 57: Number of units required to be sold for break-even for different listing prices.



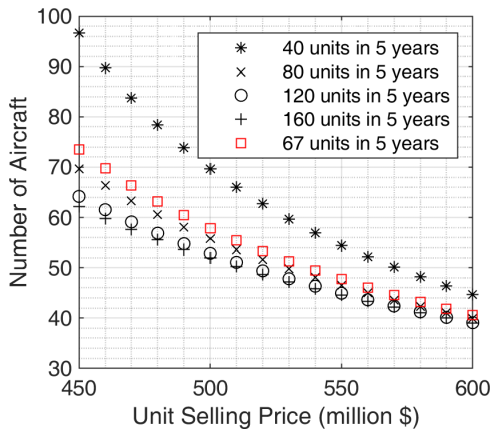
(a) A380 (No composite).



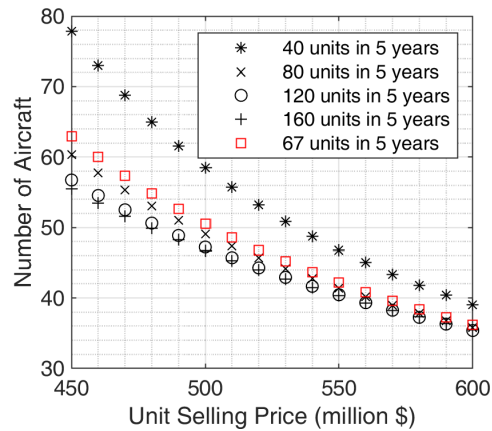
(b) BWB Iteration 5.

Figure 70: Production costs and revenue for break-even analysis.

The effect of number of produced units in 5 years are demonstrated in Figure 71, lower number of production units requires much higher total number of aircraft sold further down the line to reach profitability. In addition, when the number of production units is low, selling price has a significant impact on the required sales for profitability.



(a) A380 (No composite).



(b) BWB Iteration 5.

Figure 71: Effects of production units in 5-year period on the number of sold aircraft for break-even.

8.3 Direct Operating Cost

For economic sustainability of an airline, operating costs of the fleet are important factors in the life cycle costs of aircraft [83]. Operating costs are categorised into Direct Operating Costs (DOC) and Indirect Operating Costs (IOC), both constitute to the profitability of an airline. However, IOC is challenging to evaluate as it covers the cash outflow for a longer seasonal period where costs still incur even if the services are not provided as planned [84], and largely depends on the business strategies [83]. Therefore, DOC is typically considered efficient in weighing the costs involved when airlines acquire an aircraft and often used for comparative analysis [85].

Many different DOC estimation methods have been proposed by various authorities and literature since ATA first established an empirical schematic in calculating DOC in the 1940s. Other methods developed by NASA [86], AEA [87] and Eastlake were also among the few that made regular appearances in literature. In the comparative study carried out by Ali et al., ATA, NASA and AEA models all generated similar trend in DOC for different passenger aircraft, albeit the large differences in values for certain components.

All of the DOC models stated above are dependant on various aircraft characteristics, of which the one that has the most significant impact is the initial acquisition cost as mentioned in the previous section. The minimum selling prices estimated were therefore directly fed into the DOC model. Both the AEA and Eastlake model were used for a comparative study on the A380 and verified against literature, the method that generated the more comprehensive results were taken for further DOC estimations per nautical mile per passenger on each of the design iterations for long haul and short haul flights in different fuel price scenarios.

8.3.1 Methodology

The Eastlake model was chosen at the beginning stage for the A380 DOC estimation owing to its relative simplicity and minimum input parameter requirements. However, due to the unavailability of published DOC data from commercial airlines and the lack of usage of the Eastlake model in literature, the results could only be compared to other models for verification. Thus, the more complicated AEA model was selected for its literature results availability for various wide-body passenger aircraft.

Figure 72 and 73 shows the information flow for calculating the total DOC for both models, equations listed in Table 58 and 60 were implemented in MATLAB for iterative evaluations using different input parameters. The total flight time per year Q_{FLGT} was calculated based on the available time and turnaround time stated in Table 59 using Equation 23.

$$Q_{FLGT} = t_{available} * \frac{t_{block}}{t_{block} + TAT} \quad (23)$$

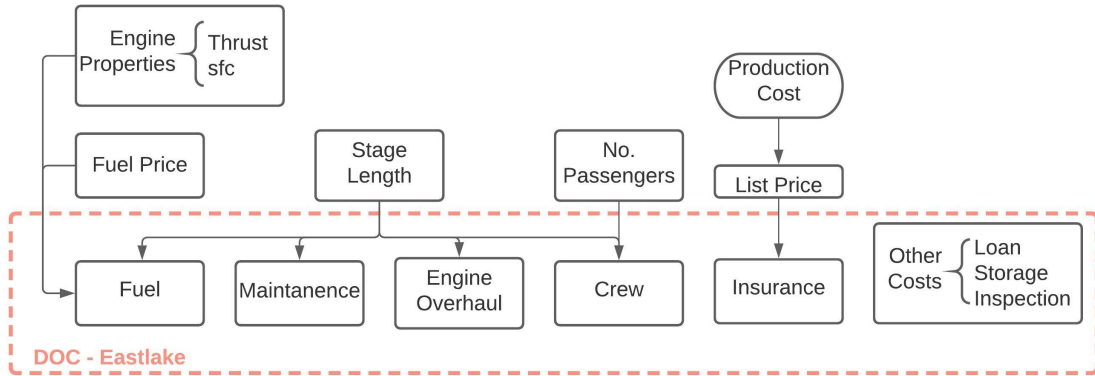


Figure 72: Direct operating cost flow diagram, derived from equations [18].

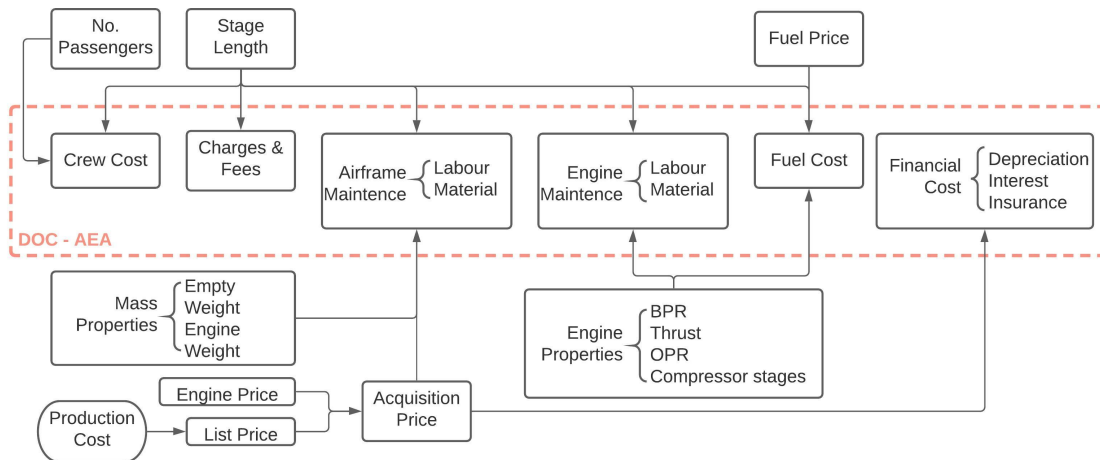


Figure 73: Direct operating cost flow diagram using AEA method, derived from equations [83]

DOC - Eastlake (\$)

Maintenance	$C_{AP} = F_{MF} * R_{AP} * Q_{FLGT}$
Storage	$C_{STOR} = 12 * R_{STOR}$
Fuel	$C_{FUEL} = T_c * sfc * Q_{QFLT} * FuelPrice$
Insurance	$C_{INS} = 500 + 0.015 * C_{AC}$
Inspection	\$15,000
Engine Overhaul	$C_{OVER} = 7.5 * N_{PP} * Q_{QFLT}$
Crew	$C_{CREW} = N_{CREW} * R_{CREW} * Q_{FLGT}$
Loan Repayment	$C_{LOAN} = \frac{P_{BORROW} * interest * Q_{FLGT}}{1 - 1/(1 + interest)^n}$
Total(\$)	$C_{YEAR} = C_{AP} + C_{STOR} + C_{FUEL} + C_{INS} + C_{INSP} + C_{OVER} + C_{LOAN}$

Table 58: DOC - Eastlake model, adapted from [18].

Range (nm)	$t_{available}(h)$	Turnaround Time(h)
<1000	4000	0.5
1000-2000	5100	1.4
>2000	6500	3

Table 59: Available hours per year and corresponding Turnaround Time [83].

DOC - AEA (\$)

Utilisation	$U = t_{available}/(t_{block} + TAT)$
Airframe Spares	$AFS = 0.1 * (MSP - ENP * NPP)$
Spare Propulsion Units	$SPU = 0.3 * ENP * NPP$
Total Investment	$TI = MSP + AFS + SPU$
Depreciation	$DEP = TI/(14 * U)$
Interest	$INT = 0.05 * TI/U$
Insurance	$INT = 0.005 * MSP/U$
Total Financial Cost	$DEP + INT + INS$
Pilot	$CPC = 380 * t_{block}$
Cabin Crew	$CAC = 60 * n_{cab} * t_{block}$
Total Crew Cost	$CPC + CAC$
Navigation	$NAV = 0.5 * Range * (MTOW/50)^{0.5}$
Landing	$LAF = 6 * MTOW$
Total Charges	$NAV + LAF$
Airframe Weight	$AFW = MWE - W_{ENG} * NPP$
Airframe Price	$AFP = MSP - ENP * NPP$
Flight Time	$t_f = t_{block} - 0.25$
Airframe Maintenance Labour	$AFL = 0.09 * AFW + 6.7 - (350/(AFW + 75)) * (0.8 + 0.68 * t_f) * R_{labor}$
Airframe Maintenance Materials	$AMF = AFP * (4.2 + 2.2 * t_f)$
Total Airframe Maintenance	$AMC = AFL + AMF$
	$C1 = 1.27 - 0.2 * BPR^{0.2}$
	$C2 = 0.4 * (OPR/20)^{1.3} + 0.4$
	$C3 = 0.032 * n_c + 0.57$
Engine Maintenance Labour	$EML = 0.21 * C1 * C3 * (1 + T_{sl})^{0.4} * R_{labor}$ $(0.8 + 0.68 * t_f) * R_{labor}$
Engine Maintenance Materials	$EMM = 2.56 * (1 + T_{sl})^{0.8} * C1 * (C2 + C3)$
Total Engine Maintenance	$EMC = NPP * (EML + EMM) * (t_f + 1.3)/(t_f - 0.25)$
Fuel	$C_{FUEL} = T_c * sfc * t_{block} * FuelPrice$
Total DOC per Block	Total Financial Cost + Total Crew Cost Total Charges + Total Maintenance + Fuel

Table 60: DOC - AEA, adapted from [83] and [85].

The fuel cost evaluation was adapted to using the available upstream thrust and sfc information rather than the original method based on fuel burn per seat-nm in the AEA model. The same fuel cost calculation was also implemented for the Eastlake model.

As the ultimate goal was to quantify DOC in nm-pax, DOC per year and per flight block outputs from the Eastlake and AEA models were transformed into the desired unit using Equations 24 - 25.

$$DOC_{nm\text{pax}_{EL}} = \frac{C_{year}}{\frac{Q_{FLGT}}{t_{block}} * Range * pax} \quad (24)$$

$$DOC_{nm\text{pax}_{AEA}} = \frac{C_{block}}{Range * pax} \quad (25)$$

The cost breakdown from both models were recorded for the A380 case, the DOCs for A380, B747 and subsequent BWB designs were plotted against number of passengers onboard and compared for long and short haul flights with different fuel prices using the AEA model. The definitions of the scenarios are listed in Tables 61 and 62.

	Flight	Range (nm)	t_{block} (hr)
Short haul	LHR-PVG	4966	11
Long haul	LHR-GLA	300	1.3

Table 61: Range and block time for long and short haul flights.

	Fuel Price (\$/gallon)
Low	0.93
Normal	1.74
High	3.89

Table 62: Fuel prices. [83]

The carbon dioxide emission was also evaluated using Equation 26 based on mass of fuel consumption per flight block where the CO_2 production ratio $3.16kg$ per kg of fuel was applied [88].

$$m_{CO_2} = 3.16 * m_{fuel} \quad (26)$$

8.3.2 Results

The DOC for A380 calculated using the Eastlake and AEA models are shown in Table 63, where it can be noticed that the AEA model predicted up to 167% higher cost compared to the Eastlake model for short haul flights. Both models predicted higher DOC for short haul flights. The long haul result obtained shows agreement with literature with only 2% discrepancy, 51% difference was found for the short haul result when compared to literature.

	Eastlake	AEA	AEA [83]
Short haul	0.141	0.377	0.25
Long haul	0.072	0.108	0.11

Table 63: A380 DOC per nm-pax for short and long haul flights at normal fuel price using the Eastlake and AEA models, and compared to the AEA results from literature [83].

The breakdown proportion for each category of costs using both models are compared in Figure 74. Fuel costs accounts for over half of the overall DOC when predicted using the

Eastlake model, which is 22% higher than that of the AEA model. The depreciation cost is not accounted for in the Eastlake model, but is the second main contribution to costs for the AEA model.

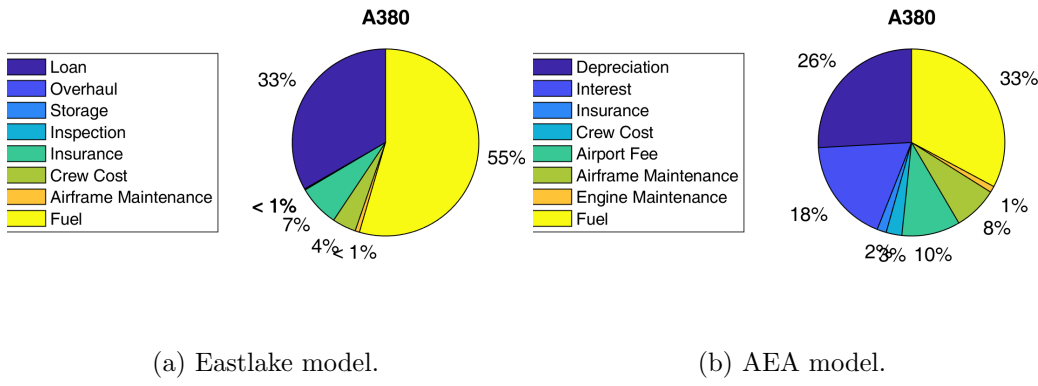


Figure 74: A380 DOC contribution for long haul flights at normal fuel price.

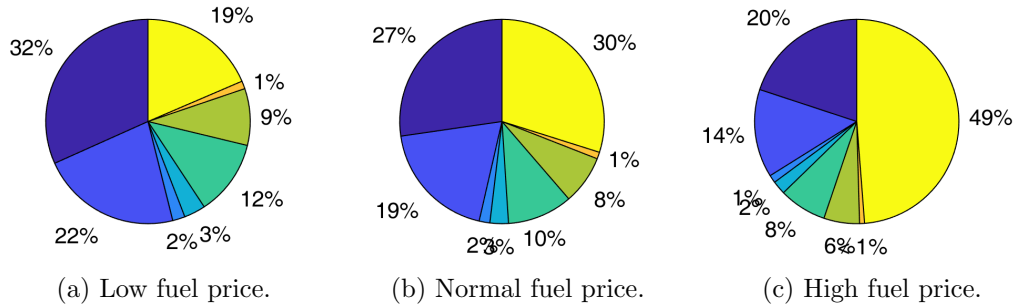


Figure 75: DOC contribution comparison for long haul flights at different fuel prices using the AEA model for BWB final design iteration.

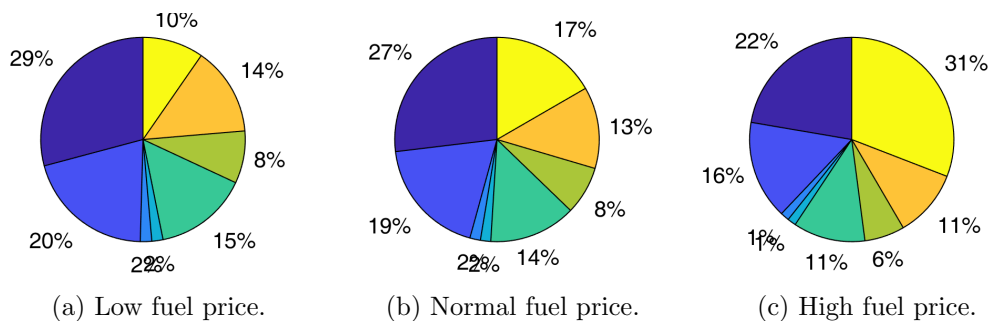


Figure 76: DOC contribution comparison for short haul flights at different fuel prices using the AEA model for BWB final design iteration.

From the cost distribution for all of the 6 scenarios considered, total fuel cost was shown to be highly sensitive to the flight stage length and fuel prices as illustrated in Figure 75 and 76, where the chart legends can be referred to Figure 74b. The total of fuel cost, depreciation and loan interest account for around 60% to 80% of the total DOC for all scenarios.

The DOC per nautical mile per passenger at full passenger load for each aircraft and BWB design iterations are illustrated in Table 64 and 65. B747 was found to be the most expensive to operate for both long and short haul flights due to its lower passenger capacity. The final BWB design iteration with the 4-engine configuration achieved up to 10.5% and 8.6% cost reduction for long and short haul flights at high fuel price compared to A380, a further 3.2% and 2% reduction was achieved respectively with the 3-engine configuration.

Fuel Price	A380	B747	Iter1	Iter2	Iter3	Iter4	Iter5	Iter5 (3-Eng)
Low	0.092	0.114	0.092	0.091	0.088	0.087	0.086	0.083
Normal	0.108	0.134	0.109	0.106	0.103	0.102	0.099	0.097
High	0.152	0.188	0.153	0.147	0.143	0.140	0.136	0.133

Table 64: DOC per nm-pax (\$) for long haul flight.

Fuel Price	A380	B747	Iter1	Iter2	Iter3	Iter4	Iter5	Iter5 (3-Eng)
Low	0.345	0.432	0.347	0.341	0.332	0.329	0.323	0.310
Normal	0.377	0.471	0.380	0.372	0.361	0.357	0.350	0.336
High	0.463	0.576	0.467	0.452	0.439	0.431	0.422	0.407

Table 65: DOC per nm-pax (\$) for short haul flight.

Figures 77 and 78 show the DOC variation with respect to number of passengers for all configurations and iterations of aircraft. The DOC curve noticeably drops throughout the design iterations. The B747 aircraft was found to be the most economical for up to 410 passengers for long haul and short haul flights at low fuel price. The final BWB design with 4 engines was able to reach similar DOC as the B747 even at lower passenger counts when the fuel price is high. The 3-engine configuration was able to surpass the cost efficiency of the B747 by up to 6% at high fuel price as demonstrated in Figure 78b. Full comparison between 6 scenarios can be found in Appendix J(a)-(b).

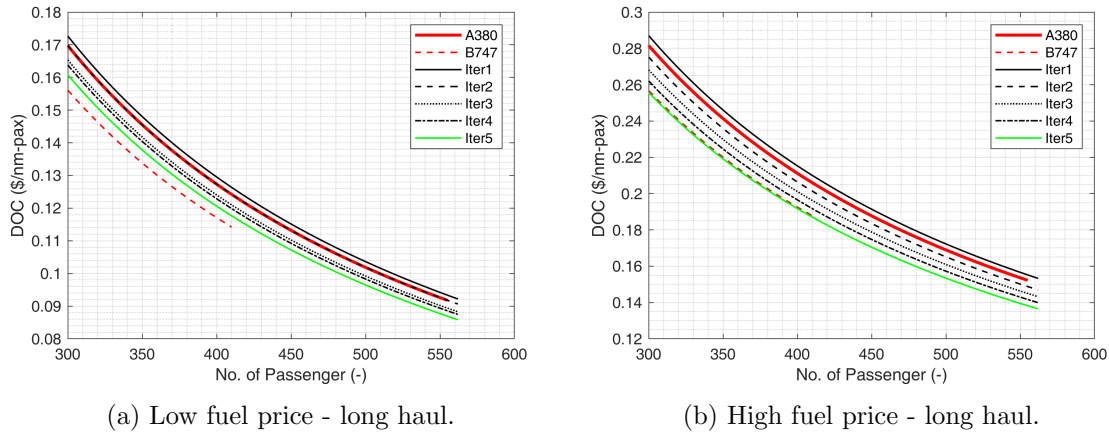


Figure 77: DOC per nm-pax for different design iterations compared to A380 and B747.

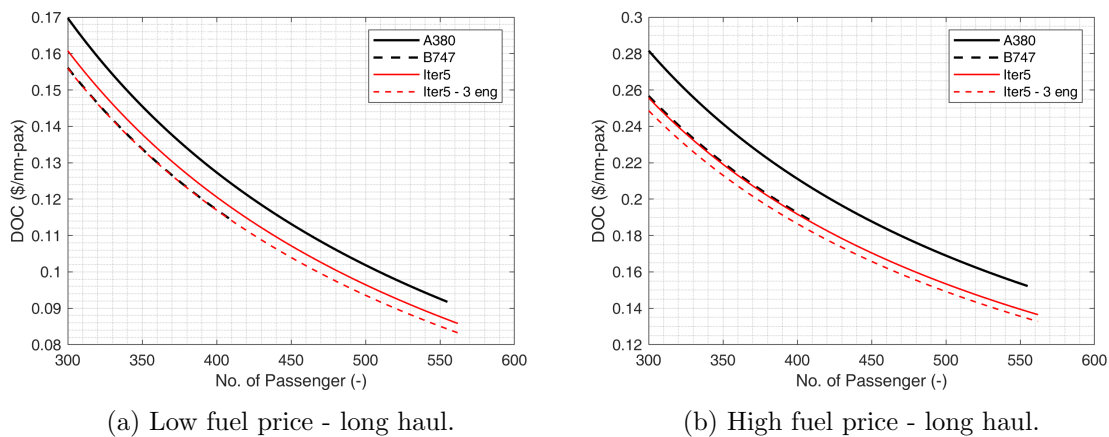


Figure 78: DOC per nm-pax for the BWB 3-engine configuration for the final design iteration for long haul flights compared to the BWB 4-engine configuration, A380 and B747.

The carbon dioxide emission for long and short haul flights are listed in Tables 66 and 67, up to around 18% reduction was achieved per nautical mile per passenger for the 3-engine BWB for both stage lengths.

	A380	B747	Iter1	Iter5	Iter5 (3-Eng)
Fuel Mass/Block(t)	214.97	193.41	219.91	182.39	178.17
CO ₂ /Block(t)	679.29	611.16	694.91	576.36	563.01
CO ₂ /nm-pax(kg)	0.246	0.300	0.249	0.207	0.202

Table 66: CO₂ emissions for long haul flight.

	A380	B747	Iter1	Iter5	Iter5 (3-Eng)
Fuel Mass/Block(t)	25.41	22.86	25.99	21.56	21.06
CO_2 /Block(t)	80.28	72.23	82.13	68.11	66.54
CO_2 /nm-pax(kg)	0.482	0.587	0.487	0.404	0.395

Table 67: CO_2 emissions for short haul flight.

8.4 Results Interpretation

8.4.1 Development Cost

With the most recent official A380 list price of \$445.6m by Airbus in 2018 [89], the Eastlake model was proven to generate reasonably accurate sales price estimation when assumed no composite materials was used. When the fraction of composite material was considered, the price was noticeably higher than the reference list price value. This could be potentially due to the complexity in labelling the price of an aircraft when trading, as airlines may customise the orders so suit their needs or make bulk orders at a discounted rate from the manufacturer which would result in large discrepancies between costs of different orders. Nevertheless, as the aim of this project was to compare the costs between different aircraft configurations as opposed to emphasise on the accuracy of the model, the acquisition cost evaluation strategy presented was deemed to be acceptable as a comparison method.

The substantial drops in list prices between iterations as demonstrated previously were primarily due to the reduction in the airframe weight as the structure was optimised. In addition, as the L/D ratio increased throughout the designs, the engine costs also decreased as the result of lower thrust requirement per engine. The relatively lower development cost of the BWB concept compared to the A380 proves it profitable from the aspect of a manufacturer.

However, it should be noted that the development cost calculated based on empirical relationships has the default assumption that the current level of technological skills is compatible with the new conceptual design, hence does not provide a comprehensive estimation on how an unprecedented design and production of a new type of aircraft impacts the overall development and manufacturing cost.

8.4.2 Direct Operating Cost

From the comparison between the Eastlake and AEA model information flow diagrams illustrated previously, the AEA model entails more input parameters that are informed by design choices that have an impact on aircraft performance characteristics, hence, it was considered more representative on the DOC variations between varied configurations. The high discrepancies in the operating costs for both models were due to the fundamental

dissimilarities in the categories of costs involved.

The AEA framework adopted in this project was able to be validated by literature that implemented similar methods for the long haul flight with the A380. The inconsistency in the short haul compared to literature may be due to the differences in defined range and block time. The difference in fuel consumption calculation methods could be another factor that affected the DOC, as the fuel burn in literature was based on published fuel economy data for commercial aircraft, whereas that in this project was determined using engine thrust and SFC considering the relevant data was unavailable for the conceptual BWB.

As the major cost contribution to both long and short haul flights is consisted of fuel, depreciation and loan interest, which are largely dependent on the acquisition price and engine thrust requirement according to the AEA model, scenarios where fuel consumption and price is high greatly benefits from the BWB design. Therefore, the advantage of reduction in weight and thrust in BWB aircraft has a great potential in reducing the DOC for an airline. Similarly, the reduction in fuel consumption also directly drives the CO_2 emission down compared to conventional aircraft. Although the bio-based fuels considered for sustainable aviation fuel as mentioned in Section 6.2.3 could possibly further offset the carbon footprint, however, the expensive fuel price is deemed non-economical without enforced carbon taxation policy.

9 Discussion

9.1 Soft Systems Methodology

It was the opinion of the team that SSM provided a good balance between the structure provided by most Systems methodologies, but still allowed the freedom to consider all research avenues, approaching the project holistically. While other systems methodologies such as the Systems V-Model provide a very structured linear approach to the running of a project and its related sequence of events; SSM provided a basis for an in depth discussion around what the eventual System would need to encapsulate. Furthermore, SSM is primarily focused on developing the learning process regarding the situation of the problem and how such complex problems should be overcome, it is not focused around a definite solution to a singular, easily quantifiable problem. Due to the previously mentioned subjective nature of what may be classed as feasible and the limited scope of the project due to its preliminary purview, such a focus was optimum for the project aim and allowed deeper, more rounded engineering knowledge and experience to be gained by the team. SSM provided a vessel for expansive thinking which need not confine itself to the direct implications of what was achievable in the real world, thus widening the horizons of traditional systems methods thinking and realising key areas of exploration to be considered for future work. Such thinking nurtured considerations from alternative perspectives and allowed the team members to remain open-minded in regards to the ways in which the project aim could be realised through different implementations.

9.2 The BWB Concept

9.2.1 Technical Feasibility

From an Aerodynamic standpoint, it is easy to see the potential of the BWB concept, while the wing area is reduced as a result of the substantially wider fuselage, the ability to employ the fuselage as a lifting surface also mean that an L/D value similar to that of a modern airliner such as an A380. The implementation of traditional wing optimisation techniques such as the implementation of washout and wing tapering were effective in both the increase in lift in reduction in drag that saw the requirements met for the aerodynamic characteristics of the airframe. All of this points towards an aerodynamically feasible design. In tracking the progress of the design, it is interesting to note the difference in wing shape that is often seen in literature surrounding the BWB topic; with the sweep and twist angles being fairly consistent with previous studies, the implementation of a larger, more blended wing has seen similar results in this case to those of studies such as that seen in Figure 52 of this report. This observation lends itself well to the wicked nature of the design task, with many solutions being presented relative to a singular design concept. Generally, as a result of the work done it can be stated, from an Aerodynamic standpoint, that the concept of the BWB can be seen to be feasible.

Furthering the aerodynamic feasibility of the BWB design, achieving such aerodynamic structures is also feasible. Despite having a much larger wing root chord compared to aircraft in its class the wings structure was able to withstands the highly demanding loads applied to it. Initial designs although acceptable in terms of stress, suffered gross skin deformation making them unsuitable where the thin skin was ill supported over the large surface area when under quite substantial loads. The issue was effectively eliminated by providing extra support to the skin by adding more, thicker ribs to the structure. This brought on its own problems of increased mass which is an issue in aircraft design where minimising mass is a priority so required addressing. Using manual optimisation was found to be a rather inefficient method of achieving this providing highly variable results. Due to this, basic means of analytical optimisation were sought after using Solidworks topology tools as an effective and time efficient means of accomplishing this. Using these tools, a lighter structure was created with superior stress characteristics due to the mass reduction and more efficient use of available material. The shearing actions on the structure were reduced as the weight of the wings resistance on the upwards lifting force is reduced, also causing the increased deflection. When the mass was further reduced by hollowing out the ribs and spars there was a further reduction in stress as this effect was exacerbated, thus producing a lightweight yet structurally sound wing that could achieve its aerodynamic goals.

The initial designs of the fuselage suffered unacceptable stress and deformation results due to the shape and thickness of the pressure shell being insufficient. Overall thickening of the structure alleviated this problem however, the structures shape still posed problems in the form of stress concentrations due to being not completely cylindrical in nature. Rounding these areas reduced the stress to acceptable results for chosen materials however like the wing structures these changes had made the mass unacceptable high. With shelling of the structure greatly reducing the mass while still remaining structurally suitable.

Materials selection for key structural components confirm that it is feasible to implement the proposed design using currently employed advanced aluminium alloys; in particular, 2024 T6 and 7075 T6 alloys which are currently employed on Airbus and Boeing aircraft. Ensuring the feasibility of the design with contemporary materials is vitally important within the aerospace industry, which is slow to adopt new material types. Aluminium alloys are easy to manufacture, relatively cheap, and can be recycled easily at the end of life. While CFRP materials are omitted for primary structural components in this feasibility study, it is accepted that as the cost of manufacture continues to fall, these components will constitute a greater percentage of the complete aircraft material makeup, following current trends in the aviation industry.

It is noted, however, that composites constitute a high percentage of the material compo-

sition on most modern commercial aircraft. While composite materials were not identified for use in the current work, which only considered a small subset of components, they would undoubtedly constitute a high proportion of materials within the complete design. As the cost and complexity of manufacturing CFRP materials continues to fall it is likely that these will be adopted for more key structural components across all aircraft, and particularly in future BWB designs.

9.2.2 Practical Feasibility

Many key issues commonly cited in the BWB literature centre around practical issues that bringing such a design to market would present: those relating to manufacturing and supply chain difficulties remained out of scope of the current body of work. However, the issue of emergency exits in such a wide-bodied aircraft was explored. Through discrete simulation, it was confirmed that evacuation of a 603 seat is possible, even with a number of aft emergency exits being made unavailable. This is a significant result for the BWB design, where aft over-wing or rear emergency exits are frequently deemed infeasible. Further optimisation of interior configuration will further reduce expected emergency egress times below the required 90 seconds.

9.2.3 Economic Feasibility

As previously discussed, the reduction in thrust requirement owing to the more superior aerodynamic performances signified by the increased L/D ratio, as well as the substantial weight saving enabled by reduction in wing area, meant lower development cost may be achieved based on empirical relationships established from historical data of conventional aircraft. Consequently, with the lower capital cost for the initial acquisition and fuel saving ability of the BWB aircraft, the cost in operating such aircraft in a fleet may also be significantly reduced to the level that is comparable or outperforms conventional aircraft, which implies economic feasibility. However, these conclusions were drawn from the assumption that the manufacturability and ease of maintenance are comparable with conventional aircraft; otherwise, with the possible additional costs associated with these factors, introduction of carbon taxation policy may strengthen the advantage of the high fuel efficiency aspect of the BWB aircraft.

9.2.4 Environmental Feasibility

Owing to the high fuel efficiency realised by the distinctive aerodynamic characteristics of BWB, CO_2 emission was found to have significantly reduced compared to conventional aircraft with the current propulsion technology.

Due to current and predicted limitations of electric and hydrogen-fuelled engines, such renewable energy sources would be incompatible with the scale of the long range, high capac-

ity BWB design. However, further carbon footprint improvements could be made through the use of SAFs, although this would impact the economic feasibility. If the considerable progress witnessed in the last decade in this industry is continued [60], the current disadvantages of production scale and cost could be overcome and would be compatible for use in the BWB design. Therefore allowing carbon offset of the design during fuel production and usage, which would work in the favour of the carbon neutrality goals for 2050.

10 Conclusion

SSM is best suited to multi-faceted problems where various aspects can be preferred for optimisation based on the perspective and concerns of the current society and values. Therefore, it was an apt fit for the projects multidisciplinary nature and the multitude of competing design elements of a commercial aircraft. SSM provided an excellent framework to assess the various design activities required and their inter-dependencies, in a manner in which it would have been easy to adjust should a certain aspect for optimisation been chosen. Through its implementation, all team members had a sound comprehension of the process and the manner in which the various aspects interlinked. This allowed for efficient team work and effective communication between the members.

The structural analysis on the BWB concept was performed to determine whether the alternative non cylindrical design and the lifting surfaces responsible for achieving competitive aerodynamic performance were structurally feasible. The structures of the wings able to support the require loads with relatively small stress results of 226 MPa, well within the limits of materials for such parts. allowing them to remain light at 63 tonnes each thanks to the use of optimisation methods. The fuselage structure also proving successful however less refined with a maximum stress value of 380 MPa however no optimisation was able to be applied to it. Overall achieving a suitable structure for the task set out remaining light enough to provide competitive weight savings compared to competitors.

By using the BWB exterior geometry dimensions, cabin floor area was able to be defined. Seating arrangements for economy and business classes were completed based on typical commercial aircraft standards as well as regulations stated by EASA. The designed BWB cabin layout in this project was able to hold comparable number of passengers with A380 with a single deck at 562 passengers in a 2-class configuration. Within the scope of work, the preliminary design of the cabin layout for both passenger classes were sufficient in proving the possible potential of high loading capabilities. When operated as a freighter, the BWB can hold up to 31.8% higher volume of cargo compared to the current highest capacity freighter B747-8F if non-standard containers may be used.

The BWB design resulted in an empty weight saving of 29.87 tonnes in comparison to the A380. Such considerable weight saving allowed for a direct decrease in development cost of the aircraft, but also an indirect decrease, through the consequent reduction in cruise thrust, of the direct operating costs. These savings presented a degree of economical advantage over the A380. The acquisition cost was first found with 6% reduction for the final 4-engine BWB configuration compared to the A380 using the Eastlake model, a further 3% decrease was achieved by the 3-engine configuration. Through break-even analyses, 59 units of aircraft need to be sold to reach profitability for the 3-engine BWB, which is up to 14 less compared to the A380, when the list price is set at \$450m. At full passenger load of over

500 passengers, the 4-engine BWB achieved 10.5% and 8.9% cost reduction from the A380 DOC for long and short haul at high fuel price, a further 2% and 3.2% reduction was found by using 3 engines. The BWB achieved up to 18% reduction in CO_2 emission from the A380.

In conclusion, the airframe weight and engine thrust reductions for the BWB aircraft were proven to be able to greatly decrease the development and operating cost compared to current conventional aircraft. With potential high efficiency engine technologies in the future, as well as the possible introduction of carbon tax in the aviation industry, the cost benefits of the BWB concept may become more substantial.

Currently, at such a preliminary design stage and based on the work done to this point by the group and in consulted literature, the BWB concept presents itself as a feasible future aircraft. However, the depth of investigation must be increased through further work before a definitive determination could be made.

11 Future Work and Perspectives

11.1 Aerodynamics

As previously discussed, the adoption of a manual design optimisation strategy was seen to be effective in producing the results required; however, an area of further work where the aerodynamics is concerned would be further shape optimisation of the airframe. While the final design iteration met the requirements and the subsequent economic analysis showed the design would be feasible, there is potentially room for shape optimisation in order to ascertain the most aerodynamically efficient design. Further to this, while the simulations provided good results in terms of the cruise portion of flight, further assessment of aerodynamic characteristic for the rest of the flight envelope would be required for a complete aerodynamic analysis.

11.2 Structure and Stability

For the aircraft structure, future work would be concerned with further optimising the rib structure with attempts to be made into creating and implementing a numerical method to carry out the optimisation. Alternative spar shapes such as I beams and alternative layouts for spars should also be explored. Such optimisation methods could also be applied to the fuselage structure to provide a better optimised design. Further decreasing the aircraft's mass, creating a more efficient design. The fuselage concept should be applied to the entire aircraft concept to identify any potential global design issues. Specific work on the landing gear layout and design should also be considered.

For stability, although the design was calculated to be suitably stable. It is based on some large underpinning assumptions. Work would need to be undertaken on more suitable methods for BWB design such as Vortex Lattice method [90] or eigenvalue analysis [33] to provide more accurate values. Lateral static stability should also be considered in further work to give a more complete picture of the aircraft's stability characteristics. The implementation of realistic control surfaces should be implemented to better analyse this, along with dynamic stability study to provide an overall picture of the design's stability characteristics.

11.3 Interior Layout

For conventional aircraft, wings are rigged at an incidence angle of maximum lift-to-drag ratio to keep the pitching angle at minimum during cruise. However, as the wings and fuselage are fully blended for a BWB configuration, the cabin floor placement may be necessary to be adjusted to offset the cruising angle to ensure a comfortable level position for passengers.

Additionally, a double-deck BWB aircraft configuration could also be explored for entering different segmentation of the aviation market. Such configuration would allow the spacious fuselage to potentially accommodate more creative facilities for enhancing passenger experience.

Furthermore, the landing gear placement can be investigated for a more comprehensive structural design, which ultimately leads to a more accurate evaluation of the loading capacity.

11.4 Propulsion

The future work that can be carried out in regards to propulsion systems of the design is extensive. The first, and most natural further work, that can be applied to the currently selected propulsion systems would be to accurately model each of the three and four engine configurations on Solidworks, or a relevant 3D modelling software, before conducting a CFD analysis of various aerodynamic parameters such as drag, lift, pressure distributions etc. In order to receive more accurate values and make a more informed decision on what is best suited to the BWB geometry.

More extensive further work methods involve further optimisation of the engines through the utilisation of an effect called Boundary Layer Ingestion (BLI), which remains a highly experimental area within the industry as discussed in section 6.2.4. Due to this highly experimental nature of the technology, it is clearly a very exciting area in terms of propulsive systems for use on the BWB, however significantly more research is required before it can be properly implemented into the real world and hence is an area of future work.

As also discussed in section 6.2.2, the effects of distributed propulsion could be utilised if sufficient technological advances in the SFC of smaller engines take place in the future, or by completely designing a new engine specifically for this operation. This would be an interesting route to take the further work down and would serve to reap the benefits of the reduced overall drag of the aircraft and hence increase propulsive efficiency.

Overall, there are an extensive amount of ways to further iterate the propulsion system in order to improve propulsive efficiency and BWB performance as a result. Any of the identified methods of future work would make for extremely interesting areas of research and would certainly add value to the industry as a result.

11.5 Materials

Future work in materials selection would primarily involve increasing the resolution of components considered, in parallel to increasing the resolution of structural design. While

current work has focused on investigating feasibility, future work should additionally include manufacturing, financial, and logistical considerations which will redefine the concept of optimality from a purely functional perspective into a one that is more well rounded.

11.6 Economics

The experience of engineers on a new conceptual technology may be considered in future development cost evaluations by implementing a quantity discount factor where labour costs decrease as number of produced units increase due to the experience gained, the resulted cost difference can be investigated between conventional aircraft that have been around for decades and the BWB design.

Different carbon tax scenarios may also be explored by adding extra relations to the DOC formulation to account for the additional cost incurred due to emission. Further to that, sensitivity analysis can be performed on the DOC by altering percentage increases in maintenance and acquisition costs due to the introduction of immature technologies and recognise how carbon taxation may favour the higher efficiency BWB aircraft.

Additional economic analysis can be performed on the passenger-cargo and freighter configuration to gain further understanding on the possible utilisation of the BWB aircraft and costs involved for different types of operations for airlines.

References

- [1] C. Goldberg, D. Nalianda, P. Pilidis, and R. Singh, “Economic viability assessment of NASA’s blended wing body N3-X aircraft,” *53rd AIAA/SAE/ASEE Joint Propulsion Conference*, 2017.
- [2] Dale Crane, *Dictionary of Aeronautical Terms, Third Edition*. Newcastle, Washington: Aviation Supplies Academics, 1997, p. 224.
- [3] R. Brar. (2014). “Design of a blended wing body aircraft,” [Online]. Available: <https://www.sjsu.edu/ae/docs/project-thesis/Brar.Randhir%5C%202Nov14.pdf>.
- [4] NASA. (2010). “Past projects: X-48b blended wing body,” [Online]. Available: <https://www.nasa.gov/centers/dryden/research/X-48B/index.html>.
- [5] Boeing. (2016). “Blended wing body back to the tunnel,” [Online]. Available: <http://www.boeing.com/features/2016/09/blended-wing-body-09-16.page>.
- [6] Airbus. (2020). “Imagine travelling in this blended wing body aircraft,” [Online]. Available: <https://www.airbus.com/newsroom/stories/Imagine-travelling-in-this-blended-wing-body-aircraft.html>.
- [7] G. C. Mapper. (2020). “Routing london heathrow airport to shanghai pudong international,” [Online]. Available: <https://www.greatcirclemapper.net/en/great-circle-mapper.html?route=EGLL-ZSPD&aircraft=73&speed=n>.
- [8] P. Checkland, “Soft Systems Methodology: A Thirty Year Retrospective,” *Systems Research and Behavioural Science*, vol. 17, 2000. DOI: [https://doi.org/10.1002/1099-1743\(200011\)17](https://doi.org/10.1002/1099-1743(200011)17).
- [9] INCISM, *Comparing hard and soft or*, University of Lancaster. [Online]. Available: <https://www.lancaster.ac.uk/users/incism/back2.html>.
- [10] S. Burge. (2015). “An overview of the soft systems methodology,” [Online]. Available: <https://www.burgehugheswalsh.co.uk/Uploaded/1/Documents/Soft-Systems-Methodology.pdf>.
- [11] P. Li, B. Zhang, Y. Chen, C. Yuan, and Y. Lin, “Aerodynamic design methodology for blended wing body transport,” *Chinese Journal of Aeronautics*, vol. 25, no. 4, pp. 508–516, 2012. DOI: [10.1016/s1000-9361\(11\)60414-7](https://doi.org/10.1016/s1000-9361(11)60414-7).
- [12] N. Qin, A. Vavalle, A. L. Moigne, M. Laban, K. Hackett, and P. Weinerfelt, “Aerodynamic considerations of blended wing body aircraft,” *Progress in Aerospace Sciences*, vol. 40, no. 6, pp. 321–343, 2004. DOI: [10.1016/j.paerosci.2004.08.001](https://doi.org/10.1016/j.paerosci.2004.08.001).
- [13] H. Smith, “College of Aeronautics Blended Wing Body Development Programme,” *Congress of International Council of Aeronautical Sciences*, 2000.
- [14] P. Okonkwo and H. Smith, *Review of evolving trends in blended wing body aircraft design*, 2016. DOI: [10.1016/j.paerosci.2015.12.002](https://doi.org/10.1016/j.paerosci.2015.12.002).

- [15] R. H. Liebeck, "Design of the Blended Wing Body Subsonic Transport," *Journal of Aircraft*, 2004.
- [16] J. Van Dommelen and R. Vos, "Conceptual design and analysis of blended-wing-body aircraft," *Proceedings of the Institution of Mechanical Engineers, Part G: Journal of Aerospace Engineering*, 2014, ISSN: 20413025. DOI: 10.1177/0954410013518696.
- [17] M. Brown and R. Vos, "Conceptual design and evaluation of blended-wing-body aircraft," in *AIAA Aerospace Sciences Meeting, 2018*, 2018, ISBN: 9781624105241. DOI: 10.2514/6.2018-0522.
- [18] Snorri Gudmundsson, *General Aviation Aircraft Design : Applied Methods*. Florida: Elsevier, 2014, p. 1048.
- [19] Airbus. (2020). "Aircraft characteristics - airport and maintenance planning," [Online]. Available: http://www.airbus.com/content/dam/corporate-topics/publications/backgrounderstechdata/aircraft_characteristics/Airbus-Aircraft-AC-A380.pdf.
- [20] EASA, *Certification specifications and acceptable means of compliance for large aeroplanes cs-25*, 2020.
- [21] N. A. Cumpsty and A. Heyes, *Jet propulsion: a simple guide to the aerodynamic and thermodynamic design and performance of jet engines*. Cambridge University Press, 2015.
- [22] Y. Li and N. Qin, "Influence of spanwise load distribution on blended-wing-body performance at transonic speed," *Journal of Aircraft*, vol. 57, no. 3, pp. 408–417, 2020. DOI: 10.2514/1.c035696.
- [23] S. Siouris and N. Qin, "Study of the effects of wing sweep on the aerodynamic performance of a blended wing body aircraft," *Proceedings of the Institution of Mechanical Engineers, Part G: Journal of Aerospace Engineering*, vol. 221, no. 1, pp. 47–55, 2007. DOI: 10.1243/09544100jaero93.
- [24] B. Blessing, J. Pham, and D. Marshall, "Using cfd as a design tool on new innovative airliner configurations," *47th AIAA Aerospace Sciences Meeting including The New Horizons Forum and Aerospace Exposition*, 2009. DOI: 10.2514/6.2009-45.
- [25] T. Ikeda and C. Bil, *Aerodynamic performance of a blended wing-body configuration aircraft*, 2006.
- [26] Z. e. a. Chen, "Assessment on critical technologies for conceptual design of blended-wing-body civil aircraft," *Chinese Journal of Aeronautics*, 2019.
- [27] W. M. Kimmel and K. R. Bradley, "A sizing methodology for the conceptual design of blended-wing-body transports," *Joint Institute for the Advancement of Flight Sciences*, 2004.
- [28] V. e. a. Schmitt, "Pressure distributions around the onera m6 wing at transonic mach numbers," *Report of the Fluid Dynamics Panel Working Group*, 1979.

- [29] G. Yu, D. Li, Y. Shu, and Z. Zhang, “Numerical simulation for engine/airframe interaction effects of the bwb300 on aerodynamic performances,” *International Journal of Aerospace Engineering*, vol. 2019, pp. 1–15, 2019. DOI: 10.1155/2019/1072196.
- [30] T. Bach and C. Huhne, “Structural optimization of stiffened composite panels for highly flexible aircraft,” *Advances in structural and Multidisciplinary Optimization*, pp. 838–849, 2007.
- [31] B. K. Stanford and P. D. Dunning, “Optimal topology of aircraft rib and spar structures under aeroelastic loads,” *Joint Institute for the Advancement of Flight Sciences*, 2014.
- [32] R. Brar, “Design of a blended wing body aircraft,” *Department of Aerospace Engineering, San Jose University*, 2014.
- [33] S. Paudel, S. Rana, and S. Ghimire, “Aerodynamic and stability analysis of blended wing body aircraft,” *International Journal of Mechanical Engineering and Applications*, 2016.
- [34] D. Raymer, *Aircraft Design: A Conceptual Approach, Fifth Edition*. 2012. DOI: 10.2514/4.869112.
- [35] EASA, *Certification specifications and acceptable means of compliance for large aeroplanes cs-25*, Revisions completed annually, 2020.
- [36] S. Guru. (2018). “British airways seat maps airbus a380-800 (388),” [Online]. Available: https://seatguru.com/airlines/British_Airways/British_Airways_Airbus_A380_new.php.
- [37] D. Scholz, *Dieter scholz: Aircraft design*, Lecture Notes, Hamburg Open Online University, 2020. [Online]. Available: https://www.fzt.haw-hamburg.de/pers/Scholz/HOOU/AircraftDesign_6_Fuselage.pdf.
- [38] SEARATES. (2021). “Uld container types,” [Online]. Available: <https://www.seirates.com/reference/uld/>.
- [39] AirBridgeCargo. (2021). “Boeing 747-8f,” [Online]. Available: <https://www.airbridgecargo.com/en/page/37/boeing-747-8f>.
- [40] F. S. E. Group. (2005). “Very efficient large aircraft,” [Online]. Available: <https://fseg.gre.ac.uk/fire/VELA.html>.
- [41] S. I. D’souza, “An analysis of the developments in blended wing body aircraft for sustainable aviation,” *University of Toronto Institute for Aerospace Studies*, 2012.
- [42] F. Global. (2006). “Airbus a380 evacuation trial full report: Everyone off in time,” [Online]. Available: <https://www.flightglobal.com/airbus-a380-evacuation-trial-full-report-everyone-off-in-time/66584.article>.

- [43] E. Galea, L. Filippidis, Z. Wang, P. Lawrence, and J. Ewer, “Evacuation analysis of 1000+ seat blended wing body aircraft configurations: Computer simulations and full-scale evacuation experiment,” in *Pedestrian and evacuation dynamics*, Springer, 2011, pp. 151–161.
- [44] EASA, *Transport of cargo in passenger compartment - exemptions under article 71(1) of regulation (eu)2018/1139 (the basic regulation)*, 2020.
- [45] EASA, *Acceptable means of compliance (amc) and guidance material (gm) to annex iv - part-cat*, 2016.
- [46] S. Guru. (2018). “Air france seat maps airbus a380-800 (380),” [Online]. Available: https://seatguru.com/airlines/Air_France/Air_France_Airbus_A380_V2.php.
- [47] S. Guru. (2018). “Emirates seat maps airbus a380-800 (388) two class,” [Online]. Available: https://seatguru.com/airlines/Emirates_Airlines/Emirates_Airlines_Airbus_A380_Two_Class.php.
- [48] M. Airlines. (2012). “Interior arrangement - mixed 494 seats,” [Online]. Available: <https://weechookeong.files.wordpress.com/2012/09/a380-layout-plan.jpg>.
- [49] K. R. Bradley, *A sizing methodology for the conceptual design of blended wing body transports*, 2004. [Online]. Available: <https://ntrs.nasa.gov/citations/20040110949>.
- [50] I. Kroos, *Aircraft design: Synthesis and analysis*, Desktop Aeronautics Inc., Version 0.99, 2001.
- [51] P. Kumar and A. Khalid, “Blended Wing Body Propulsion System Design,” *International Journal of Aviation, Aeronautics, and Aerospace*, vol. 4, no. 6, 2017. DOI: <https://doi.org/10.15394/ijaaa.2017.1187>.
- [52] E. Tulapurkara, A. Venkattraman, and V. Ganesh. (2007). “An example of airplane preliminary design procedure - jet transport,” [Online]. Available: <https://nptel.ac.in/courses/101/106/101106035/>.
- [53] M. Afsar, *16598 aero-design 1 notes*, 2018.
- [54] I. Taylor, *Me425 aerospace propulsion notes*, 2020.
- [55] P. LI, B. ZHANG, Y. CHEN, C. YUAN, and Y. LIN, “Aerodynamic design methodology for blended wing body transport,” *Chinese Journal of Aeronautics*, vol. 25, no. 4, pp. 508–516, 2012, ISSN: 1000-9361. DOI: [https://doi.org/10.1016/S1000-9361\(11\)60414-7](https://doi.org/10.1016/S1000-9361(11)60414-7). [Online]. Available: <https://www.sciencedirect.com/science/article/pii/S1000936111604147>.
- [56] J. Flaig, *Hydrogen-electric passenger aircraft flies for eight minutes in 'momentous' world first*, 2020. [Online]. Available: <https://www.imeche.org/news/news-article/hydrogen-electric-passenger-aircraft-flies-for-eight-minutes-in-'momentous'-world-first>.

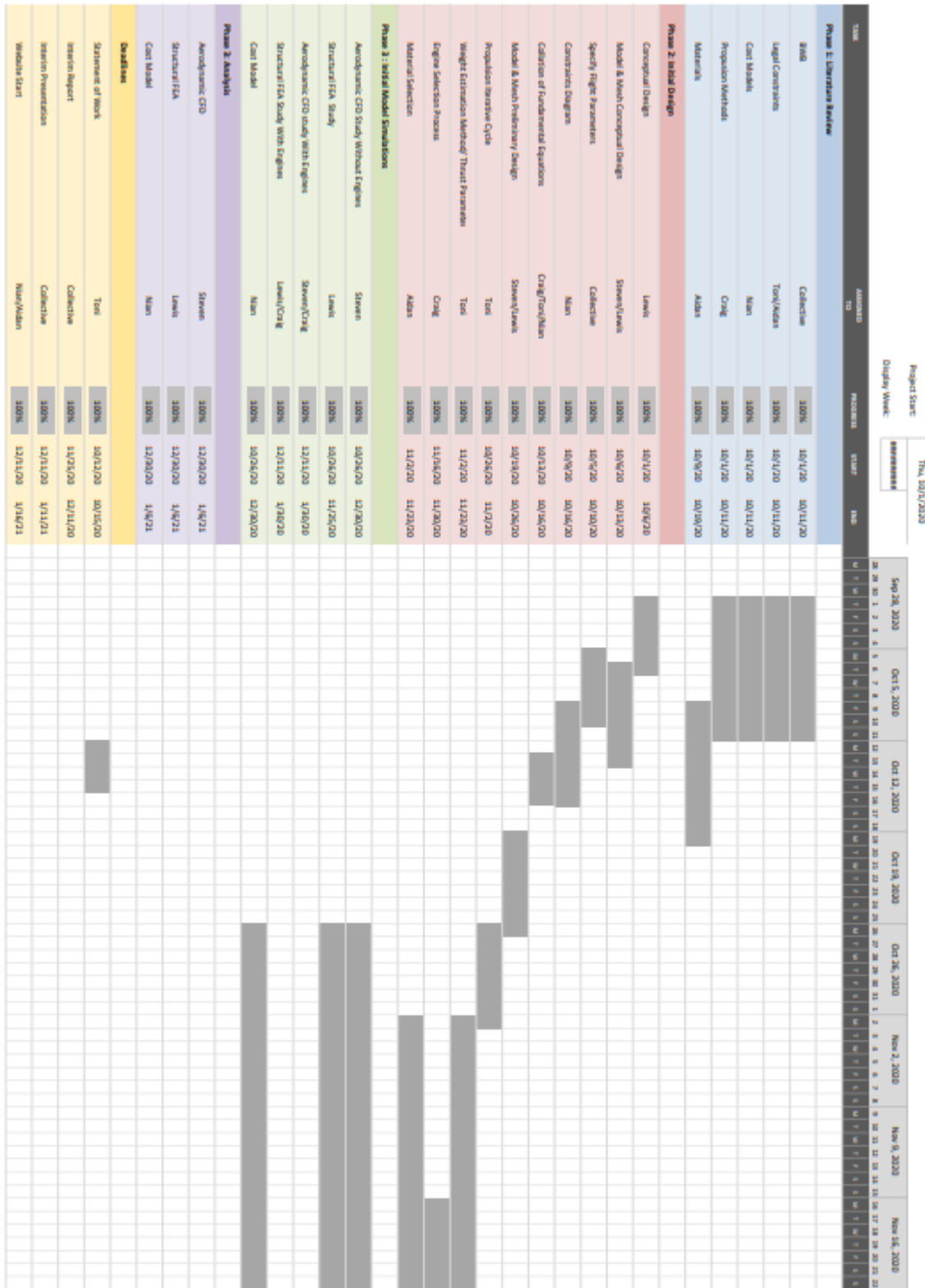
- [57] M. Holder, *Electric plane hits the skies in 'uk first' for climate-friendly flight*, 2020. [Online]. Available: <https://www.businessgreen.com/news/4016849/electric-plane-hits-skies-uk-climate-friendly-flight>.
- [58] T. Robinson, *Airbus spearheads european 'moonshot' for zero-carbon aviation*, 2020. [Online]. Available: https://www.aerosociety.com/news/airbus-spearheads-european-moonshot-for-zero-carbon-aviation/?utm_source=raes_newsletter&utm_medium=email&utm_campaign=15_october_2020.
- [59] Airbus, *E-fan x: A giant leap towards zero-emission flight*, 2020. [Online]. Available: <https://www.airbus.com/innovation/zero-emission/electric-flight/e-fan-x.html0>.
- [60] EASA. (2021). “Sustainable aviation fuels,” [Online]. Available: <https://www.easa.europa.eu/eaer/climate-change/sustainable-aviation-fuels>.
- [61] NASA. (2021). “Boundary layer,” [Online]. Available: <https://www1.grc.nasa.gov/aeronautics/bli/>.
- [62] N. G. R. Centre. (2021). “Boundary layer ingestion propulsion,” [Online]. Available: <https://www.grc.nasa.gov/www/k-12/airplane/boundlay.html>.
- [63] N. G. R. Centre. (2017). “Reduce fuel burn with a dose of bli,” [Online]. Available: <https://www.nasa.gov/aero/reduce-fuel-burn-with-a-dose-of-bli>.
- [64] N. Meier. (2020). “Civil turbojet/turbofan specifications,” [Online]. Available: <http://www.jet-engine.net/civtfspec.html>.
- [65] EASA. (2019). “Type-certificate data sheet ge-90 series engines,” [Online]. Available: https://www.easa.europa.eu/sites/default/files/dfu/EASA%20TCDS%20IM%20E%20002_GE90%20series_Issue4_Final_18Dec2019.pdf.
- [66] MIT. (2020). “Aircraft range: The breguet range equation,” [Online]. Available: <https://web.mit.edu/16.unified/www/FALL/thermodynamics/notes/node98.html>.
- [67] G. Electric. (2021). “Ge9x commercial aircraft engine,” [Online]. Available: <https://www.geaviation.com/commercial/engines/ge9x-commercial-aircraft-engine>.
- [68] K. Jayakrishna, V. R. Kar, M. T. Sultan, and M. Rajesh, “1 - materials selection for aerospace components,” in *Sustainable Composites for Aerospace Applications*, ser. Woodhead Publishing Series in Composites Science and Engineering, M. Jawaid and M. Thariq, Eds., Woodhead Publishing, 2018, pp. 1–18, ISBN: 978-0-08-102131-6. DOI: <https://doi.org/10.1016/B978-0-08-102131-6.00001-3>. [Online]. Available: <https://www.sciencedirect.com/science/article/pii/B9780081021316000013>.
- [69] A. P. Mouritz, *Introduction to aerospace materials*. Elsevier, 2012.

- [70] J. Macdonald. (2018). "Using thermoplastics in aerospace applications," [Online]. Available: <https://www.aerodefensetech.com/component/content/article/adt/features/articles/32727#:~:text=Thermoplastics%20can%20be%20machined%20to,can%20be%20critical%20for%20aerospace.&text=Aerospace%2Dgrade%20polymers%20such%20as,effective%20way%20to%20reduce%20weight..>
- [71] *granta edupack software*2020. Granta Design Limited, 2020.
- [72] P. Jerome, "Composite materials in the airbus a380-from history to future," in *Beijing: Proceedings 13th International Conference on Composite Materials (ICCM-13)*, 2001.
- [73] W. G. Roeseler, B. Sarh, M. U. Kismarton, J. Quinlivan, J. Sutter, and D. Roberts, "Composite structures: The first 100 years," in *16th International Conference on Composite Materials*, Japan Society for Composite Materials Kyoto, Japan, 2007, pp. 1–41.
- [74] M. H. Industries, "Production technology of large-scale composite wings for commercial aircraft," in *Mitsubishi Heavy Industries Technical Review Vol. 51 No. 4 (December 2014)*, 2014.
- [75] M. F. Ashby and D. Cebon, "Materials selection in mechanical design," *Le Journal de Physique IV*, vol. 3, no. C7, pp. C7–1, 1993.
- [76] T. Materia. (2009). "Aluminum alloy development for the airbus a380," [Online]. Available: <https://www.totalmateria.com/page.aspx?ID=CheckArticle&LN=EN&site=ktn&NM=227>.
- [77] C. Goldberg, D. Nalianda, V. Sethi, P. Pilidis, R. Singh, and K. Kyprianidis, "Assessment of an energy-efficient aircraft concept from a techno-economic perspective," *Applied Energy*, 2018, ISSN: 03062619. DOI: 10.1016/j.apenergy.2018.03.163.
- [78] P. Clark, *Buying the Big Jets: Fleet planning for airlines*. 2018. DOI: 10.4324/9781315195780.
- [79] B. Graver, K. Zhang, and D. Rutherford, "3CO₂ emissions from commercial aviation, 2018," *International Council on Clean Transportation, 2019*, 2019.
- [80] C. N. Eastlake and H. W. Blackwell, "Cost estimating software for general aviation aircraft design," in *ASEE Annual Conference Proceedings*, 2000. DOI: 10.18260/1-2--8243.
- [81] Airbus. (2021). "Orders and deliveries," [Online]. Available: <https://www.airbus.com/aircraft/market/orders-deliveries.html>.
- [82] A. W. Shen, J. L. Guo, and Z. J. Wang, "Analysis of the influence of advanced materials for aerospace products R&D and manufacturing cost," in *IOP Conference Series: Materials Science and Engineering*, 2015. DOI: 10.1088/1757-899X/103/1/012004.

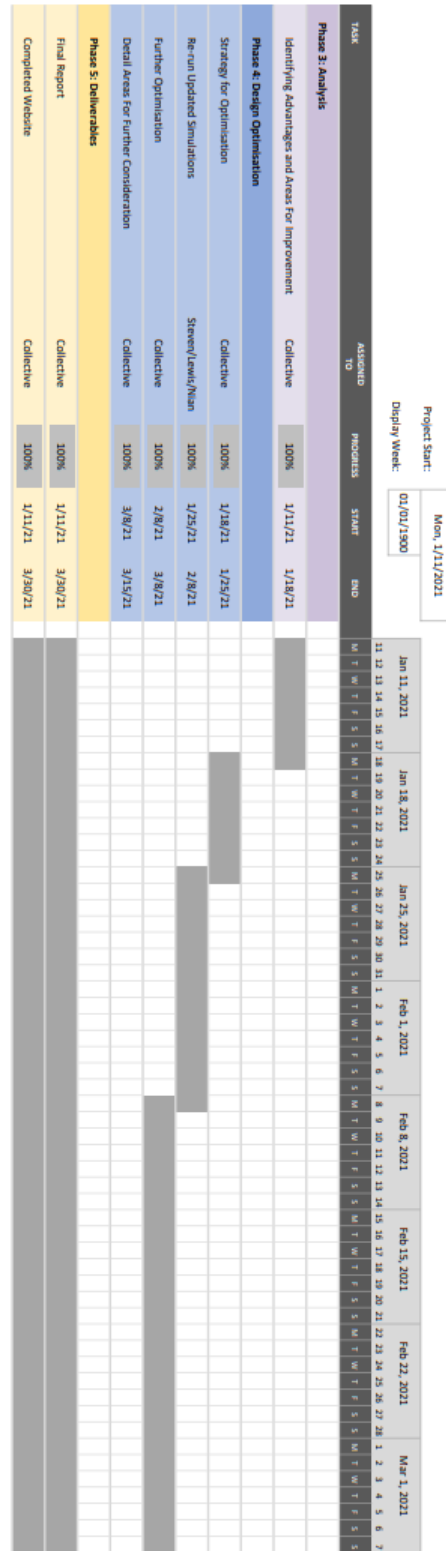
- [83] M. LEE, L. K. LI, and W. SONG, “Analysis of direct operating cost of wide-body passenger aircraft: A parametric study based on Hong Kong,” *Chinese Journal of Aeronautics*, 2019, ISSN: 10009361. doi: 10.1016/j.cja.2019.03.011.
- [84] M. A. Camilleri, “Aircraft Operating Costs and Profitability,” in, 2018. doi: 10.1007/978-3-319-49849-2_12.
- [85] R. Ali and O. Al-Shamma, “A Comparative Study of Cost Estimation Models used for Preliminary Aircraft Design,” *Global Journal of Researches in Engineering: B Automotive Engineering*, 2014.
- [86] R. H. Liebeck, D. A. Andrastek, J. Chau, R. Girvin, R. Lyon, B. K. Rawdon, P. W. Scott, and R. A. Wright, “Advanced subsonic airplane design and economic studies,” *NASA Contractor Report*, 1995.
- [87] A. of European Airlines, *Short medium range aircraft: AEA requirements*. 1989.
- [88] EESI. (2019). “Fact sheet — the growth in greenhouse gas emissions from commercial aviation,” [Online]. Available: <https://www.eesi.org/papers/view/fact-sheet-the-growth-in-greenhouse-gas-emissions-from-commercial-aviation>.
- [89] Airbus. (2018). “Airbus commercial aircraft list prices 2018,” [Online]. Available: www.airbus.com/content/dam/corporate-topics/publications/backgrounder/Airbus-Commercial-Aircraft-list-prices-2018.pdf.
- [90] R. Merino-Martinez, “Design and analysis of the control and stability of a blended wing body aircraft,” *Polytechnic University of Madrid*, 2015.
- [91] G. W. Records. (2012). “Highest recorded temperature on earth,” [Online]. Available: <https://www.guinnessworldrecords.com/world-records/highest-recorded-temperature>.
- [92] Britannica. (2021). “Temperature stress,” [Online]. Available: <https://www.britannica.com/science/temperature-stress>.

12 Appendices

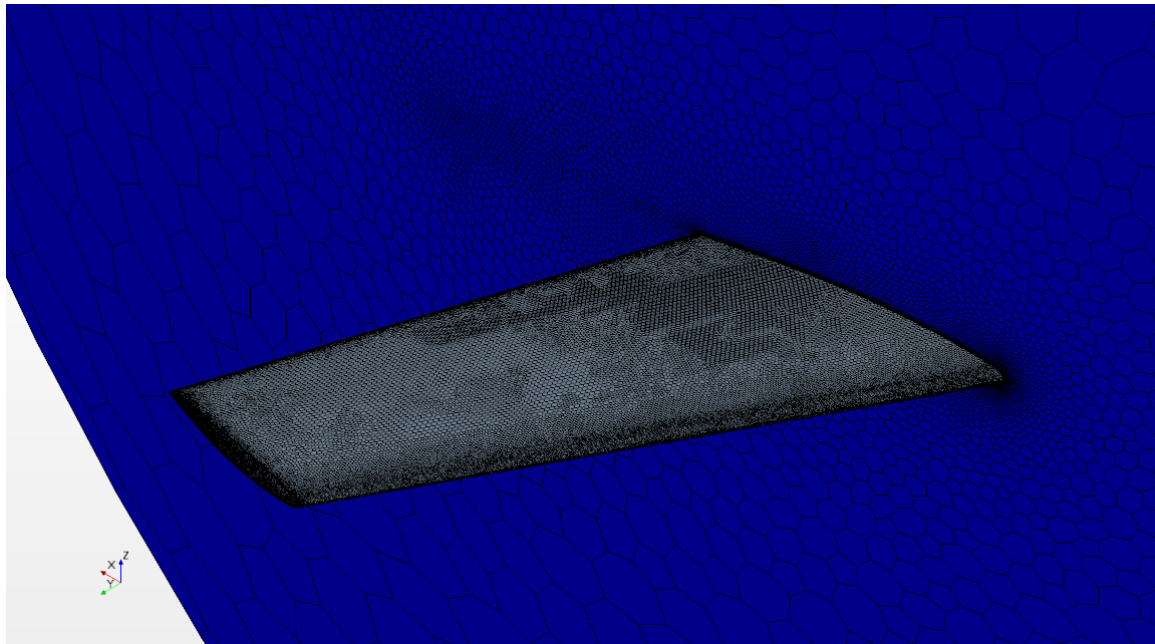
12.1 Appendix A : Semester 1 Gantt Chart



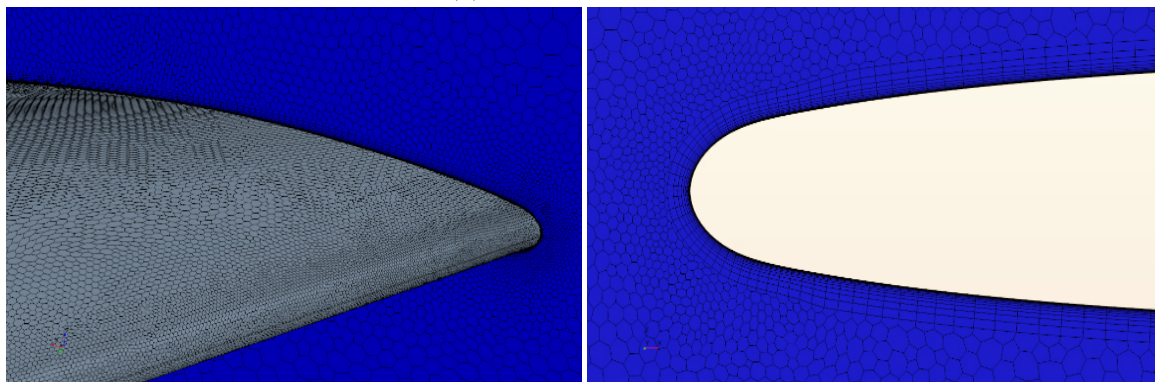
12.2 Appendix B : Semester 2 Gantt Chart



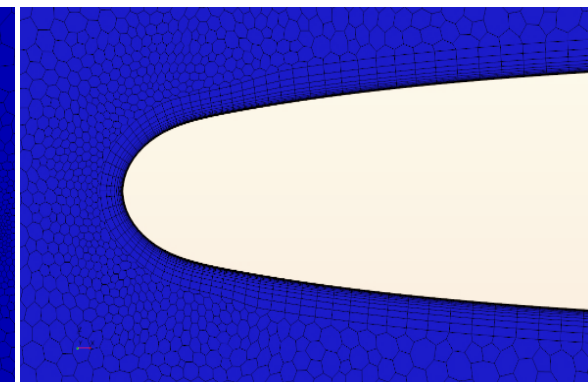
12.3 Appendix C : ONERA M6 Mesh Characteristics



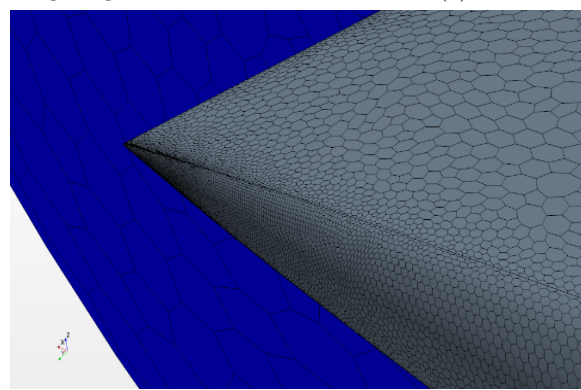
(a) ONERA M6 Mesh.



(b) ONERA Leading Edge Mesh.



(c) ONERA Prism Layers.



(d) ONERA Trailing Edge Mesh.

Figure 79: ONERA M6 Meshing Characteristics

12.4 Appendix D: Regulations of Predominant Importance of Regarding Transport of Cargo in Passenger Compartment

From existing guidelines regarding stowage in standard operations (CAT.OP.MPA.160), where cargo includes everything that is not luggage [45]:

- Baggage and cargo must be stowed in a location capable of restraining it
- Items should not be stowed in lavatories or against bulkheads incapable of restraining movement unless bulkheads have a placard specifying greatest mass capabilities
- Baggage and cargo placed in lockers must allow the latched doors to be secured
- Baggage and cargo can not impede access to emergency equipment
- Checks must be carried out before take-off, before landing and when the fasten seat belts sign is illuminated
- Mass of the cargo should not exceed the structural loading of the floor/seats
- Number/type of restraint devices and their attachment points must be capable of restraining cargo in accordance with Certification Specifications
- In the event of emergency evacuation, the cargo should not hinder or impair the crew's view

Further new operational aspects that must be considered from the new EASA guideline [44]:

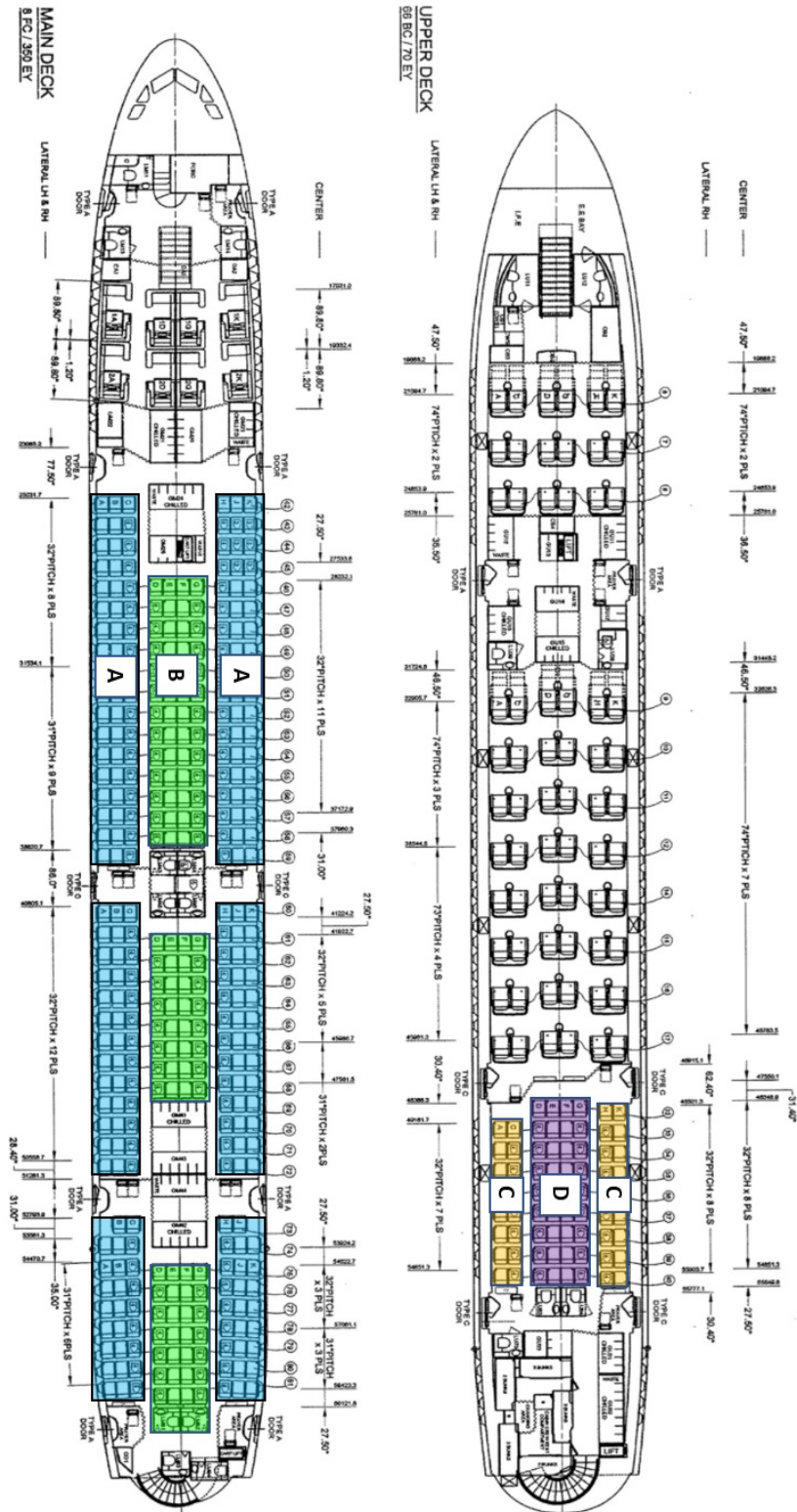
- Despite prohibition of any passengers in the compartment, whilst transporting cargo, cabin occupants (crew members, operator's employee or authorised consignment officer) are required to survey and access all areas during all phases of flight and to fight any fire that may occur.
- New risk assessment should be performed with adequate procedures for managing emergencies, both of which should be included in the temporary revision to the operating manual.
- Exact weight and position of the cargo should be reflected in the mass and balance documentation, with the pilot-in-command being supplied with a cargo manifest.
- Cargo must not exceed structural loading limits.
- Cargo must only be stored where it is capable of being restrained.
- Cargo must not impede access to emergency equipment or hinder any aisle access in case of evacuation.

- Cabin occupants must use existing cabin crew seating and not share rows with the cargo, ensuring a clear separation of at least one empty seat row.
- If nets are used for cargo restraint, they must be (E)TSO approved and load limitations adhered to.
- If nets are used, their deformation due to cargo movement during emergency landing, flight or ground loads should not come into excessive contact with other objects nor block the pathways to emergency equipment and pathways.

Furthermore, the absence of passengers allows the transportation of dangerous goods granted they are carried in the hold only, with goods and loading conforming to the specifications in the Technical Instructions for Cargo Aircraft. If carrying dangerous goods, all crew members must be made aware of which are loaded, the risks and consequences of the dangerous goods, and any changes in loading limits or emergency procedures [44]. In addition to dangerous goods, the following items are prohibited in the passenger compartment:

- Mail
- Batteries (including those contained within equipment)
- Cargo of a piercing, dense, rigid, or penetrating nature, or cargo with sharp edges or corners, such as rods, pipes, extrusions, or beams, that could become a projectile hazard during flight operations
- Live animals

12.5 Appendix E : Malaysia Airlines Interior Layout Drawing



12.6 Appendix F : A380 Cargo Loading Calculations

Section A

Max. volume (V) = 3.54m³, Max. height (h) = 1.27m, Section width (w) = 1.334m

$$\begin{aligned}
 V &= lwh \\
 3.54 &= l(1.334)(1.27) \\
 3.54 &= 1.69l \\
 l &= 2.09m
 \end{aligned} \tag{27}$$

$$\begin{aligned}
 l_{lat} &= 2.09 + (2(0.38)) \\
 &= 2.85m
 \end{aligned} \tag{28}$$

$$\begin{aligned}
 N_{la} &= \frac{43.61}{2.85} \\
 &= 15.3 \\
 &= 15
 \end{aligned} \tag{29}$$

$$\begin{aligned}
 V_{sect} &= 15(3.54) \\
 &= 53.1m^3
 \end{aligned} \tag{30}$$

Section B

Max. volume (V) = $3.54m^3$, Max. height (h) = $1.27m$, Section width (w) = $1.778m$

$$\begin{aligned}
 V &= lwh \\
 3.54 &= l(1.778)(1.27) \\
 3.54 &= 2.26l \\
 l &= 1.57m
 \end{aligned} \tag{31}$$

$$\begin{aligned}
 l_{lat} &= 1.57 + (2(0.38)) \\
 &= 2.33m
 \end{aligned} \tag{32}$$

$$\begin{aligned}
 N_{la} &= \frac{35.23}{2.33} \\
 &= 15.12 \\
 &= 15
 \end{aligned} \tag{33}$$

$$\begin{aligned}
 V_{sect} &= 15(3.54) \\
 &= 53.1m^3
 \end{aligned} \tag{34}$$

Section C

Max. volume (V) = $3.54m^3$, Max. height (h) = $1.27m$, Section width (w) = $0.889m$

$$\begin{aligned}
 V &= lwh \\
 3.54 &= l(0.889)(1.27) \\
 3.54 &= 1.129l \\
 l &= 3.14m
 \end{aligned} \tag{35}$$

$$\begin{aligned}
 l_{lat} &= 3.14 + (2(0.38)) \\
 &= 3.9m
 \end{aligned} \tag{36}$$

$$\begin{aligned}
 N_{la} &= \frac{32.94}{3.9} \\
 &= 8.45 \\
 &= 8
 \end{aligned} \tag{37}$$

$$\begin{aligned}
 V_{sect} &= 8(3.54) \\
 &= 28.32m^3
 \end{aligned} \tag{38}$$

Section D

Max. volume (V) = 3.54m³, Max. height (h) = 1.27m, Section width (w) = 1.778m

$$\begin{aligned}
 V &= lwh \\
 3.54 &= l(1.778)(1.27) \\
 3.54 &= 2.26l \\
 l &= 1.57m
 \end{aligned} \tag{39}$$

$$\begin{aligned}
 l_{lat} &= 1.57 + (2(0.38)) \\
 &= 2.33m
 \end{aligned} \tag{40}$$

$$\begin{aligned}
 N_{la} &= \frac{32.94}{2.33} \\
 &= 14.14 \\
 &= 14
 \end{aligned} \tag{41}$$

$$\begin{aligned}
 V_{sect} &= 14(3.54) \\
 &= 49.56m^3
 \end{aligned} \tag{42}$$

12.7 Appendix G : BWB Cargo Loading Calculations

Section A

Section length (l) = 0.46m, Section width (w) = 1.334m, Max. height (h) = 1.27m

$$\begin{aligned}
 V &= lwh \\
 &= (0.46)(1.334)(1.27) \\
 &= 0.78m^3
 \end{aligned} \tag{43}$$

$$\begin{aligned}
 V_{sect} &= 30(0.78) \\
 &= 23.4m^3
 \end{aligned} \tag{44}$$

Section B

Split into two sections with 0.38m access.

Section length (l) = 1.26m, Section width (w) = 1.334m, Max. height (h) = 1.27m

$$\begin{aligned}
 V &= 2lwh \\
 &= (2)(1.26)(1.334)(1.27) \\
 &= 4.26m^3
 \end{aligned} \tag{45}$$

$$\begin{aligned}
 V_{sect} &= (31)(4.26) \\
 &= 132.06m^3
 \end{aligned} \tag{46}$$

Section C

Split into two sections with 0.38m access.

Section length (l) = 1.29m, Section width (w) = 1.334m, Max. height (h) = 1.27m

$$\begin{aligned}
 V &= 2lwh \\
 &= (2)(1.29)(1.334)(1.27) \\
 &= 4.36m^3
 \end{aligned} \tag{47}$$

$$\begin{aligned}
 V_{sect} &= (4)(4.36) \\
 &= 17.44m^3
 \end{aligned} \tag{48}$$

Section D

Split into two sections with 0.38m access and one seat volume deducted.

Section length (l) = 1.26m, Section width (w) = 1.334m, Max. height (h) = 1.27m

$$\begin{aligned} V &= 2[lwh - ((0.445)(0.46)(1.27))] \\ &= 2[(1.26)(1.334)(1.27) - 0.26] \\ &= 3.74m^3 \end{aligned} \quad (49)$$

$$\begin{aligned} V_{sect} &= (4)(3.74) \\ &= 14.96m^3 \end{aligned} \quad (50)$$

Section E

Section length (l) = 2.05m, Section width (w) = 1.334m, Max. height (h) = 1.27m

$$\begin{aligned} V &= lwh \\ &= (2.05)(1.334)(1.27) \\ &= 3.47m^3 \end{aligned} \quad (51)$$

$$\begin{aligned} V_{sect} &= (2)(3.47) \\ &= 6.94m^3 \end{aligned} \quad (52)$$

Section F

Split into two sections with 0.38m access.

Section length (l) = 1.665m, Section width (w) = 1.334m, Max. height (h) = 1.27m

$$\begin{aligned} V &= 2lwh \\ &= (2)(1.665)(1.334)(1.27) \\ &= 5.64m^3 \end{aligned} \quad (53)$$

$$\begin{aligned} V_{sect} &= (2)(5.64) \\ &= 11.28m^3 \end{aligned} \quad (54)$$

Section G

Section length (l) = 0.46m, Section width (w) = 0.445m, Max. height (h) = 1.27m

$$\begin{aligned}
 V &= lwh \\
 &= (0.46)(0.445)(1.27) \\
 &= 0.26m^3
 \end{aligned} \tag{55}$$

$$\begin{aligned}
 V_{sect} &= (4)(0.26) \\
 &= 1.04m^3
 \end{aligned} \tag{56}$$

Section H

Section length (l) = 0.46m, Section width (w) = 1.334m, Max. height (h) = 1.27m

$$\begin{aligned}
 V &= 2lwh \\
 &= (2)(0.46)(0.445)(1.27) \\
 &= 0.52m^3
 \end{aligned} \tag{57}$$

$$\begin{aligned}
 V_{sect} &= (2)(0.52) \\
 &= 1.04m^3
 \end{aligned} \tag{58}$$

12.8 Appendix H : MATLAB Script for Weight Estimation

```

1 clc
2 clear all
3
4 %% Script Aim
5
6 %The purpose of the script is to have a system in place to give
    an accurate
7 %weight estimation of the aircraft depending on parameters
    effected by design
8 %change. Components of the overall TOW equation will be
    calculated for 3,
9 %4 and 8 engine configurations before being given at the end.
    After
10 %this , parameters affected by weight in propulsion will be
    calculated .

11
12 %% Aircraft Known Values
13
14 %%Areas
15 S_wing = 263.3;           %Wing area (m^2)
16 S_cabin = 479.59;         %Cabin area (m^2)
17 S_aft = 273.3;           %Aft area (m^2)
18 S_sc = 0.33*S_wing;      %Surface control area(m^2)

19
20 %%Masses
21 m_3eng = 7484.27;        %Individual engine dry weight for 3 engine
    config
22 m_4eng = 7074.22;        %Individual engine dry weight for 4 engine
    config
23 m_8eng = 3259;          %Individual engine dry weight for 8 engine
    config

24
25 %%Miscellaneous
26 lambda_aft = 3.3;        %Aft taper ratio
27 Isc = 0.147;              %Assuming fully powered surface controls (
    kg/m^2)
28 N_passengers = 562;       %Number of max. passengers
29 F_Tc = 206.32;            %Cruise thrust based on weight (kN)
30 sfc = 0.0162;             %sfc

```

```

31 t = 36480; %Time of flight path (s)
32
33 %Letting TOW be integers in a reasonable range
34 x_3 = [0:1000000];
35 x_4 = [0:1000000];
36 x_8 = [0:1000000];
37
38 TOW_3eng = x_3;
39 TOW_4eng = x_4;
40 TOW_8eng = x_8;
41
42 %% TOW Weight Equation
43
44 %TOW = m_empty + m_payload + m_empty
45
46 %m_empty has to consider aspects such as wings, propulsion, cabin
47 , %aft, landing gear, surface controls, auxiliary power unit (APU),
48 %instruments and navigational equipment, electrical components,
49 %hydraulics and pneumatics, furnishings, air con and anti-icing
50 and
51 %operating items. All masses will be expressed in kg.
52 %% Empty mass (m_empty)
53 %% Wings
54
55 %From Ko et al's BWB 450 design having 59591kg mass for a 1245 m
56 ^2
57 %surface area, assume BWB wing mass can be taken at 60000kg.
58 Revise
59 %this when material choice and design is settled.
60
61 %% Propulsion
62 %From Bradlely m_prop = 1.6*m_engdry
63
64 m_prop3eng = 3*1.6*m_3eng;
65 m_prop4eng = 4*1.6*m_4eng;
66 m_prop8eng = 8*1.6*m_8eng;
67

```

```

68 %% Cabin
69 %From Bradley
70
71 m_cabin3eng = (5.698865)*(0.316422)*(TOW_3eng.^0.166552)*(S_cabin
    ^1.061158);
72 m_cabin4eng = (5.698865)*(0.316422)*(TOW_4eng.^0.166552)*(S_cabin
    ^1.061158);
73 m_cabin8eng = (5.698865)*(0.316422)*(TOW_8eng.^0.166552)*(S_cabin
    ^1.061158);

74 %% Aft
75 %From Bradley. Calculated for each engine configuration using the
76 %general eq.
78 %m_aft = (1 + 0.05 N_engine)*(0.53)*(S_aft)*(MTOW^2)*(lambda_aft +
    0.5)

79
80 m_aft3eng = (1 + (0.05*3))*(0.53)*(S_aft)*(TOW_3eng.^0.2)*(
    lambda_aft + 0.5);
81 m_aft4eng = (1 + (0.05*4))*(0.53)*(S_aft)*(TOW_4eng.^0.2)*(
    lambda_aft + 0.5);
82 m_aft8eng = (1 + (0.05*8))*(0.53)*(S_aft)*(TOW_8eng.^0.2)*(
    lambda_aft + 0.5);

83
84 %% Landing Gear
85 %From Kroos
86
87 m_gear3eng = 0.04*TOW_3eng;
88 m_gear4eng = 0.04*TOW_4eng;
89 m_gear8eng = 0.04*TOW_8eng;

90
91 %% Surface Controls
92 %From Kroos
93
94 m_sc = Isc*S_sc;

95
96 %% APU
97 %From Kroos
98
99 m_APU = 0.454*(7*N_passenger);

100 %% Instruments & Navigational Equipment

```

```

102 %From Kroos , for long range .
103
104 m_IN = 544.31 ;
105
106 %% Electrical & Electronics
107 %From Kroos
108
109 m_elec = 0.454*((13*N_passengers)+ 1500) ;
110
111 %% Hydraulics & Pneumatics
112 %From Kroos
113
114 m_HP = 0.65*S_wing ;
115
116 %% Furnishings
117 %From Kroos
118
119 m_furn = 0.454*(101.6*N_passengers) ;
120
121 %% Air-conditioning & Anti-icing
122 %From Kroos
123
124 m_AA = 0.454*(15*N_passengers) ;
125
126 %% Operating Items
127 %From Kroos
128
129 m_opi = 0.454*(40*N_passengers) ;
130
131 %% Empty Weight
132 %Empty weight calculated for every engine configuration execpt
      terms
133 dependent on TOW.
134
135 m_empty3eng = m_wings + m_prop3eng + m_sc + m_APU + m_IN
136 + m_elec + m_HP + m_furn + m_AA + m_opi ;
137 m_empty4eng = m_wings + m_prop4eng + m_sc + m_APU + m_IN
138 + m_elec + m_HP + m_furn + m_AA + m_opi ;
139 m_empty8eng = m_wings + m_prop8eng + m_sc + m_APU + m_IN
140 + m_elec + m_HP + m_furn + m_AA + m_opi ;
141

```

```

142 %% Payload
143 %Accounting for 3 flight crew , 12 cabin crew and max number of
144 %passengers. Using the passenger mass estimations given in NPTEL.
145
146 m_payload = 110*(N_passengers + 3 + 12);
147
148 %% Fuel
149 %Basing the fuel consumption on cruise conditions as it is the
150 %of the flight , and using cruise thrust and sfc calculated .
151
152 %Alternative way to do it is based of Cd (from Kumar & Khalid)
153 %F_T = D_total = 0.5*rho*v_cruise*Sref*Cd
154 %m_fuel = F_T*sfc*t
155
156 m_fuel = F_Tc*sfc*t;
157
158
159 %% TOW
160 % Take off weight based on full passenger payload , calculated for
161 % all
162 % configurations .
163
164 %% 3 engine configuration
165 y_3 = m_empty3eng + ((5.698865)*(0.316422)*(TOW_3eng.^0.166552)
166 *(S_cabin^1.061158)) + ((1 + (0.05*3))*(0.53)*(S_aft)*(TOW_3eng
167 .^0.2))
168 *(lambda_aft + 0.5)) + (0.04*TOW_3eng) + m_payload + m_fuel -
169 TOW_3eng;
170
171 [y_3_min , y_3i] = min(abs(y_3));
172
173 x_zero3 = x_3(y_3i);
174 y_zero3 = y_3(x_zero3);
175 hold on;
176 grid on;
177 plot(x_zero3 , y_zero3 , 'ro');
178

```

```

179 formatSpec = '%.0f';
180 fprintf('Take-off Weights \n');
181 fprintf('For 3 engine configuration is %s kgs.\n', num2str(x_zero3
    ,formatSpec));
182
183 %% 4 engine configuration
184
185 y_4 = m_empty4eng + ((5.698865)*(0.316422)*(TOW_4eng.^0.166552)
186 *(S_cabin^1.061158)) + ((1 + (0.05*4))*(0.53)*(S_aft)*(TOW_4eng
    .^0.2)
187 *(lambda_aft + 0.5)) + (0.04*TOW_4eng) + m_payload + m_fuel -
    TOW_4eng;
188
189 plot(x_4, y_4);
190
191 [y_4_min, y_4i] = min(abs(y_4));
192
193 x_zero4 = x_4(y_4i);
194 y_zero4 = y_4(x_zero4);
195 hold on;
196 grid on;
197 plot(x_zero4, y_zero4, 'ro');
198
199 formatSpec = '%.0f';
200 fprintf('For 4 engine configuration is %s kgs.\n', num2str(x_zero4
    ,formatSpec));
201
202 %% 8 engine configuration
203
204 y_8 = m_empty8eng + ((5.698865)*(0.316422)*(TOW_8eng.^0.166552)
205 *(S_cabin^1.061158)) + ((1 + (0.05*8))*(0.53)*(S_aft)*(TOW_8eng
    .^0.2)
206 *(lambda_aft + 0.5)) + (0.04*TOW_8eng) + m_payload + m_fuel -
    TOW_8eng;
207
208 plot(x_8, y_8);
209
210 [y_8_min, y_8i] = min(abs(y_8));
211
212 x_zero8 = x_8(y_8i);
213 y_zero8 = y_8(x_zero8);

```

```

214 hold on;
215 grid on;
216 plot(x_zero8, y_zero8, 'ro');
217
218 formatSpec = '%.0f';
219 fprintf('For 8 engine configuration is %s kgs.\n', num2str(
    x_zero8,formatSpec));
220
221 %% Total Empty Weight
222 %% 3 engine configuration
223
224 m_emptytotal3eng = x_zero3 - m_payload - m_fuel;
225
226 fprintf('\n');
227 fprintf('<strong>Total Empty Weight </strong>\n');
228 fprintf('For 3 engine configuration is %s kg.\n', num2str(
    m_emptytotal3eng));
229
230 %% 4 engine configuration
231
232 m_emptytotal4eng = x_zero4 - m_payload - m_fuel;
233
234 fprintf('For 4 engine configuration is %s kg.\n', num2str(
    m_emptytotal4eng));
235
236 %% 8 engine configuration
237
238 m_emptytotal8eng = x_zero8 - m_payload - m_fuel;
239
240 fprintf('For 8 engine configuration is %s kg.\n', num2str(
    m_emptytotal8eng));
241
242 %% Stall Speed
243 %From the new weight estimations, stall speed is calculated
    assuming
244 rho = 1.225;
245 Cl_max = 1.7;
246
247 %% 3 engine configuration stall
248
249 V_stall3 = sqrt((2*9.81*x_zero3)/(rho*S_wing*Cl_max));

```

```

250
251 fprintf( '\n');
252 fprintf( '<strong>Stall Speeds </strong>\n');
253 fprintf( 'For 3 engine configuration is %s m/s.\n', num2str(
254     V_stall3));
255 %% 4 engine configuration stall
256
257 V_stall4 = sqrt((2*9.81*x_zero4)/(rho*S_wing*Cl_max));
258
259 fprintf( 'For 4 engine configuration is %s m/s.\n', num2str(
260     V_stall4));
261 %% 8 engine configuration stall
262
263 V_stall8 = sqrt((2*9.81*x_zero8)/(rho*S_wing*Cl_max));
264
265 fprintf( 'For 8 engine configuration is %s m/s.\n', num2str(
266     V_stall8));
267 %% Lift off speeds
268 %% 3 engine configuration
269
270 V_liftoff3 = 1.1.*V_stall3;
271
272 fprintf( '\n');
273 fprintf( '<strong>Lift-off Speeds </strong>\n');
274 fprintf( 'For 3 engine configuration is %s m/s.\n', num2str(
275     V_liftoff3));
276 %% 4 engine configuration
277
278 V_liftoff4 = 1.1.*V_stall4;
279
280 fprintf( 'For 4 engine configuration is %s m/s.\n', num2str(
281     V_liftoff4));
282 %% 8 engine configuration
283
284 V_liftoff8 = 1.1.*V_stall8;
285

```

```

286 fprintf( 'For 8 engine configuration is %s m/s.\n', num2str(
287   V_liftoff8));
288 %% Take off speeds
289 %% 3 engine configuration
290
291 V_takeoff3 = 1.2*V_stall3;
292
293 fprintf( '\n');
294 fprintf( '<strong>Take-off Speeds </strong>\n');
295 fprintf( 'For 3 engine configuration is %s m/s.\n', num2str(
296   V_takeoff3));
297 %% 4 engine configuration
298
299 V_takeoff4 = 1.2*V_stall4;
300
301 fprintf( 'For 4 engine configuration is %s m/s.\n', num2str(
302   V_takeoff4));
303 %% 8 engine configuration
304
305 V_takeoff8 = 1.2*V_stall8;
306
307 fprintf( 'For 8 engine configuration is %s m/s.\n', num2str(
308   V_takeoff8));
309 %% Cruise Speed
310
311 %Assuming flight at 11000m,
312 M_cruise = 0.85;
313 gamma = 1.4;
314 R = 287; % J/kgK
315 T = 216.66; % K
316
317 V_cruise = M_cruise*(sqrt(gamma*R*T));
318
319 fprintf( '\n');
320 fprintf( '<strong>Cruise Speed </strong>\n');
321 fprintf( 'The cruise speed is the same for all configurations at %
322   s m/s.\n',

```

```

322 num2str(V_cruise));
323
324 %% Climb Thrust at 10 degrees
325
326 %Adjust from Steven & Lewis sims
327 LD = 20.8;
328
329 %% 3 engine configuration
330
331 F_Tclimb3_10 = (9.81*x_zero3*((cosd(10)/LD) + sind(10)))/3;
332
333 fprintf('\n');
334 fprintf('<strong>Climb Thrust for 10 degrees </strong>\n');
335 fprintf('For 3 engines is %s N per engine.\n', num2str(
    F_Tclimb3_10));
336
337 %% 4 engine configuration
338
339 F_Tclimb4_10 = (9.81*x_zero4*((cosd(10)/LD) + sind(10)))/4;
340
341 fprintf('For 4 engines is %s N per engine.\n', num2str(
    F_Tclimb4_10));
342
343 %% 8 engine configuration
344
345 F_Tclimb8_10 = (9.81*x_zero8*((cosd(10)/LD) + sind(10)))/8;
346
347 fprintf('For 8 engines is %s N per engine.\n', num2str(
    F_Tclimb8_10));
348
349 %% Climb Thrust at 15 degrees
350 %% 3 engine configuration
351
352 F_Tclimb3_15 = (9.81*x_zero3*((cosd(15)/LD) + sind(15)))/3;
353
354 fprintf('\n');
355 fprintf('<strong>Climb Thrust for 15 degrees </strong>\n');
356 fprintf('For 3 engines is %s N per engine.\n', num2str(
    F_Tclimb3_15));
357
358 %% 4 engine configuration

```

```

359
360 F_Tclimb4_15 = (9.81*x_zero4*((cosd(15)/LD) + sind(15)))/4;
361
362 fprintf('For 4 engines is %s N per engine.\n', num2str(
363   F_Tclimb4_15));
364
365 %% 8 engine configuration
366
367 F_Tclimb8_15 = (9.81*x_zero8*((cosd(15)/LD) + sind(15)))/8;
368
369 fprintf('For 8 engines is %s N per engine.\n', num2str(
370   F_Tclimb8_15));
371
372 %% Take-off Distance (assumed at 10 degrees)
373 %% 3 engine configuration
374
375 %%Same as before Cl_max = 1.7, S_wing = 1300 and TOW = x_zero3
376 %%Maybe change this to S_ref to account for lift of the body?
377
378 TW3 = F_Tclimb3_10/(x_zero3*9.81);
379 WS3 = (x_zero3*9.81)/S_wing;
380
381 S_TO3 = ((1.1^2)/(Cl_max*rho*9.81*TW3))*WS3;
382
383 fprintf('<strong>Take-off Distance for 10 degrees </strong>\n');
384 fprintf('For 3 engines is %s m.\n', num2str(S_TO3));
385
386 %% 4 engine configuration
387
388 %%Same as before Cl_max = 1.7, S_wing = 1300 and TOW = x_zero4
389 %%Maybe change this to S_ref to account for lift of the body?
390
391 TW4 = F_Tclimb4_10/(x_zero4*9.81);
392 WS4 = (x_zero4*9.81)/S_wing;
393
394 S_TO4 = ((1.1^2)/(Cl_max*rho*9.81*TW4))*WS4;
395
396 fprintf('For 4 engines is %s m.\n', num2str(S_TO4));
397 %% 8 engine configuration

```

```

398
399 %Same as before Cl_max = 1.7, S_wing = 1300 and TOW = x_zero8
400 %Maybe change this to S_ref to account for lift of the body?
401
402 TW8 = F_Tclimb8_10/(x_zero8*9.81);
403 WS8 = (x_zero8*9.81)/S_wing;
404
405 S_TO8 = ((1.1^2)/(Cl_max*rho*9.81*TW8))*WS8;
406
407 fprintf('For 8 engines is %s m.\n', num2str(S_TO8));
408
409 %% Take-off Distance (assumed at 15 degrees)
410 %% 3 engine configuration
411
412 %Same as before Cl_max = 1.7, S_wing = 1300 and TOW = x_zero3
413 %Maybe change this to S_ref to account for lift of the body?
414
415 TW3_15 = F_Tclimb3_15/(x_zero3*9.81);
416 WS3_15 = (x_zero3*9.81)/S_wing;
417
418 S_TO3_15 = ((1.1^2)/(Cl_max*rho*9.81*TW3_15))*WS3_15;
419
420 fprintf('\n');
421 fprintf('<strong>Take-off Distance for 15 degrees </strong>\n');
422 fprintf('For 3 engines is %s m.\n', num2str(S_TO3_15));
423
424 %% 4 engine configuration
425
426 %Same as before Cl_max = 1.7, S_wing = 1300 and TOW = x_zero4
427 %Maybe change this to S_ref to account for lift of the body?
428
429 TW4_15 = F_Tclimb4_15/(x_zero4*9.81);
430 WS4_15 = (x_zero4*9.81)/S_wing;
431
432 S_TO4_15 = ((1.1^2)/(Cl_max*rho*9.81*TW4_15))*WS4_15;
433
434 fprintf('For 4 engines is %s m.\n', num2str(S_TO4_15));
435
436 %% 8 engine configuration
437
438 %Same as before Cl_max = 1.7, S_wing = 1300 and TOW = x_zero8

```

```

439 %Maybe change this to S_ref to account for lift of the body?
440
441 TW8_15 = F_Tclimb8_15/(x_zero8*9.81);
442 WS8_15 = (x_zero8*9.81)/S_wing;
443
444 S_TO8_15 = ((1.1^2)/(Cl_max*rho*9.81*TW8_15))*WS8_15;
445
446 fprintf( 'For 8 engines is %s m.\n', num2str(S_TO8_15));
447
448 %% Take-off Distance (assumed at 10 degrees)
449 %% 3 engine configuration
450
451 %Same as before Cl_max = 1.7, S_wing = 1300 and TOW = x_zero3
452 %Maybe change this to S_ref to account for lift of the body?
453
454 TW3 = F_Tclimb3_10/(x_zero3*9.81);
455 WS3 = (x_zero3*9.81)/S_wing;
456
457 S_TO3 = ((1.1^2)/(Cl_max*rho*9.81*TW3))*WS3;
458
459 fprintf( '\n');
460 fprintf( '<strong>Take-off Distance for 10 degrees </strong>\n');
461 fprintf( 'For 3 engines is %s m.\n', num2str(S_TO3));
462
463 %% 4 engine configuration
464
465 %Same as before Cl_max = 1.7, S_wing = 1300 and TOW = x_zero4
466 %Maybe change this to S_ref to account for lift of the body?
467
468 TW4 = F_Tclimb4_10/(x_zero4*9.81);
469 WS4 = (x_zero4*9.81)/S_wing;
470
471 S_TO4 = ((1.1^2)/(Cl_max*rho*9.81*TW4))*WS4;
472
473 fprintf( 'For 4 engines is %s m.\n', num2str(S_TO4));
474
475 %% 8 engine configuration
476
477 %Same as before Cl_max = 1.7, S_wing = 1300 and TOW = x_zero8
478 %Maybe change this to S_ref to account for lift of the body?
479

```

```
480 TW8 = F_Tclimb8_10/(x_zero8*9.81);  
481 WS8 = (x_zero8*9.81)/S_wing;  
482  
483 S_TO8 = ((1.1^2)/(Cl_max*rho*9.81*TW8))*WS8;  
484  
485 fprintf('For 8 engines is %s m.\n', num2str(S_TO8));  
486  
487 %% Cruise Thrust  
488 %% 3 engine configuration  
489  
490 F_Tcruise3 = ((x_zero3*9.81)/LD)/3;  
491  
492 fprintf('\n');  
493 fprintf('<strong>Cruise Thrust </strong>\n');  
494 fprintf('For 3 engines is %s N per engine.\n', num2str(F_Tcruise3));  
495  
496 %% 4 engine configuration  
497  
498 F_Tcruise4 = ((x_zero4*9.81)/LD)/4;  
499  
500 fprintf('For 4 engines is %s N per engine.\n', num2str(F_Tcruise4));  
501  
502 %% 8 engine configuration  
503  
504 F_Tcruise8 = ((x_zero8*9.81)/LD)/8;  
505  
506 fprintf('For 8 engines is %s N per engine.\n', num2str(F_Tcruise8));
```

12.9 Appendix I: Development Cost Breakdown

	C_{ENG} (\$b)	C_{DEV} (\$b)	C_{FT} (\$b)	C_{TOOL} (\$b)	C_{MFG} (\$b)	C_{QC} (\$b)	C_{MAT} (\$b)	C_{AVIO} (\$k)	C_{PP} (\$m)	C_{LIAB} (\$b)
A380 (No Comp.)	8.98	1.48	0.12	3.02	5.79	1.15	6.20	100	60.45	4.56
A380	11.22	1.66	0.12	3.77	6.15	1.38	6.20	100	60.45	5.20
Iter1	8.80	1.45	0.12	2.96	5.66	1.13	6.05	100	63.28	4.46
	-2%	-2%	-1%	-2%	-2%	-2%	-2%	0%	5%	-2%
Iter2	8.80	1.46	0.12	2.96	5.67	1.13	6.05	100	60.13	4.46
Iter3	8.57	1.42	0.12	2.88	5.51	1.10	5.86	100	58.89	4.34
Iter4	8.57	1.42	0.12	2.88	5.51	1.10	5.86	100	56.67	4.34
Iter5	8.43	1.41	0.12	2.83	5.41	1.08	5.75	100	54.12	4.26
	-6%	-5%	-3%	-6%	-6%	-6%	-7%	0%	-10%	-6%
Iter5 (3 Engine)	8.16	1.37	0.11	2.74	5.23	1.04	5.53	100	50.62	4.12
	-9%	-7%	-4%	-9%	-10%	-10%	-11%	0%	-16%	-9%

Table 68: Breakdown development costs for each analysed aircraft using the Eastlake model.

12.10 Appendix J(a) : DOC per nm-pax Comparison for 4-Engine

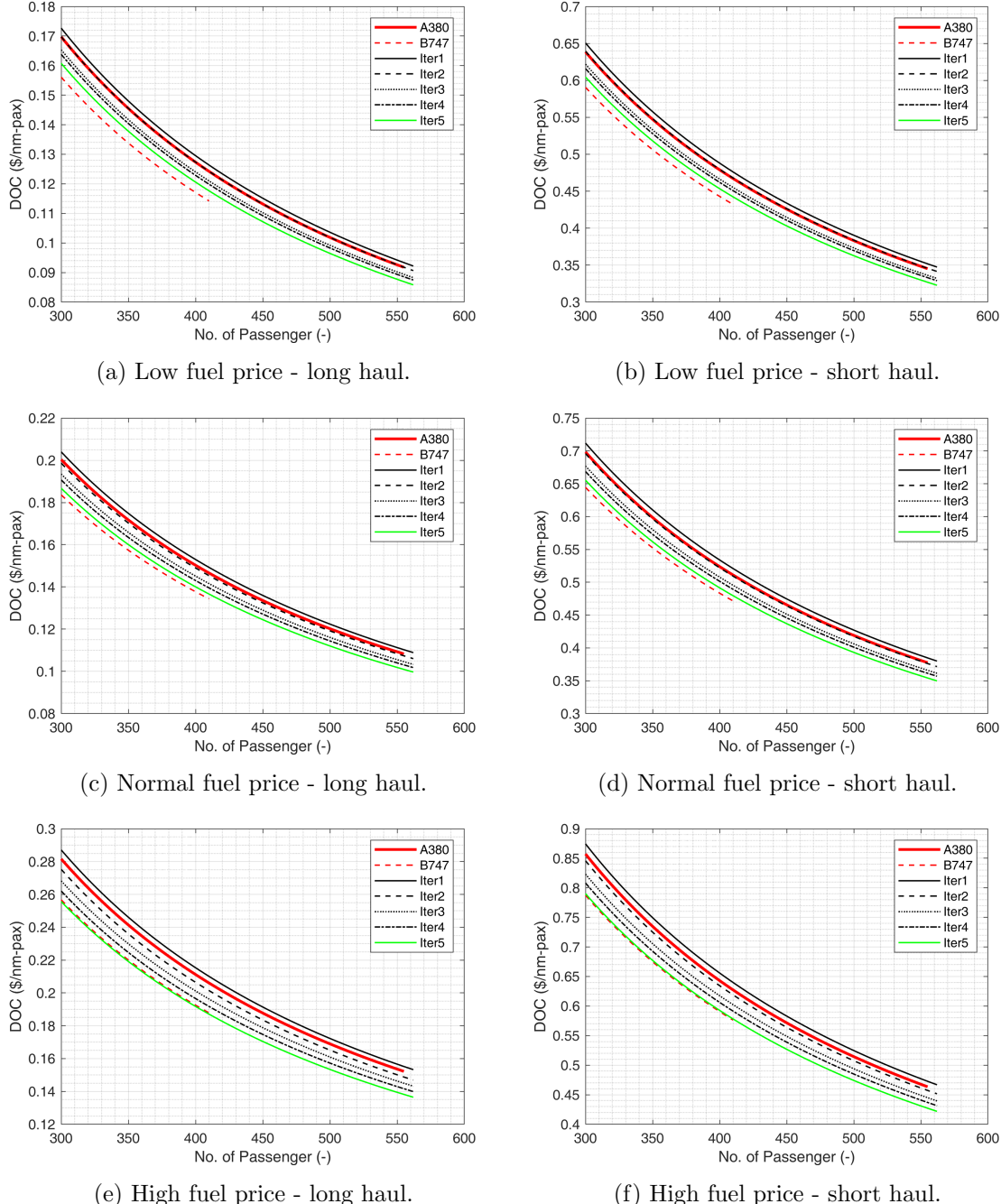
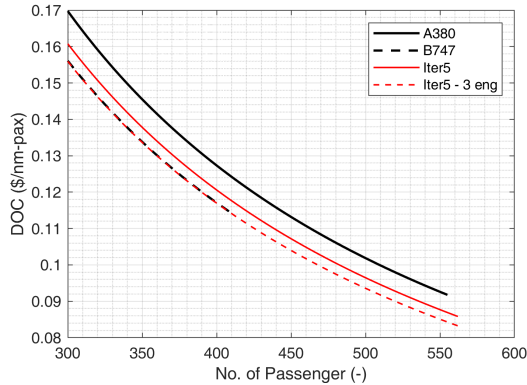
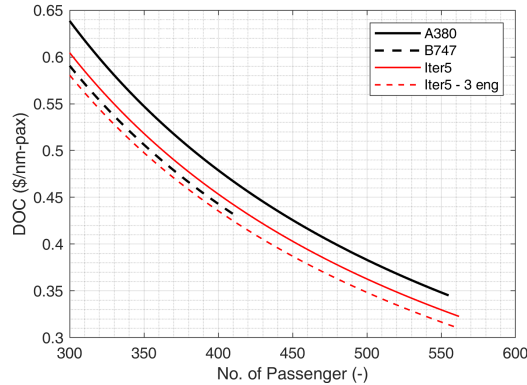


Figure 80: DOC per nm-pax for BWB 4-engine configurations through different design iterations at various fuel price scenarios for long haul and short haul flights compared to A380 and B747.

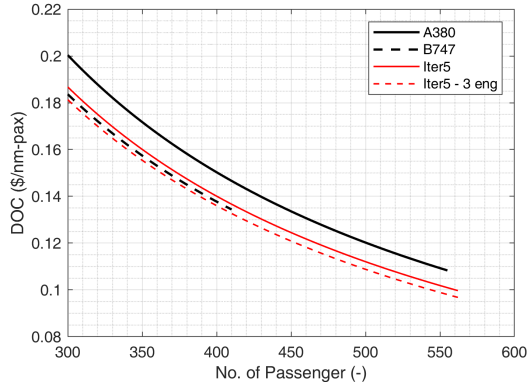
12.11 Appendix J(b) : DOC per nm-pax Comparison for 3 and 4-Engine



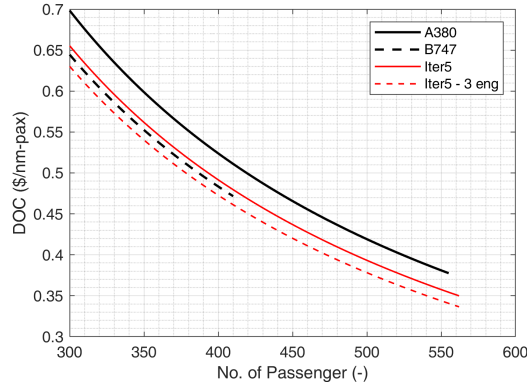
(a) Low fuel price - long haul.



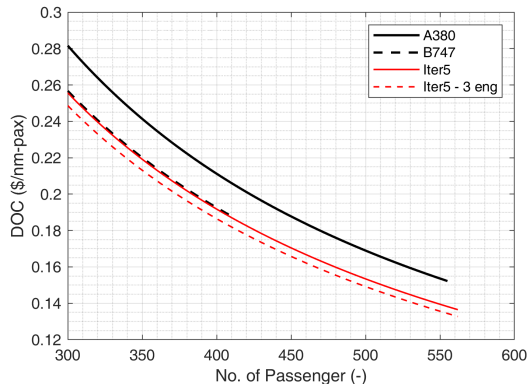
(b) Low fuel price - short haul.



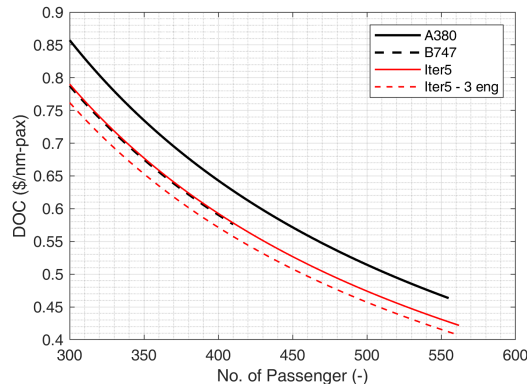
(c) Normal fuel price - long haul.



(d) Normal fuel price - short haul.



(e) High fuel price - long haul.



(f) High fuel price - short haul.

Figure 81: DOC per nm-pax for the BWB 3-engine configuration for the final design iteration at various fuel price scenarios for long haul and short haul flights compared to the BWB 4-engine configuration, A380 and B747.

12.12 Appendix K: Evacuation simulation

```
1 #cell 0
2 from PIL import Image, ImageDraw
3 import networkx as nx
4 import matplotlib.pyplot as plt
5 import numpy as np
6 from ast import literal_eval as make_tuple
7 from numpy import genfromtxt
8 import itertools
9 import pickle
10 import copy
11 import random
12
13 #cell 1
14 ## Initialisation Functions
15
16 #cell 2
17 # Define 'maze'
18
19 , ,
20 Schema:
21
22     0: Unobstructed
23     1: Wall
24     2: Seating
25     3: Impasse
26     4: Exit
27 , ,
28
29 def initTestMaze():
30
31     a = np.array([
32         [1, 1, 1, 1, 1, 1, 1, 1, 1],
33         [4, 0, 0, 0, 0, 0, 0, 0, 1],
34         [4, 0, 0, 0, 0, 2, 2, 2, 1],
35         [1, 2, 2, 2, 0, 3, 3, 3, 1],
36         [1, 0, 0, 0, 0, 3, 3, 3, 1],
37         [1, 2, 2, 2, 0, 3, 3, 3, 1],
38         [1, 0, 0, 0, 0, 0, 0, 0, 1],
39         [1, 2, 2, 2, 0, 2, 2, 2, 1],
```

```
40         [1, 1, 1, 1, 1, 1, 1, 1, 1],
41     ])
42
43     return a
44
45 def initMaze(file='floorPlanA380.csv', horizontalFlag = False):
46
47     a = genfromtxt(file, delimiter=',')
48
49     if horizontalFlag:
50         return np.transpose(a)
51     else:
52         return a
53
54
55 #cell 3
56 # Create graph network from 'maze'
57 def initGraph(maze):
58
59     # Node type dict
60     nodeMap = {0: "Path",
61                1: "Wall",
62                2: "Seating",
63                3: "Impasse",
64                4: "Exit"}
65
66     # Define edge logic
67     types = ['Path', 'Wall', 'Seating', 'Impasse', 'Exit']
68     edgeMap = {}
69
70     barriers = ["Wall", "Impasse"]
71
72     for d in ['up', 'side', 'down']:
73         edgeMap[d] = {}
74         for ty in types:
75             edgeMap[d][ty] = {}
76             for t in types:
77                 if (ty in barriers) or (t in barriers):
78                     val = 1000000
79                 else:
80                     val = 1
81             edgeMap[d][ty][t] = val
```

```

81
82     # Path edge cases
83     edgeMap[ 'up' ][ 'Path' ][ 'Seating' ] = 100
84     edgeMap[ 'side' ][ 'Path' ][ 'Seating' ] = 5
85     edgeMap[ 'down' ][ 'Path' ][ 'Seating' ] = 3
86
87     # Exit edge cases
88     edgeMap[ 'up' ][ 'Exit' ][ 'Seating' ] = 100
89     edgeMap[ 'side' ][ 'Exit' ][ 'Seating' ] = 5
90     edgeMap[ 'down' ][ 'Exit' ][ 'Seating' ] = 3
91
92     # Seating edge cases
93     edgeMap[ 'up' ][ 'Seating' ][ 'Path' ] = 2
94     edgeMap[ 'side' ][ 'Seating' ][ 'Path' ] = 5
95     edgeMap[ 'down' ][ 'Seating' ][ 'Path' ] = 100
96
97     edgeMap[ 'up' ][ 'Seating' ][ 'Exit' ] = 2
98     edgeMap[ 'side' ][ 'Seating' ][ 'Exit' ] = 5
99     edgeMap[ 'down' ][ 'Seating' ][ 'Exit' ] = 100
100
101    edgeMap[ 'up' ][ 'Seating' ][ 'Seating' ] = 100
102    edgeMap[ 'side' ][ 'Seating' ][ 'Seating' ] = 5
103    edgeMap[ 'down' ][ 'Seating' ][ 'Seating' ] = 100
104
105    G = nx.Graph()
106    for i in range(len(maze)):
107        for j in range(len(maze[i])):
108            k = (i, j)
109            G.add_node(k, type = nodeMap[maze[i][j]], pos = (j,
110                                              len(maze)-i))
111
112            for i in range(len(maze)):
113                for j in range(len(maze[i])):
114                    k = (i, j)
115                    sourceType = G.nodes[k][ 'type' ]
116                    # Assign upwards edge
117                    if i > 0:
118                        l = (i-1,j)
119                        targetType = G.nodes[l][ 'type' ]
w = edgeMap[ 'up' ][ sourceType ][ targetType ] # Edge weight

```

```

120             G.add_edge(k,l,weight = w)
121             # Assign right edge
122             if j < (len(a[i])-2):
123                 l = (i,j+1)
124                 targetType = G.nodes[l]['type']
125                 w = edgeMap['side'][sourceType][targetType] #
126                               Edge weight
126             G.add_edge(k,l,weight = w)
127             # Assign left edge
128             if j > 0:
129                 l = (i,j-1)
130                 targetType = G.nodes[l]['type']
131                 w = edgeMap['side'][sourceType][targetType] #
131                               Edge weight
132             G.add_edge(k,l,weight = w)
133             # Assign downwards edge
134             if i < (len(a)-2):
135                 l = (i+1,j)
136                 targetType = G.nodes[l]['type']
137                 w = edgeMap['down'][sourceType][targetType] #
137                               Edge weight
138             G.add_edge(k,l,weight = w)
139         return G, nodeMap, edgeMap
140
141 #cell 4
142 def initOccupancy(maze):
143     # Initialise occupancy grid. Individuals spawned into all
143       seat locations.
144     # Individual IDs assigned on encounter
145
146     # Note maze is a numpy array so is passed by REFERENCE -
146       modification WILL change
147     # Py default is pass by ASSIGNMENT
148
149     occupancy = np.zeros(a.size).reshape(a.shape)
150
151     individualID = 1
152
153     for i in range(len(a)):
154         for j in range(len(a[i])):
155             if a[i,j] == 2:

```

```

156             occupancy[i,j] = individualID
157             individualID += 1
158
159         return occupancy
160
161     #cell 5
162     def initPopulation(graph, occupancy):
163         population = []
164         for i in range(len(occupancy)):
165             for j in range(len(occupancy[i])):
166                 if occupancy[i,j] > 0:
167                     # Get initial path selection
168                     # No need to pass G, but included for clarity
169                     path = getPath(graph, (i,j))
170
171                     # Append individual to population with default
172                     # state
173                     population.append({ 'ID': int(occupancy[i,j]),
174                                         'location': (i,j),
175                                         'path': path,
176                                         'step': 0,
177                                         'lastMove': 0,
178                                         'lastPathChange': 0,
179                                         'moved': False,
180                                         'canMove': True,
181                                         'escaped': False,
182                                         'firstMove': random.randint(5,
183                                         20) })
184
185     return population
186
187     #cell 6
188     def softmax(x):
189         e_x = np.exp(x - np.max(x))
190         return e_x / e_x.sum(axis=0)
191
192     #cell 7
193     def searchNodes(G, attr, val):
194         return [x for x,y in G.nodes(data=True) if y[attr]==val]
195
196     #cell 8

```

```

195 def getPath(graph, source, pathFlag = False, individual = []):
196     ## Given a graph and a source, find the shortest paths and
197     # select one for an individual
198
199     exits = searchNodes(G, 'type', 'Exit')
200     paths = []
201     for exit in exits:
202         paths.extend([[item for item in path] for path in
203                     itertools.islice(nx.all_shortest_paths(G, source, exit,
204                                     weight = "weight"), 3)])
205
206     # Sort paths from shortest to longest
207     paths = sorted(paths, key=len)
208     # Remove paths of equal length (reduce diversity)
209     while len([len(p) for p in paths]) != len(set([len(p) for p
210             in paths])):
211         for i, path in enumerate(paths):
212             if len(path) == len(paths[i-1]):
213                 paths.pop(i)
214
215     p = []
216     for path in paths:
217         for i, l in enumerate(path):
218             if (a[1] == 3) or (a[1] == 1) or ((i > 0) and a[1] ==
219                 2):
220                 break
221             else:
222                 p.append(path)
223     paths = p
224
225     if pathFlag:
226         paths = [p for p in paths if p[1] != individual['path'][individual['step'] + 1]]
227
228     if len(paths) > 0:
229         # Logic to select path
230         lenPaths = np.array([len(p) for p in paths]) # Get array
231             of path lengths
232         lenPaths = sum(lenPaths) - lenPaths # Invert so shortest
233             paths have greatest value

```

```

228     pPath = softmax(lenPaths) # Calculate probabilities
229     path = paths [np.random.choice(len(paths), 1, p=pPath) [0]]
230             # Select path based on probability
231
232     else :
233         path = []
234
235
236 #cell 9
237 ## Simulation Functions
238
239 #cell 10
240 def moveIndividual(a, G, occ, item, i, t, nodeMap, edgeMap):
241
242     movedFlag = False
243     if t > 50:
244         moveTimeLimit = 1
245     else :
246         moveTimeLimit = 5
247
248     if t < 15:
249         item [ 'lastMove' ] = t
250
251     if item [ 'moved' ]:
252
253         item [ 'canMove' ] = False
254
255     else :
256
257         if occ [ item [ 'path' ] [ item [ 'step' ] + 1 ] ] > 0:
258             item [ 'canMove' ] = False
259             if t > item [ 'firstMove' ]:
260                 if (t-item [ 'lastMove' ]) > moveTimeLimit:
261
262                     newPath = updatePath(G, item, occ, a)
263                     if len(newPath) > 0:
264                         item [ 'path' ] = newPath
265                         item [ 'step' ] = 0
266
267             elif t > item [ 'firstMove' ]:

```

```

268     if a[item[ 'path '][item[ 'step '] + 1]] == 4:
269         if t < 11.1:
270             item[ 'canMove '] = False
271             item[ 'moved '] = True
272             item[ 'lastMove '] = t
273             movedFlag = True
274     else:
275         item[ 'canMove '] = False
276         item[ 'moved '] = True
277         item[ 'lastMove '] = t
278         movedFlag = True
279         # Remove current position from occupancy
280         occ[item[ 'location ']] = 0
281         item[ 'step '] += 1
282         item[ 'location ']= item[ 'path '][item[ 'step ']]
283             # Update location
284         occ[item[ 'location ']] = 0
285         item[ 'escaped '] = True
286
287     else:
288         # If individual NOT blocked
289         item[ 'canMove '] = False
290         item[ 'moved '] = True
291         item[ 'lastMove '] = t
292         movedFlag = True
293
294         # Remove current position from occupancy
295         occ[item[ 'location ']] = 0
296         item[ 'step '] += 1
297         item[ 'location ']= item[ 'path '][item[ 'step ']] # Update location
298
299         occ[item[ 'location ']] = item[ 'ID ']
300
301         G = updateGraph(item[ 'location '], a, occ, G,
302                         nodeMap, edgeMap)
303     else:
304         item[ 'canMove '] = False
305     return movedFlag

```

```

306 #cell 11
307 def updatePath(G, item, occ, a):
308     # Is there a free adjacent square?
309     freeMoves = False
310     loc = item['location']
311     for i,j in [(0,-1), (1,0), (-1,0), (0,1)]:
312         target = ((loc[0] + i), (loc[1] + j))
313         if (occ[target] == 0) and (a[target] == 0):
314             freeMoves = True
315             break
316     if freeMoves:
317         path = getPath(G, loc, True, item)
318     else:
319         path = []
320
321     return path
322
323 #cell 12
324 def updateGraph(source, a, occ, G, nodeMap, edgeMap):
325
326     dirMap = {(0,-1): 'side',
327                (1,0): 'up',
328                (-1,0): 'down',
329                (0,1): 'side'}
330
331     for i,j in [(0,-1), (1,0), (-1,0), (0,1)]:
332         target = (source[0] + i, source[1] + j)
333
334         c = (0,0)
335         b = a.shape
336
337         if all([(c < target) for c, target in zip(c,target)]) and \
338             \
339             all([(target < b) for target, b in zip(target,b)]):
340             # Update based on MAZE
341             sourceType = nodeMap[a[source]]
342             targetType = nodeMap[a[target]]
343             mazeWeight = edgeMap[dirMap[(i,j)][sourceType][
344                                         targetType]
345
346             # Update based on OCCUPANCY

```

```

345         occWeight = 1000 if occ[target] > 0 else 0
346         weight = max(mazeWeight, occWeight)
347         #print(f'Source: {source}')
348         #print(f'Target: {target}')
349         #print(f'Weight: {weight}')
350         G[source][target]['weight'] = weight
351
352     return G
353
354
355 #cell 13
356 ## Initialise simulation
357
358
359
360 #cell 14
361 #filenames
362 base = 'BWB_restricted_exit'
363 if 'A380' in base:
364     horizontalFlag = True
365 else:
366     horizontalFlag = False
367 mazeFilename = base + '.csv'
368 pklFile = base + '.pkl'
369 floorplan = base + '.png'
370 floorplanPop = base + '_with_pop.png'
371 gifName = base + '.gif'
372
373 #cell 15
374 # Initialisation process can be longest part. Pickle setup for
375 # speed.
375 pklFlag = False
376 filename = pklFile
377
378 if not pklFlag:
379     # Initialise MAZE
380     flag = True
381     if flag:
382         a = initMaze(mazeFilename, horizontalFlag) # global
383     else:
384         a = initTestMaze() # global

```

```

385
386     # Initialise GRAPH
387     G, nodeMap, edgeMap = initGraph(a) # global (NOTE: GRAPH
388         object passed by REFERENCE by default)
389     # Hence okay not to pass G between functions as would be
390         edited as if global anyway
391
392
393     # Initialise OCCUPANCY GRID
394     occ = initOccupancy(a)
395
396     # Initialise POPULATION
397     pop = initPopulation(G, occ)
398
399 else:
400     with open(filename, 'rb') as f:
401         a, G, occ, pop, nodeMap, edgeMap = pickle.load(f)
402
403 timestep = 1/2
404 endFlag = False
405 t = 0
406
407 #cell 16
408 ## Utilities
409
410 #cell 17
411 # Draw image of base 'maze'
412 def draw_matrix(a, zoom, borders):
413     im = Image.new('RGB', (zoom * len(a[0]), zoom * len(a)), (255, 255, 255))
414     draw = ImageDraw.Draw(im)
415     for i in range(len(a)):
416         for j in range(len(a[i])):
417             color = (255, 255, 255)
418             r = 0
419             if a[i][j] == 1:
420                 color = (0, 21, 36)
421             elif a[i][j] == 2:
422                 color = (21, 97, 109)

```

```

423         elif a[i][j] == 3:
424             color = (181, 182, 130)
425         elif a[i][j] == 4:
426             color = (255, 125, 0)
427             draw.rectangle((j*zoom+r, i*zoom+r, j*zoom+zoom-r-1,
428                             i*zoom+zoom-r-1), fill=color)
429
430     return im
431
432 a = initMaze(mazeFilename, horizontalFlag) # global
433
434 zoom = 20 # global
435 borders = 6 # global
436 im = draw_matrix(a, zoom, borders) # global
437
438 im.save(floorplan, )
439
440 #cell 18
441 def drawPop(occ, im):
442     draw = ImageDraw.Draw(im)
443     zoom = 20
444     borders = 6
445     for i in range(len(occ)):
446         for j in range(len(occ[i])):
447             if occ[i,j] > 0:
448                 r = borders
449                 draw.ellipse((j * zoom + r, i * zoom + r, j *
450                               zoom + zoom - r - 1, i * zoom + zoom - r - 1),
451                               fill=(255,0,0))
452
453     return im
454
455 a = initMaze(mazeFilename, horizontalFlag) # global
456
457 zoom = 20 # global
458 borders = 6 # global
459 im = draw_matrix(a, zoom, borders) # global
460 im = drawPop(occ, im)
461
462 im.save(floorplanPop, )
463
464 #cell 19

```

```

462 ## Simulation
463
464 #cell 20
465
466 # Init gif
467 baseIm = draw_matrix(a, 20, 6)
468 images = []
469
470 while not endFlag:
471
472     # At start of each iteration noone has moved and everyone can
        move
473     for i in pop:
474         i[ 'moved' ] = False
475         i[ 'canMove' ] = True
476
477     # Draw population
478     images.append(drawPop(occ, baseIm.copy()))
479
480     # Loop until no population moves are possible (blocked or
        have moved)
481     while any([m[ 'canMove' ] for m in pop]):
482
483         for i, item in enumerate(pop):
484
485             movedFlag = moveIndividual(a, G, occ, item, i, t,
                nodeMap, edgeMap)
486
487             if movedFlag:
488                 for m in pop:
489                     m[ 'canMove' ] = True
490                 # break
491
492             pop = [p for p in pop if p[ 'escaped' ] != True]
493
494
495             images.append(drawPop(occ, baseIm.copy()))
496             print(f'Timestep: {t} \t Population: {len(pop)}')
497             t += timestep
498
499             if len(pop) == 0:

```

```
500         endFlag = True
501
502     print(f"Time taken: {t} seconds")
503
504 images[0].save(gifName,
505                 save_all=True, append_images=images[1:],
506                 optimize=False, duration=333, loop=0)
```

12.13 Appendix L: Required material operating temperature

An upper bound on the required material operating temperatures can be assessed by considering the highest ground temperatures an aircraft is likely to encounter. This is no more than 60°, with the highest recorded land temperature being 56.7°[91].

A lower bound on required material operating temperatures can be assessed by considering the average temperatures encountered by an aircraft at cruise altitude (at most around 42000ft). This may be as low as -57°[92], however the ram-rise temperature increase during flight will raise this temperature slightly.

Considering these lower and upper bounds with a significant factor of safety, a temperature bound of -100° to 100° is suggested. As is recognised in Section 7.3, all materials identified as part of materials selection are able to withstand a much greater range of operating temperatures.